I.O.S.

SWANSEA BAY (SKER) PROJECT
TOPIC REPORT : 6

A D HEATHERSHAW AND F D C HAMMOND

Offshore Sediment Movement and its Relation to Observed Tidal Current and Wave Data

Report No 93

1979

NATURAL ENVIRONMENT RESEARCH COUNCIL

INSTITUTE OF OCEANOGRAPHIC SCIENCES

INSTITUTE OF OCEANOGRAPHIC SCIENCES

Wormley, Godalming,
Surrey, GU8 5UB.
(0428 - 79 - 4141)

(Director: Dr. A.S. Laughton)

Bidston Observatory,
Birkenhead,
Merseyside, L43 7RA.
(051 - 653 - 8633)

(Assistant Director: Dr. D.E. Cartwright)

Crossway,
Taunton,
Somerset, TA1 2DW.
(0823 - 86211)

(Assistant Director: M.J. Tucker

Institute of Oceanographic Sciences Report No 93/1979

Erratum

Page 7

The dimensions of the coefficient β in equation (3) should be gm $cm^{-4} s^{2}$

Addendum

Page 10

In equation (7) δ is an empirical constant which takes a value of 26.4

SWANSEA BAY (SKER) PROJECT

TOPIC REPORT : 6

A D HEATHERSHAW AND F D C HAMMOND

Offshore Sediment Movement and its Relation to Observed Tidal Current and Wave Data

Report No 93

1979

This project was supported financially by the Department of the Environment

Institute of Oceanographic Sciences
Crossway
Taunton
Somerset

A NOTE ON SYMBOLS

Where possible use of the same symbol for different meanings has been avoided. However, in some cases it has been desirable to preserve original notation

CONTENTS

		page
1.	INTRODUCTION	2
2.	DYNAMICS OF SEDIMENT TRANSPORT	2
	2.1 Fundamental processes	2
	2.2 Non-linear effects	3
3.	DISTRIBUTION OF SEDIMENTS	4
4.	BED LOAD TRANSPORT	4
	4.1 Techniques	4
	4.2 Choice of sediment transport formula	6
5.	SUSPENDED LOAD TRANSPORT	8
	5.1 Suspended sediment transport formulae	8
	5.2 Near-bottom suspended sediment and velocity profile measurements	9
6.	SEDIMENT TRANSPORT PATHS	14
7.	THE EFFECTS OF WAVES	15
	7.1 Bijker's formula	15
	7.2 Thresholds of sediment movement under waves and currents	17
	7.3 Mass transport effects due to waves	18
8.	SUMMARY AND CONCLUSIONS	19
9.	ACKNOWLEDGEMENTS	21
REFERENCES		22
TABLES		26
FIGURES		30
APPENDICES		78

1. INTRODUCTION

This report describes measurements of sediment transport rates and the sediment circulation pattern in Swansea Bay (see Figure 1).

The specific objective of this study has been to identify and quantify those processes which are capable of transporting sand towards and away from the foreshore on the E side of the Bay, particularly the area to the S of Port Talbot (see Figures 2 and 3). However, the findings of this report may have broader implications in terms of sediment transport processes in the sea.

Observed and predicted transport rates have been used to determine the relative magnitudes of suspended and bed load transport, principally under tidal currents, and in the selection of a suitable sediment transport formula for the prediction of sediment transport paths in the area. The role of surface wave activity in modifying the sediment transport processes is also briefly considered.

Previous studies of sediment transport processes in Swansea Bay (eg Davies, 1974, 1975; Ferentinos and Collins, 1978; Collins et al, 1979) have concentrated largely on a fundamental description of the origins, transport and deposition of both non-cohesive and the cohesive sediments in the area. Sediment transport paths have been inferred from grain size distributions and the asymmetry of large amplitude bedforms; current measurements have also been used to describe the various hydrodynamic regimes.

In this report we examine the previous and largely sedimentological interpretations of the area and show that in general these are consistent with the observed fluid dynamical processes and predictions from sediment transport theory. However, there are some important differences.

2. DYNAMICS OF SEDIMENT TRANSPORT

2.1 Fundamental processes

Sediment may be moved on or above the sea bed in two modes:

(a) bed load in which grains roll or saltate along the sea bed, perhaps at heights of up to a few grain diameters;

(b) suspended load in which grains are transported within the body of the fluid at some distance (many grain diameters) from the boundary.

Under tidal currents the motile agencies for these modes consist respectively of:

(c) the action of an applied stress at the sea bed by the action of the tidal current flowing above it;

(d) the production of turbulent kinetic energy by shear in the bottom boundary layer.

In some cases (c) and (d) will be modified by the effects of wave activity.

2.2 Non-linear effects.

The principal difficulty involved in measuring and predicting sediment transport is its extreme non-linearity. From a dynamic point of view bed load transport (q_{sb}) is related to the friction velocity u_* times the excess shear stress $(\tau - \tau_{cr})$ at high transport rates and to u_* times the excess shear stress squared $(\tau - \tau_{cr})^2$ at low transport rates. Suspended sediment transport (q_{ss}) is dynamically related to the friction velocity u_* to a power greater than unity, times the excess shear stress. Here τ is the shear stress exerted on the sea bed and τ_{cr} is a critical value of τ related to the threshold of movement of material as bed load or in suspension.

Thus to summarise:

$$q_{sb} \propto \begin{cases} u_*(\tau - \tau_{cr}) \propto u_*^3 & \text{at high transport rates} \\ u_*(\tau - \tau_{cr})^2 \propto u_*^5 & \text{at low transport rates} \end{cases}$$

and

$$q_{ss} \propto u_*^{n}(\tau - \tau_{cr}) \propto u_*^{n+2}$$

where $n = 1$ at least.

Further difficulties arise in computing bed load transport on rippled beds due to the uncertainty in partitioning the bed shear stress into that part which overcomes form drag and that part which is due solely to skin friction (see, eg Smith 1977; Smith and McLean, 1977).

Whereas it is possible to calculate bed load transport from a knowledge of the sediment and flow characteristics alone, calculation of suspended load transport also requires a knowledge of the concentration at a specified height above the sea bed. This information, which requires special measuring techniques, is frequently not available, and successful suspended load prediction, particularly on the continental shelf, is one of the major difficulties presently confronting sedimentologists, geologists and oceanographers.

3. DISTRIBUTION OF SEDIMENTS

The range and diversity of sediments in Swansea Bay is considerable: this in itself makes the prediction of sediment transport rates difficult. Figure 2 shows the range of sediment types observed on the E side of the Bay and illustrates a five fold variation in grain size from the fine silty material of about 50 μm grain size, in the area off Port Talbot, to the coarse 250 μm grain size material in the vicinity of Sker Point. This distribution reflects closely the variation in tidal current amplitude in the area and the residual water movements (see Heathershaw and Hammond, 1979).

Grain size analyses of sediment samples from the foreshore on the E side of the Bay (see Appendix A) indicate a median grain size (d_{50}) of about 173 μm . This material is similar in size to the sediments lying in the vicinity of the Kenfig Patches, Hugo Bank and Scarweather Sands. Here, box core and grab samples have indicated a median grain size of about 161 μm (see Figure 4 and Appendix A).

Further details of the geophysical interpretations and sediment characteristics of the area are given in Blackley (1978).

In the present study therefore, we have been concerned primarily with the movement of material having a median (d_{50}) grain size of about 170 μm . The manner in which this size of material moves through the population of grain sizes found in the area is by no means clear; in particular the way in which a non-cohesive sand size material moves across cohesive material of the type found off Port Talbot is not known and this is clearly one of the major difficulties in predicting the movement of coarse grained material.

4. BED LOAD TRANSPORT

4.1 Techniques

In order to predict sediment transport rates and directions, near bottom current measurements were made at a number of locations in Swansea Bay (see Figure 3). These observations were made using conventional recording current meter techniques and full details of this work are given in Heathershaw and Hammond (1979).

The bulk of these measurements were made at a height of 2 m above the seabed and thus estimates of the near bottom velocity field ($\overline{u}_{200}$) have been used, with an appropriate sediment transport formula, to predict sediment transport rates and directions over the area as a whole.

The choice of a suitable formula has been determined by comparing bed load transport estimates from two radioactive tracer experiments, at positions T1 and T2 in Figure 3, with predicted transport rates using current measurements from Stations A and C. Further details of the tracer experiment and comparisons of sediment transport formulae are given in Heathershaw and Carr (1977) and in Appendices B and C of this report.

Examples of tracer dispersion patterns are given in Figure 5, and it should be noted that these reflect strongly the phase of the tide following the release of the tracer (ie ebb at T1 and flood at T2) and cannot be used to infer directions of net sediment movement until the tracer has come into equilibrium with the sea bed. Heathershaw and Carr (1977) have found that this may take as long as 10 - 20 days.

The various sediment transport formulae examined here, utilise estimates of the friction velocity u_*, or the friction velocity and the depth mean flow $\hat{u}$. To obtain these estimates from our measurements of $\bar{u}_{200}$ it is necessary to assume some form for the vertical velocity distribution in the bottom boundary layer. It is usual to assume that this is logarithmic and of the form

$$\bar{u}(z) = \frac{u_*}{\kappa} \ln \frac{z}{z_0}, \qquad (1)$$

where $\bar{u}$ is the mean flow at a height z above the sea bed, z_0 is the roughness length and κ is von Karman's constant, usually taken as 0.4 for suspension-free flows. However, it should be noted that logarithmic velocity profiles may not be applicable at all times throughout the tidal cycle (eg Sternberg, 1968, 1972) and we will show later that the form of the profile may be influenced by vertical stratification effects of the type reported by Smith and McLean (1977) and Taylor and Dyer (1977).

The use of a logarithmic velocity distribution (equation 1) in predicting sediment transport rates on the continental shelf presents a major difficulty since in the majority of cases z_0 is not known. In this study we have found that reported z_0 values fall roughly into four categories according to the sediment types most frequently encountered on the continental shelf. These are summarised in Table 1 and it should be noted that these values are quite independent of any changes which may occur over the tidal cycle.

Various of the sediment transport formulae (eg Bagnold, 1963, Yalin,

1963) require specification of a critical or threshold velocity u_{cR}. In this study values of u_{cR} have been calculated using a logarithmic velocity profile (equation 1) and a critical friction velocity, u_{*cR}, obtained from Yalin's (1972) modified Shields' (1936) curve (see Appendix D for details).

Thus at each location where sediment transport predictions were made, values of z_o and u_{cR} were specified, the appropriate adjustments being made in the few cases where current measurements were not made at a height of 2m above the sea-bed. Full details of these calculations are also given in Appendix D.

Comparisons of measured and predicted bed load transport rates can only be made in terms of net or tidally averaged quantities since those are all that can be determined from the radioactive tracer experiments described in Appendix B.

4.2 Choice of sediment transport formula

Five sediment transport formulae (see Table 2) were chosen for evaluation in this study. Full details of the formulae and the comparisons between them are given in Appendix C.

These comparisons indicate a two order of magnitude variation in the predicted net bed load transports given by the five formulae. Figure 6 summarises the comparisons of predicted and observed net or tidally averaged transport rates at Stations A and C, using the 5 different formulae, and from the tracer experiments at T1 and T2.

Best estimates of the net bed load transport appear to be given by Bagnold's (1963) formula, in a modified form due to Gadd et al (1978), which gives estimates to within a factor of 0.5 - 2 of the measured rates (see Table 3 and Figure 6). Bagnold's original formula expressed the bed load transport rate q_{sb} in terms of the stream power ω and an efficiency factor K, that is

$$q_{sb} = \frac{\rho_s}{\rho_s - \rho} K \omega \qquad (2)$$

where ρ_s is the sediment density, ρ is the density of sea water and ω is the stream power given by the product of the bed stress τ and the friction velocity u_*. The application of this formula

requires specification of the efficiency factor K which has been shown (eg Sternberg, 1972) to be a function not only of grain size but also of bed form amplitude. This dependence has been removed by Gadd et al (1978), who, using the flume data of Guy et al (1966), have expressed (2) in terms of the current at 100cm above the sea bed, $\overline{u}_{100}$, and a threshold velocity u_{cr} . (Note that Bagnold's original formula - equation 2 - predicts sediment transport at all flow speeds). Thus

$$q_{sb} = \beta (\overline{u}_{100} - u_{cr})^3 , \qquad (3)$$

where β is a coefficient, having the dimensions of gm $cm^{-4}s^{-2}$, which was obtained from flume data. For this study equation (3) has been written in terms of the measured currents at a height of 200cm above the sea bed ($\overline{u}_{200}$) by assuming a logarithmic velocity profile and by taking an appropriate roughness length z_0 (see Table 1). The value of the coefficient β varies according to grain size and Gadd et al (1978) give values of β for d_{50} grain sizes of 180μm and 450μm . In this investigation we have been particularly concerned with the prediction of sediment transport rates and directions for the size of material found on the foreshore and sand banks of the E side of the Bay. This material (see Tables A.1 and A.2) has a median grain size (d_{50}) of about 170μm which corresponds fairly closely to the mean tracer particle sizes which were of the order 160 - 170μm $\pm$ 20μm . We have thus taken a value of β of 7.55×10^{-5} gm cm^4s^{-2}, which correponds in Gadd et al's calibration of equation (3) to a grain size of 180μm , and is therefore considered a reasonable value.

Bagnold's formula is one of the simplest expressions currently in use by oceanographers and engineers and is based on the physics of the stream power concept. Indeed, its success in this particular application may owe much to this simplicity.

To obtain net transport rates from the predictions based upon current meter records, successive 10 minute samples of current speed and direction were converted to sediment transport rates and directions and then vector averaged over a large number of tidal cycles, the exact number being determined by the length of the current meter record. Smoothed progressive vector diagrams of sediment transport rates and directions are shown in Appendix E, Figures E1.1 to E11.1. The net transport rates used in the

comparisons of sediment transport formulae and in the eventual prediction of sediment transport paths, as described in this report, are thus the resultants of the appropriate progressive vector diagrams, examples of which are shown in Appendix E. The sediment transport progressive vector diagrams may be compared with those for the water movements given by Heathershaw and Hammond (1979). It is clear from these comparisons that residual sediment and water movements can be in significantly different directions.

The more sophisticated techniques, eg Ackers and White's (1973) formula (see Appendix C), tend to yield lower estimates (see Figure 6). However, it is worth noting that in the absence of a tracer estimate and in terms of their median performance we might equally well have chosen Engelund and Hansen's (1967) or Einstein's (1950) formulae.

5. SUSPENDED LOAD TRANSPORT

5.1 Suspended sediment transport formulae

It is not possible to predict directly, suspended sediment transport rates from a knowledge of the near bottom velocity field and the sediment characteristics alone. The solution of the steady state diffusion equations (see Yalin, 1972) gives the mass concentration at a height z above the sea bed, $C(z)$, in terms of a reference concentration $C(a)$ measured at a height a. The resultant profile, known as the Rouse concentration profile, is

$$\frac{C(z)}{C(a)} = \left(\frac{h - z}{h - a} \cdot \frac{a}{z} \right)^{\frac{w_s}{\kappa u_*}} \qquad (4)$$

where h is the total flow depth and w_s the settling velocity. However, various attempts have been made to relate $C(a)$ to a near bed concentration which might in turn be related to the bed load. In particular Smith (1977) and Smith and McLean (1977) have suggested that the reference concentration $C(a)$ may be expressed in terms of the bed load concentration at a height equal to the roughness length. Thus $C(a)$ may be written as

$$C(a) = C(0) \gamma_0 s / (1 + \gamma_0 s) \qquad (5)$$

where s is the normalised excess shear stress given by

$$s = (\tau - \tau_{cr}) / \tau_{cr}$$

and γ_0 is an empirically determined constant of order 10^{-3}, provided a is taken as approximately equal to z_0. $C(0)$, notionally, at least, is the maximum permissible concentration at the bed and for $s \rightarrow \infty$ ie, large excess shear stresses, $C(a) \rightarrow C(0)$. For low excess shear stresses Smith (1977) has shown that

$$C(a) = \gamma_1 e_s s \qquad (6)$$

for $a \simeq z_0$. For material having a mean grain size of approximately 180μm. Smith and McLean (1977) have found $\gamma_0 = 2.4 \times 10^{-3}$ and $\gamma_1 = 1.24 \times 10^{-3}$. However, Dyer (1980), measuring on a rippled sand bed having a mean grain size of 250μm, has found a value of γ_1 significantly different from that reported by Smith and McLean (1977) and about an order of magnitude lower.

The methods outlined above may provide a means of predicting suspended sediment transport rates from a knowledge of the velocity field and sediment characteristics alone. However, as we have seen considerable uncertainty still surrounds the values of the empirical coefficients γ_0 and γ_1.

5.2 Near-bottom suspended sediment and velocity profile measurements

Full details of the suspended sediment and velocity profile measurements are given in Appendix F of this report.

Suspended sediment measurements in Swansea Bay at locations PS2, PS4 and PS5 (see Figure 3) using the pumped sampling equipment shown in Figure 7 and described in detail in Appendix F, have revealed a complex pattern of behaviour.

Grain size analyses show that at PS2 (see Figure 8) the median grain sizes of the material in suspension and on the sea bed are broadly similar ($d_{50} \simeq 70\mu m$). However, at PS5 (see Figure 9) while the material in suspension is similar in size to that at PS2 there is considerably more variation in the sea-bed samples which are up to a factor of 2 times coarser. It is also interesting to note that at both sites there is little systematic variation of mean grain size with height.

Concentration measurements were made at heights of 10, 15, 25, 40, 80 and 180cm above the seabed to give one profile approximately every half hour throughout the tidal cycle. Concentration profile measurements were considered

important at this stage to determine the validity of equation (4).

Near-bottom velocity profile measurements were also made at locations PS2, PS4 and PS5 (see Figure 3) with the equipment described in Appendix F. Logarithmic velocity profiles (equation 1) were fitted to velocity measurements in the bottom boundary layer, averaged over a period of 10 minutes, using a least squares regression technique to give the friction velocity u_* and roughness length z_0 . The velocity measurements were made at heights of 15, 40, 100 and 180cm above the seabed. Only 45% of the velocity profiles could be fitted at the 95% confidence level and nearly all profiles showed a tendency to be concave downwards, even at the 99% confidence level, indicating possible stratification effects (see later discussion).

Examples of concentration and velocity profiles are shown in Figures 10, 11 and 12, while Figures 13 and 14 show the variation of u_* , $\bar{u}_{100}$ and the concentrations at different heights above the sea bed, through the tidal cycle at PS2 and PS4. The variations of z_0 with u_* at PS2 and PS4 are shown in Figures 15 and 16 and indicate an order of magnitude variation in z_0 over the tidal cycle with, on Springs, flood values being higher than ebb values. At PS2, on Springs, the situation appears to be similar. However, with the exception of the ebb values which lie in the range .1 to .5cm the observed roughness lengths are in general higher than would be expected given the flow conditions and sediment characteristics for the area. This behaviour may be due in part to the presence of ripples on the sea bed and the way in which their amplitudes vary over the tidal cycle. Alternatively it may be due to high suspended sediment concentrations, particularly near the bed, where the presence of a moving layer of grains may modify the velocity profile and provide an effective bed roughness which is related to the thickness of a moving, or saltating layer, and which in turn is related to the excess shear stress. Under these circumstances z_0 is given (see Smith, 1977) by

$$z_0 = \frac{\delta(\tau - \tau_{cr})}{(\rho_s - \rho) g} + z_N \,, \qquad (7)$$

where z_N is the flat bed roughness related to the grain size d , by $z_N \simeq d/30$ (Yalin, 1972). However, analysis of our data does not reveal any obvious correlations of the form shown in equation (7), although Figures 15 and 16 do suggest that z_0 may be proportional to u_*^4 , which is a similar result to that of Dyer (1980). It seems more likely that the

complex pattern of behaviour observed in the measured z_0 values is a consequence of the stabilising effect of suspensions in the boundary layer. This will lead to modified forms of the equilibrium velocity and concentration profiles in a constant stress layer. The effect of a density gradient may be expressed in terms of the Monin-Obukhov length L (see Taylor and Dyer, 1977, for discussion) defined by

$$L = \frac{-\bar{\rho} u_*^3}{\kappa g \overline{\rho' w'}} , \tag{8}$$

where ρ' and w' are the fluctuating parts of the density and vertical velocity fields, $\bar{\rho}$ is the mean density and $\overline{\rho' w'}$ represents a density or buoyancy flux.

The velocity profile (1) may now be written as

$$\bar{u} = \frac{u_*}{\kappa}\left(\ln \frac{z+z_0}{z_0} + \frac{\Lambda z}{L}\right) \tag{9}$$

(the $\ln \frac{z+z_0}{z_0}$ form is used for computational ease at this stage) where Λ is an empirically determined constant which from atmospheric boundary layer experiments (Businger et al, 1971) has been found to be $4.7 \pm .5$.

Taylor and Dyer (1977), using the results of Barenblatt (1953, 1955) have shown that (9) may be expressed in terms of the suspended sediment concentrations and settling velocity as

$$\bar{u} = \frac{u_*}{\kappa}\left[\zeta + \frac{1}{B}\ln\left\{1 + \frac{AB}{(1-B)}\left(e^{(1-B)\zeta} - 1\right)\right\}\right], \tag{10}$$

where

$$\zeta = \ln\left[(z+z_0)/z_0\right] . \tag{11}$$

A and B are given by

$$A = \frac{\Lambda w_s \kappa g \gamma C_0 z_0}{u_*^3} \quad \text{and} \quad B = \frac{w_s}{\kappa u_*} , \tag{12}$$

where, C_0 is now the 'surface concentration' of sediment, which is analogous in some respects to $C(0)$ in equation (5), and γ is now given by $\gamma = (\rho_s - \rho)/\rho$ where ρ_s is the sediment particle density. The concentration profile corresponding to (10) is of the form

$$\ln \frac{C(z)}{C_0} = -BS - \ln\left[1 + \frac{AB}{(1-B)} \cdot \left(e^{(1-B)S} - 1\right)\right]. \qquad (13)$$

Figures 17 and 18 show velocity and concentration profiles of the form predicted by equations (10) and (13) where values of A and B have been calculated using the observed total concentration of suspended sediment ($\alpha > 0$) at z = 10cm.

As a result of fitting logarithmic velocity profiles of the form $\bar{u} = \frac{u_*}{\kappa} \ln \frac{z}{z_0}$ to a velocity distribution of the type given in equation (10) the roughness length (z_0) and friction velocity (u_*) will be systematically overestimated. This is clear from Figure 17 where in order to fit equation (10) to the data it has been necessary to take a z_0 value of .5cm and a friction velocity estimate, u_* , of 2.5cm s^{-1} which may be compared with the measured values of z_0 = 1.07cm and u_* = 3.42 cm s^{-1}. A z_0 value of .5cm would still be considered high for the area (see Table 1). However the theory does serve to illustrate that even quite moderate concentrations, of the order of 200mg l^{-1} at z = 10cm) may modify the turbulent and mean flow characteristics of the bottom boundary layer leading to the concave downwards form of the measured velocity profiles shown in Figures 11, 12 and 17, and lead to overestimates of friction velocity and roughness length z_0 .

Figure 18 shows measured and predicted concentrations of the form given in equations (4) and (13). Here the agreement between the measured values and those predicted by Monin-Obukhov theory is not so good except perhaps nearer the bed where there is some evidence to suggest the measured values may follow equation (13). Since we have attempted to fit equation (10) to the measured velocity profile, the concentration profile given by equation (13) will not necessarily pass through the measured concentration values.

Despite the fact that velocity and concentration profiles may not be of the usual form, suspended sediment transport rates have been calculated by numerically integrating the product of equations (1) and (4) over the entire flow depth, that is

$$q_{ss} = \int_{z_0}^{\lambda} C(z) \frac{u_*}{\kappa} \ln \frac{z}{z_0} \, dz \, , \qquad (14)$$

where z_o is the measured roughness length and h the total flow depth. In equation (4) the settling velocity w_s has been taken as .32cm s^{-1} corresponding to a mean particle size for the suspension, which shows no systematic variation with height, of about 70μm (see Figures 8 and 9). κ has been taken as .4 and u_* calculated from the measured velocity profiles. The depth increment dz was taken as .1cm and Table 3 shows suspended sediment transport rates, for $d > 0$, obtained from Rouse profiles (equation 4) fitted by a least squares regression to the measurements at PS2, PS4 and PS5 at the 95% confidence level. It is important to note, however, that only 42% of concentration profiles could be fitted at the 95% level (this may be compared with 45% for the velocity profiles).

The bulk of the suspended sediment data indicate that the ratio of material coarser than 40μm is about 1/50 of the total concentration of all sizes. Thus, the transport rates for coarse material, shown in Table 4 have been derived using this ratio. Also shown are bed load transport rates, calculated using Bagnold's formula (equation 3). Table 4 shows that while total suspended load transport rates are on average a factor of 10 times larger than the bed load transport, suspended load transport of material coarser than 40μm is a factor of 6 times lower than the bed load transport.

A conspicuous feature of the concentration profiles shown in Figure 10 is the almost uniform concentration with depth in the lower 2m of the flow. Furthermore, Figures 13 and 14 show little systematic variation in concentration over the tidal cycle and suggest that in general the suspension behaves as 'washload'. This situation occurs when the settling velocity (w_s) is small compared with the friction velocity u_*. Fitting profiles of the form given in equation (4) to the measured concentrations and integrating over the entire flow depth, yields depth mean concentrations for the area of about 90mg l^{-1}. This figure is lower than the surface and and near-bed concentrations reported by Davies (1974), which were of the order of 100 and 400mg l^{-1} respectively, but higher than the values given by Ferentinos and Collins (1978) which lie typically in the range 6 - 60mg l^{-1} near the bed. However, it is interesting to note that our figures for concentrations of material coarser than 40μm ($d > 40\mu m$) are similar to those given by Ferentinos and Collins.

Taking the area of Swansea Bay bounded by a line of longitude $3^{\circ}58.6'W$ running S through Mumbles Head, a line of latitude $57^{\circ}30'N$ and the coast, (see Figure 3) gives an area of approximately $1.77 \times 10^{8} m^{2}$. This also corresponds to the area bounded by the topographically high features in the area, namely the White Oyster Ledge in the W (not shown), Kenfig Patches and Scarweather Sands in the S. Taking the mean depth over the area as 15m gives a mean tidal volume of $2.66 \times 10^{9} m^{3}$. Thus, a depth mean concentration of the order of $90mg\ l^{-1}$ yields a total of about 2.4×10^{5} tonnes of sand and silt in suspension. This figure may be compared with the natural and artificial inputs of suspended sediment to the area given by Collins et al (1979); suspended sediment from rivers contributes about 200 tonnes day^{-1} and maintenance dredging of Port Talbot and Swansea harbours contributes about 1.2×10^{6} tonnes of sand and silt annually. Approximately 9×10^{6} tonnes of fine sand, silt and gravel were deposited on spoil grounds, within the area being considered, from capital dredging at Port Talbot (Davies, 1975).

6. SEDIMENT TRANSPORT PATHS

The principal objectives of this study (see Carr, 1975; Carr et al, 1976, 1977; Heathershaw et al, 1978) have been to examine the supply of sand to Swansea Bay, particularly the foreshore on the E side of the Bay, S of Port Talbot.

Comparisons of suspended and bed load transport rates have established that for material coarser than 40 μm the principal mode of transport is likely to be bed load. Table 4 shows that bed load transport of this size of material is on average about 6 times larger than the corresponding suspended load transport rate. Thus we are only concerned here with bed load transport paths and using Bagnold's modified formula (equation 3) and near bottom current measurements we have predicted sediment transport rates and directions for the area as shown in Figure 19. The directions give some agreement with previously published transport paths for the area (Ferentinos and Collins, 1978; Collins et al, 1979) and with geophysical evidence (eg sand wave alignment and asymmetry, sand ribbon orientation) presented by Collins et al (1979). Figure 19, which may be compared with the residual water circulation pattern shown in Figure 19a after Heathershaw and Hammond, 1979, suggests that in terms of the transport rates, the sediment circulation system consists of a strong westward flowing stream

of sand by-passing the Bay, with transport rates in the Bay being nearly two orders of magnitude lower than those in the offshore area. Furthermore, Figure 19 indicates that in general there are no major sediment transport paths into the area and that such transport as occurs from the westward flowing stream is likely to be due to second order effects, eg wave induced transport during storms. In particular we note that there is unlikely to be a transport of material into the area from the E in the vicinity of Sker Point, where transport is to the S, and that the only inputs of material into the Bay from the W appear to be a weak and variable transport near Mumbles Head and a strong eastward movement of material at the E end of the Scarweather Sands, which is almost certainly associated with those processes maintaining the sand banks in the area in equilibrium.

The calculated directions of sediment movement do in fact indicate three major features of sedimentological significance. These are:

(a) An area of divergence in net sediment transport in the area to the S of Port Talbot characterised by low transport rates of the order of .02 tonnes $m^{-1}day^{-1}$, but which increase in a southerly direction along the coast.
(b) an area of convergence in net sediment transport in the vicinity of the Scarweather Sands;
(c) the presence of a strong westward transport of sediment outside the Bay of the order of 2 tonnes $m^{-1}day^{-1}$.

The observed water and sediment circulations in the vicinity of the Scarweather Sands are consistent with the mechanisms of sand bank formation proposed by Pingree (1978) and Pingree and Maddock (1979). The results of these observations are described elsewhere (Heathershaw and Hammond, 1980) and show that vorticity generated by tidal streaming at a point of abrupt change in the coastal geometry (this occurs in the Porthcawl area) leads to secondary circulation effects giving rise to a near-bottom convergence and mid-depth divergence in the mean circulation on the flanks of the sand bank.

7. THE EFFECTS OF WAVES

7.1. Bijker's formula

The theory of wave tidal current interaction is still poorly understood although recent theoretical developments (eg Grant and Madsen, 1979) go some way towards improving our understanding of the physical processes involved. The effect of this interaction on sediment transport is still more tenuous since sediment transport theories, as we have seen, can in themselves give widely differing estimates. Present approaches are largely empirical (eg Owen and Thorn, 1979) and it is likely to be some time before theories are available which are capable of dealing with the wide range of conditions encountered on the continental shelf.

One approach which has been used is that developed by Bijker (1967) which, although semi-empirical, does attempt to deal with the physical interaction of the waves and the currents. The theory consists of making a vector addition of the orbital velocity (u_0) of the wave and the velocity due to the tidal current alone, at a height above the sea bed equivalent to the thickness of the viscous sublayer. The resultant velocity is converted to a bed shear stress using Prandtl mixing length theory in which the bed shear stress is given by

$$\tau = \rho l^2 \left[\frac{\partial u(z)}{\partial z} \right]^2_{z \to 0} , \qquad (15)$$

where $u(z)$ is the combined velocity at a height z above the bed, ρ is the density, τ is the bed shear stress and l is the mixing length given by $l = \kappa z$ for small values of z . Thus, according to Bijker's theory, the maximum enhancement of the bed shear stress is given by,

$$\psi = \frac{\tau_{wc}}{\tau_c} = 1 + \frac{1}{2} \left(\xi \frac{u_0}{\bar{u}} \right)^2 \qquad (16)$$

where τ_{wc} is now the resultant bed shear stress due to waves and currents, τ_c is the bed shear stress due to currents alone, ξ is given by $\xi = \rho g [(\lambda/z_0) - 1]$, λ is the mean depth, ρ is an empirically determined constant, which Bijker (1967) found equal to 0.45, and $\bar{u}$ is the steady depth mean current. In this report ψ is referred to as the Bijker magnification factor.

To obtain an upper limit to the enhancement of the bed sheer stress due to wave activity, equation (16) has been evaluated for typical and extreme wave conditions. ξ has been calculated with a roughness

length z_0 of .05cm and the depth mean current in (16) has been calculated in terms of the current at a height of 1m above the sea bed by integrating the logarithmic velocity profile (1) over the entire flow depth. The variation of ψ with wave height H, for a wave period of 8s (typical for the area, see Fortnum and Hardcastle, 1979) and water depth of 20m, is plotted in Figure 20. This shows for example that even moderate wave conditions (H = 1m) increase sediment transport rates (calculated using Bagnold's formula) by a factor of about 5 at peak tidal flows (ie = 50cm s^{-1}) with the effect becoming more pronounced as the steady current ($\bar{u}_{100}$) decreases in strength.

7.2. Thresholds of movement under waves and currents

In considering the effects of waves, it should be borne in mind that sediment particles which are suspended by enhanced bed shear stresses, are likely to move in a direction which is governed principally by the tidal currents. Furthermore, the waves are not a persistent feature of the near-bed water movements. This is illustrated in Figure 21 which shows exceedance curves for wave induced and tidal currents. Typical current threshold values are also indicated, that for the waves having been calculated using Komar and Miller's (1974) threshold criterion,

$$\frac{\rho}{\rho_s - \rho} \cdot \frac{u_{0cr}^2}{g d} = .21 \left(\frac{u_{0cr} T}{\pi d} \right)^{1/2}, \qquad (17)$$

where u_{0cr} is the critical near bed orbital velocity and T the wave period. For these calculations T has been taken as 8s. The grain size d has been taken as the median grain size of 170 μm and the steady current threshold, u_{cr} , calculated from Shields' curve. A roughness length of z_0 = .05cm has been assumed in calculating the corresponding current at 2m above the sea bed from the logarithmic velocity profile (1). A roughness length of z_0 = .05cm corresponds to the value which was prescribed for sediment transport calculations at Station A. This figure gives a threshold velocity (u_{cr}) at 200cm above the bed of about 27cm s^{-1}. At Station C, for the purposes of calculating sediment transport rates, z_0 was taken as .1cm (see Table 1 and Appendix D for details of roughness lengths and threshold velocities); this would give a threshold velocity at 200cm above the bed of about 25cm s^{-1}. In Figure 21, for simplicity, the lower threshold only is shown.

These results suggest that in the offshore areas ($\lambda \simeq 20m$) the threshold due to waves is on average exceeded for only 25% of the time and that if waves were capable of directly influencing sediment movement then the effect would be minimal. This observation is corroborated to some extent by the apparent lack of movement of tracer towards the coast from site T2 in Figure 3. However, transport may occur in shallower water and as reported by Heathershaw and Carr (1977), some movement of tracer towards the coast at T1 may have occurred due to a wave induced mass transport effect (see later discussion). The figure of 25% exceedance for the threshold of movement under waves may be compared with exceedance levels of 65 -85% for the threshold of sediment transport in a unidirectional flow at Stations A and C (see Figure 21).

7.3. Mass transport effects due to waves

From observation and theory it appears that on average the direction of sediment movement is controlled by the tidal currents with perhaps some intensification of transport by wave activity. It is interesting to note that in Figure 5 the observed transport rates are consistently higher than those predicted by most of the theories examined. This may be due to an enhanced transport in the tidal current direction by waves.

The mass transport effect arises from the fact that the wave particle orbits are not closed, giving rise to a steady movement of the water particle at the surface and near the bed in the direction of wave propagation. Heathershaw and Hammond (1979) have examined the Stokes drift u_s at different depths using Longuet-Higgins' (1953) solution for flow in the interior of the fluid. At the bed this gives the well known expression

$$u_s = \frac{5}{4} \cdot \frac{a^2 \sigma k}{\sinh^2 kh} , \qquad (18)$$

where a is the wave amplitude, σ its angular frequency, k its wave number equal to $2\pi/\lambda$, where λ is the wavelength, and h the total depth. Equation (18), which strictly speaking is only valid for laminar flow, but which Longuet-Higgins (1957), in an appendix to the paper by Russell and Osorio (1957), has shown may also apply to turbulent flow, predicts a steady forward mass transport at the sea-bed.

We must conclude therefore that during periods of prevailing SW wave activity there is likely to be a steady shoreward drift at the bed and for

wave height of 2 m, wave period of 8 s and water depth of 20 m, equation (18) predicts that this will be of the order of 2cm s^{-1}.

8. SUMMARY AND CONCLUSIONS

Observed and predicted transport rates have indicated that for sand size material (d_{50} =170μm) bed load is likely to be the dominant mode of transport in the area. However it is necessary to look at this process against a background of high concentrations of fine particle matter ($d<40\mu m$). Although the mean particle size of the suspension is about 70μm with a settling velocity of .32cm s^{-1}, the finer particulate matter will have considerably lower settling velocities and we would thus anticipate little variation in the concentrations over the tidal cycle (see Figures 11 and 12). In fact a depth mean concentration of the order of 90 mg l^{-1} would appear to be present for most of the time as 'washload'. However, this work has shown that these concentrations are sufficiently high to modify the turbulent structure of the bottom boundary layer by inducing density gradients near the sea bed leading to equilibrium velocity profiles (Figure 17) of the form predicted by Monin-Obukhov similarity arguments (eg see Taylor and Dyer, 1977). These profiles may lead to overestimates of the roughness length z_0 and friction velocity u_* derived from fitted logarithmic velocity profiles of the form given in equation (1).

The variations of z_0 with u_* as shown in Figures 15 and 16 may also suggest a more complex pattern of behaviour in which z_0 varies with both the thickness of the bed load layer and changes in amplitude of bed forms on the sea bed (see Dyer, 1979).

Suspended sediment measurements have not indicated any systematic variation of depth mean concentration in moving from the weaker nearshore tidal flows to the higher energy environment further offshore. The observed depth mean concentrations are in general higher than those reported by Ferentinos and Collins, 1978, and for the area on the E side of the Bay we have found these to be, on average, of the order 90mg l^{-1}. However, at peak tidal flow rates, near-bed concentrations of 200-500mg l^{-1} have been observed (see Figures 10, 13 and 14) at Stations PS2, PS4 and PS5.

Bed load transport rates have been predicted using a modified form (Equation (3)) of Bagnold's (1963) formula. Comparisons with radioactive tracer estimates have shown that this formula gives the best predictions (within a factor of 0.5 - 2) of the observed transport rates. Although the

net transport rates predicted by the various formulae may vary by as much as 2 orders of magnitude, they all predict similar directions of sediment movement.

The observed sediment distribution, transport rates and circulation pattern reflect strongly the tidal dynamics of the area (see Heathershaw and Hammond, 1979). The area immediately offshore of Port Talbot is an area of low tidal energy and therefore likely to be an area of net deposition for fine sediments. The areas further offshore and alongshore towards the S exhibit stronger tidal currents and therefore increasing sediment mobility. These differences are illustrated in Figure 22 which shows measured tidal current exceedance curves at current meter stations situated on lines running offshore and alongshore from Port Talbot. These indicate quite clearly that while the threshold velocity, u_{cr} , for sand size material is exceeded for about 20% of the time at Station B, it is exceeded for about 70% of the time at Station E and 85% of the time at Station C.

Predicted bed load transport paths for the area are presented schematically in Figure 23. These give general agreement with geophysical evidence and indicate a westward movement of sediment close to the coast S of Porthcawl, and across the southern extremity of the Bay through the sand bank system comprising the Scarweather Sands and possibly Nash Bank, towards the Gower coast and westward through the Helwick Bank. The rate of movement of material in this area is estimated to be of the order of 2.10^{-1} gm cm^{-1} s^{-1}, that is about 2 tonnes $m^{-1} day^{-1}$. Moving inshore there is a general decrease in transport, reflecting the diminishing tidal energy (see Heathershaw and Hammond, 1979), until in the vicinity of Port Talbot and the River Neath transport rates two orders of magnitude lower and equal to about .02 tonnes m^{-1} day^{-1} are observed.

These differences suggest that the Bay is effectively by-passed by the offshore westward movement of sediment. In fact the only predicted movements of sand size material into the Bay from the W occur in the vicinity of Mumbles Head and at the western extremity of the Scarweather Sands, the latter probably being associated with bank forming processes. The observed transport pattern suggests that if movement of material into the Bay does occur it can only occur by a transfer of material from the W flowing stream in the area between Mumbles Head and the S extremity of the White Oyster

Ledge. We should note here that radioactive tracer experiments carried out in this area, and referred to by Collins et al (1979), have indicated an easterly movement of material into the Bay. However, in one case tracer having a mean size of 15 μm was used and would thus have simulated suspended load transport, and in the other case, although a coarser material was used (mean size of 140 μm), the tracer was released at the surface on a flooding tide and the observed dispersion patterns are likely to be biased in an easterly direction. The interpretation presented in Figure 22 is in general agreement with the conjectural sediment circulation patterns given by Ferentinos and Collins (1978) and Collins et al, (1979), except that transport into the Bay by tidal currents seems improbable. It is possible that a wave-induced transport, particularly during periods of strong SW winds, is the most likely mechanism although we have no direct evidence of its occurrence. However, against this hypothesis must be balanced the finding that wave induced mass transport effects in the area are small and of the order 2cm s^{-1} at the bed and that tracer studies do not indicate any appreciable shoreward movement of material (see Figure 5) even over long periods of time when appreciable wave activity is known to have occurred. Furthermore, despite the presence of the W flowing sand stream close to the Gower coast, we should not discount the possibility, as suggested by Collins et al, 1979, of an easterly littoral transport from close inshore, probably induced by wave activity.

9. ACKNOWLEDGEMENTS

We would like to acknowledge the support and co-operation of our colleagues at the Institute of Oceanographic Sciences, Taunton. This work was supported financially by the Department of the Environment.

REFERENCES

ABRAMOWITZ, A and I A STEGUN (1965). Handbook of Mathematical Functions, Dover Publications Inc., New York, pp 1046.

ACKERS, P (1972). Sediment Transport in Channels: An alternative approach. Hydraulics Research Station Report No INT 102, pp 31

ACKERS, P and W R WHITE (1973). Sediment Transport: New approach and analysis Proc ASCE, J Hyd Div HY 11, 2041-2060

BAGNOLD, R A (1963). Mechanics of marine sedimentation in Hill, M N (ed), The Sea Interscience Publications, Vol 3, 507-582.

BARENBLATT, G F (1953). On the motion of suspended particles in a turbulent stream. Prikl Matem Mekh, 17, 261-274 (English translation)

BARENBLATT, G F (1955). Concerning the motion of suspended particles in turbulent flow occupying a half-space, or flat open channel of finite depth. Prikl Matem Mekh, 19, 61-68 (English translation)

BIJKER, E W (1967). Some considerations about scales for coastal models with moveable beds. Delft Hydraulics Laboratory Report No 50, pp 142.

BLACKLEY, M W L, (1978). Swansea Bay (Sker) Project Topic Report: 3. Geophysical Interpretation and Sediment Characteristics of the offshore and foreshore areas, Institute of Oceanographic Sciences Report No 60/78, pp 42.

BOWDEN, K F (1955). Physical Oceanography of the Irish Sea. Fishery Invest London, Series 2, 18, pp 67.

BUSINGER, J A, J C WYNGAARD, I IZUMI and E F BRADLEY (1971). Flux-profile relationships in the Atmospheric surface layer. Journal Atmospheric Sciences, 281, 181-189.

CARR A P, (1975) Swansea Bay (Sker) Project. Progress Report for the period to March 1975 and subsequent developments, Institute of Oceanographic Sciences Report No 27/75, pp

CARR, A P, A D HEATHERSHAW and M W L BLACKLEY (1976). Swansea Bay (Sker) Project. Progress Report for the period August 1975 to July 1976, Institute of Oceanographic Sciences Report No 26/76, pp 28.

CARR, A P, A D HEATHERSHAW and M W L BLACKLEY (1977). Swansea Bay (Sker) Project Progress Report for the period August 1976 to July 1977, Institute of Oceanographic Sceicnes Report No 48/77, pp 63.

COLLINS, M B, G FERENTINOS and F T BANNER (1979). The Hydrodynamics and Sedimentology of a High (Tidal and Wave) Energy Embayment. (Swansea Bay, Northern Bristol Channel). Estuarine and Coastal Marine Science, 8, 49-74.

COURTOIS, G and G SAUZAY, (1966). Les methodes de bilan des taux de comptage de traceurs radioactifs appliquees a la mesure des debits massiques de charriage. La Houille Blanche, 3, 279-284

COURTOIS, G and A MONACO, (1969). Radioactive methods for the quantitative determination of coastal drift rate. Marine Geology, 7, 183-206.

CRICKMORE, M J and R F AKED, (1975). Pump samplers for measuring sand transport in tidal waters. IERE Conference Proceedings on Instrumentation in Oceanography, No 32, 311-326.

DAVIES, C M (1974). Variability of suspended sediment in rotary currents, Swansea Bay (Bristol Channel), Great Britain. Marine Geology, 16, M31-M38.

DAVIES, C M (1975). Paths of suspended sediment transport in Swansea Bay. Proceedings Challenger Society, 4, 259-260.

DYER, K R (1980). Velocity profiles over a rippled bed and the threshold of movement of sand. Estuarine Coastal Marine Science (in press).

EINSTEIN, H A (1950). The bed load function for sediment transportation in open channel flows. Soil Conservation Service US Department of Agriculture Technical Bulletin No 1026, pp 78.

ENGELUND, F and E HANSEN (1967). A monograph on sediment transport in alluvial streams. Teknisk Vorlag, Copenhagen, pp 62.

FERENTINOS, G and M B COLLINS (1978). Sediment transport through the area to the south of Eastern Gower, as related to the sediment budget of Swansea Bay. University College of Swansea, Final Report to Institute of Oceanographic Sciences, Taunton, pp 120.

FLEMMING, C A and J N HUNT (1976). A mathematical sediment transport model for unidirectional flow. Proceedings Institution of Civil Engineers, 61, 297-310.

FORTNUM, B C H and HARDCASTLE P J (1979). Waves recorded at Scarweather Bank in the Bristol Channel. Institute of Oceanographic Sciences Report No 79, pp 7.

GADD, P E, J W LAVELLE and D J P SWIFT (1978). Estimates of sand transport on the New York Shelf using near-bottom current meter observations. Journal Sed.Pet. 48, 239-252.

GUY, H P, D B SIMONS and E V RICHARDSON (1966). Summary of alluvial channel data from flume experiments 1955-1961. US Geol Surv Prof Paper, 4621, pp 96.

GRAF, W M (1971). Hydraulics of sediment transport. McGraw Hill Inc pp 513.

GRANT, W D and O S MADSEN (1979). Combined Wave and Current Interaction with a Rough Bottom. Journal Geophysical Research, 84, No C4, 1797-1808.

HEATHERSHAW, A D and A P CARR, (1977). Measurements of sediment transport rates using radioactive tracers. ASCE Proceedings Coastal Sediments '77, Charleston South Carolina, USA, pp 20

HEATHERSHAW A D, A P CARR, M W L BLACKLEY and F D C HAMMOND, (1978). Swansea Bay (Sker) Project. Progress Report for the period August 1977 to July 1978. Institute of Oceanographic Sciences Report No 74/78, pp 47.

HEATHERSHAW A D and F D C HAMMOND (1979). Swansea Bay: Tidal currents: observed and residual circulations and their response to meteorological conditions. Institute of Oceanographic Sciences Report (in preparation).

HEATHERSHAW A D and F D C HAMMOND (1980). Secondary circulation and Sand Banks (in preparation).

KACHEL N V and R W STERNBERG (1971). Transport of bedload on ripples during an ebb current. Marine Geology, 10, 229-244.

KOMAR P D and M C MILLER (1974). Sediment threshold under oscillatory waves. Proceedings 14th Coastal Engineering Conference, Copenhagen, 756-775.

LONGUET-HIGGINS, K S (1953). Mass Transport in Water Waves. Philosophical Transactions of the Royal Society of London, Series A, 245, 535-581.

LONGUET-HIGGINS M S (1957). The mechanics of the boundary-layer near the bottom in a progressive water wave. Appendix to Russell and Osorio (1957).

OWEN M W and M F C THORN (1979). Effect of Waves on Sand Transport by Currents. Proceedings 16th Conference on Coastal Engineering, Hamburg (in press).

PINGREE, R D (1978). The formation of the Shambles and other Banks by tidal stirring of the Seas. Journal Marine Biological Association of the United Kingdom, 58, 211-226.

PINGREE R D and L MADDOCK (1979). The tidal physics of Headland flows and offshore Tidal Bank formation. Marine Geology, 32, 269-289.

RUSSELL R C H and J D C OSORIO (1957). An experimental investigation of drift profiles in a closed channel. Proceedings 6th Conference on Coastal Engineering, Miami, 171-193.

SHIELDS A (1936). Anwendung der Ahnlichkeitsmechanik und Turbulenzforschung aug die Geschiebebewegung, Mitteil, PVWES, Berlin, No 26.

SMITH J D (1977). Modelling of sediment transport on continental shelves. In E D Goldberg, I N McCave, J J O'Brien, and J H Steele (Eds). The Sea, 6, Wiley Interscience, New York. pp 539-577.

SMITH J D and S R McLEAN (1977). Spatially Averaged Flow over a Wavy Surface. Journal Geophysical Research, 82, 1735-1746

STERNBERG, R W (1968). Friction factors in tidal channels with differing bed roughness. Marine Geology, 6, 243–260.

STERNBERG, R W (1972). Predicting initial motion and bedload transport of sediment particles in the shallow marine environment. In D J P Swift, D B Duane and O H Pilkey (Eds), Shelf sediment transport: Process and pattern. Dowden, Hutchinson and Ross, Stroudsberg. pp 61–81.

SWART, D H (1976). Coastal sediment transport. Delft Hydraulics Laboratory Report No R968, pp 61.

TAYLOR P A, and K R DYER (1977). Theoretical models of flow near the bed and their implications for sediment transport. In E D Goldberg, I N McCave, J J O'Brien and J H Steele (Eds). The Sea, 6, Wiley Interscience, New York, pp 579–601.

VANONI V A (1975). Sedimentation Engineering, American Society of Civil Engineers, pp 745.

WHITE W R (1972). Sediment Transport in Channels: A general function. Hydraulics Research Station Report No INT 104, pp 25.

WHITE W R, H MILLI and A O CRABBE (1975). Sediment transport theories: a review. Proceedings Institution of Civil Engineers, Part 2, 59, 265–292.

WHITE W R, H MILLI and A D CRABBE (1978). Sediment transport: An appraisal of available methods, (2 volumes). Hydraulics Research Station Report No IT 119, pp 101.

YALIN M W (1963). An expression for bed load transportation. Proceedings ASCE, J Hyd Div 221–250.

YALIN M S (1972) Mechanics of Sediment Transport. Pergamon Press, Oxford, pp 290.

TABLE 1

Roughness length (z_0) and threshold velocity (u_{cr}) values used in calculating bed load transport rates in Swansea Bay

Station	Sediment	Bedform	Roughness length z_0 (cm)	Threshold velocity u_{cr} (cm s^{-1})
D, H, K	Sand or Gravel	Rippled) Irregular)	.5	20
C, E, F, I, J	Sand/gravel or Gravel/sand	Irregular) Irregular)	.1	25
A, B, G	Muddy sand or sandy mud	Planar) Planar)	.05	27
	Mud	Planar	.01	

Note: the roughness length figure for a mud substrate has been included in Table 1 for completeness.

TABLE 2

Sediment transport formulae used in comparisons of observed and predicted sediment transport rates in Swansea Bay

Originators		Date	Type	Mode
Bagnold	a	1963	Deterministic	Bed load
Yalin	a	1963	Deterministic	Bed load
Einstein	a	1950	Stochastic	Bed load
Ackers and White	b,c	1973	Deterministic	Total load
Engelund and Hansen	b,c	1967	Deterministic	Total load

Used recently by (a) Gadd et al 1978
(b) Swart 1976
(c) Flemming and Hunt 1976

TABLE 3

Comparisons of net bed-load transport rates ($\bar{q}_{sb}$)

	Location	Transport rates ($gm\ cm^{-1}s^{-1}$/tonnes $m^{-1}day^{-1}$) min.	max.
Measured			
(Heathershaw and Carr, 1977)	T1	.039/.34	.14/1.21
	T2	.037/.32	.097/.84
Predicted			
(Bagnold's 1963 formula)	C	.2/1.73	.3/2.59
	A	.014/.12	.059/.51

Predicted sediment transport rates were calculated using Bagnold's (1963) formula in a modified form due to Gadd et al (1978) (see equation 3).

TABLE 4

Comparisons of instantaneous suspended and bed load transport rates

	Location (Profile No)	u_* (cm s^{-1})	q_{ss} $d>0$ (gm $cm^{-1}s^{-1}$)	q_{ss} $d>40\mu m$ (gm $cm^{-1}s^{-1}$)	q_{sb} $d_{50}=170\mu m$ (gm $cm^{-1}s^{-1}$)	$\overline{u}_{100}$ (cm s^{-1})
Springs	PS2/64	2.05	3.54	.071	.20	38.95
	PS4/83	2.27	4.08	.082	.44	43.14
	PS5/62	2.94	10.50	.21	2.15	55.87
Neaps	PS2/25	1.88	0.95	.019	.092	35.72

Figure 1 Location of study area

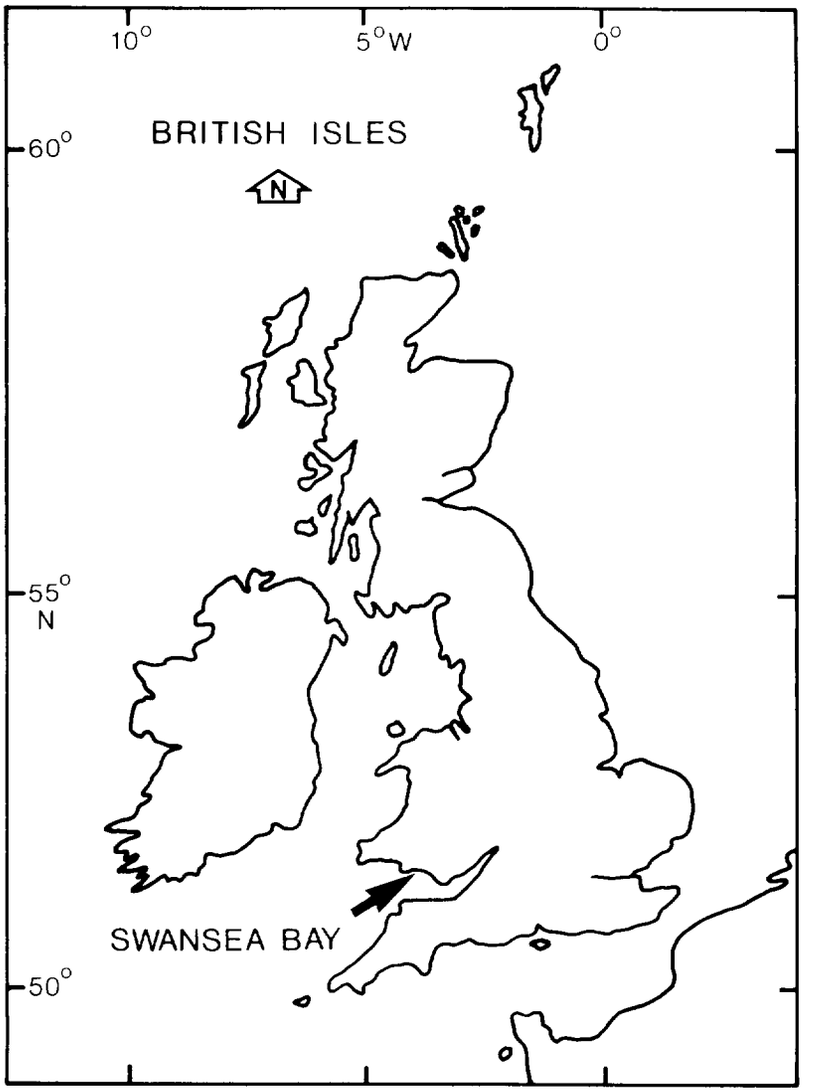

Fig.1

Figure 2 Sediment distribution on E side of Swansea Bay

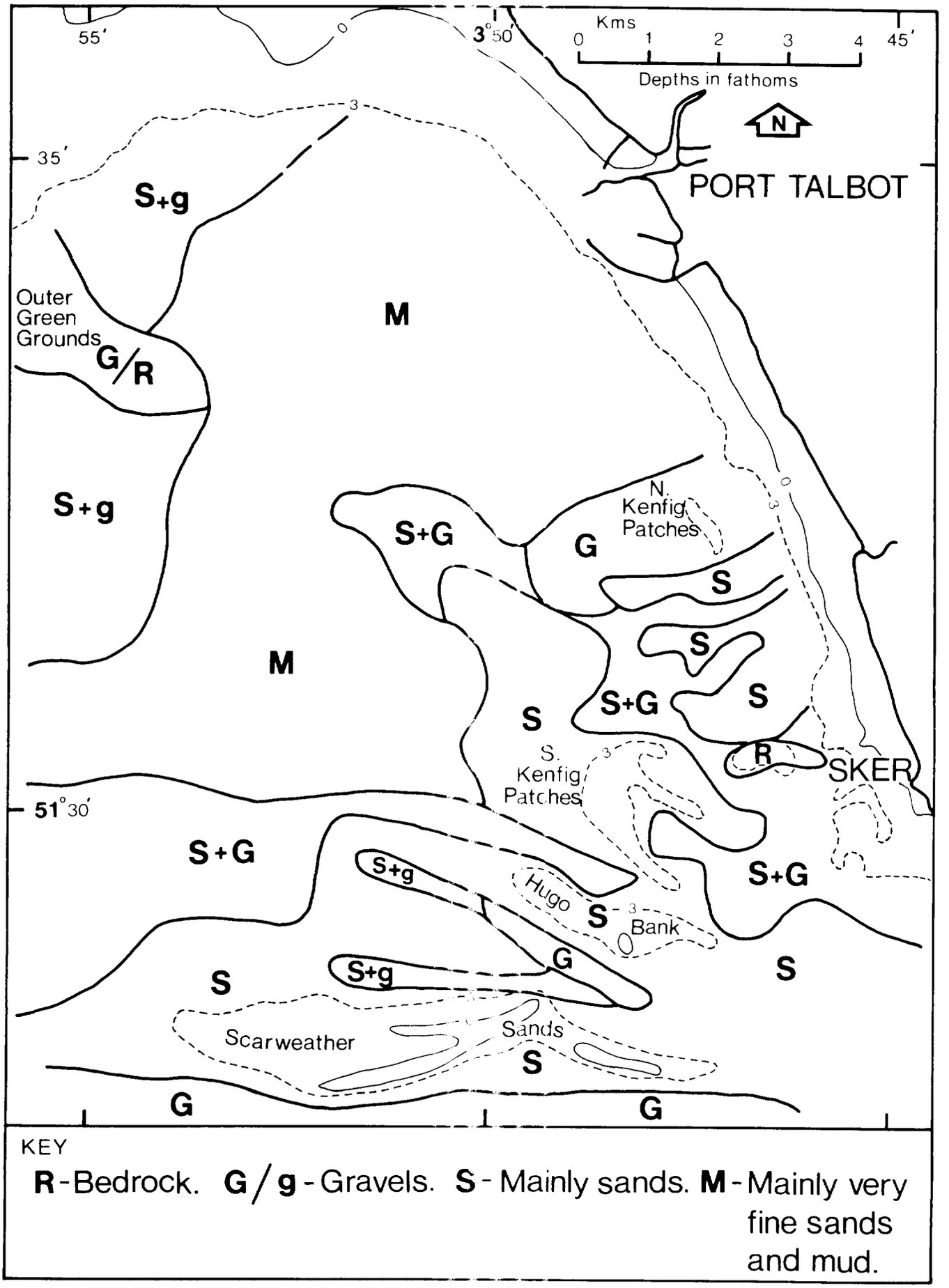
55'
3°50'
45'
Kms
0 1 2 3 4
Depths in fathoms
N
35'
PORT TALBOT
S+g
Outer
Green
Grounds
G/R
M
S+g
S+G
G
N.
Kenfig
Patches
S
S
M
S
S+G
S
S
S.
Kenfig
Patches
R
SKER
51°30'
S+G
S+g
Hugo
S
Bank
S+G
G
S+g
S
S
Scarweather
Sands
S
G
G
KEY
R-Bedrock. G/g-Gravels. S-Mainly sands. M-Mainly very fine sands and mud.

Fig.2

Figure 3 Location of recording current meter moorings and positions at which near bottom velocity profile and suspended sediment measurements were made. The locations of radioactive tracer experiments (T1 and T2) are also indicated.

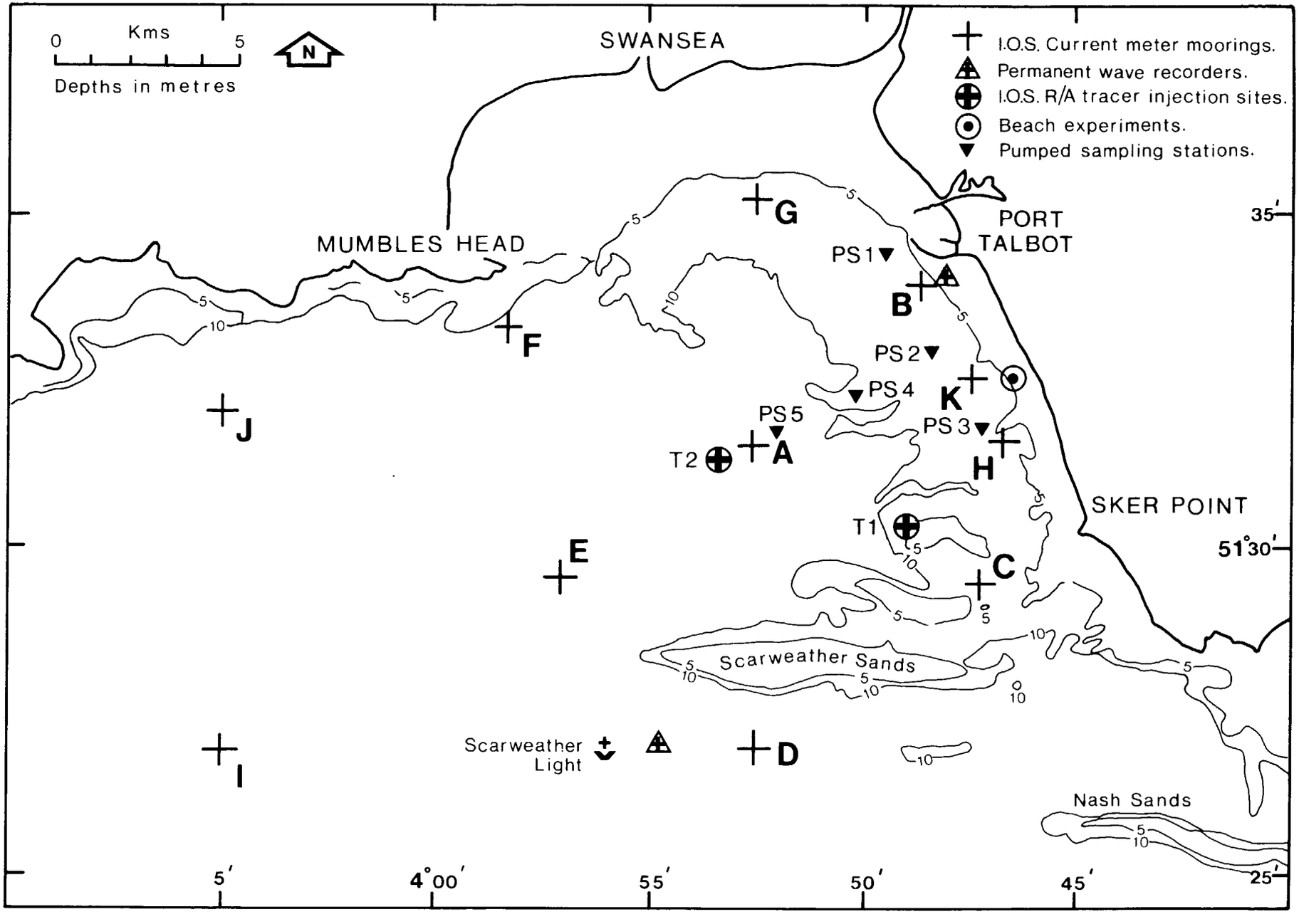
0 Kms 5
Depths in metres
N
SWANSEA
I.O.S. Current meter moorings.
Permanent wave recorders.
I.O.S. R/A tracer injection sites.
Beach experiments.
Pumped sampling stations.
MUMBLES HEAD
PORT TALBOT
SKER POINT
Scarweather Sands
Scarweather Light
Nash Sands
G
B
F
J
K
H
A
E
C
D
I
PS1
PS2
PS3
PS4
PS5
T1
T2
35′
51°30′
5′
4°00′
55′
50′
45′
25′

Fig.3

Figure 4 Typical grain size distributions for sediments on E side of Swansea Bay in the vicinity of the Scarweather Sands and Kenfig Patches (details of the location of box-core and grab samples are given in Blackley 1978)

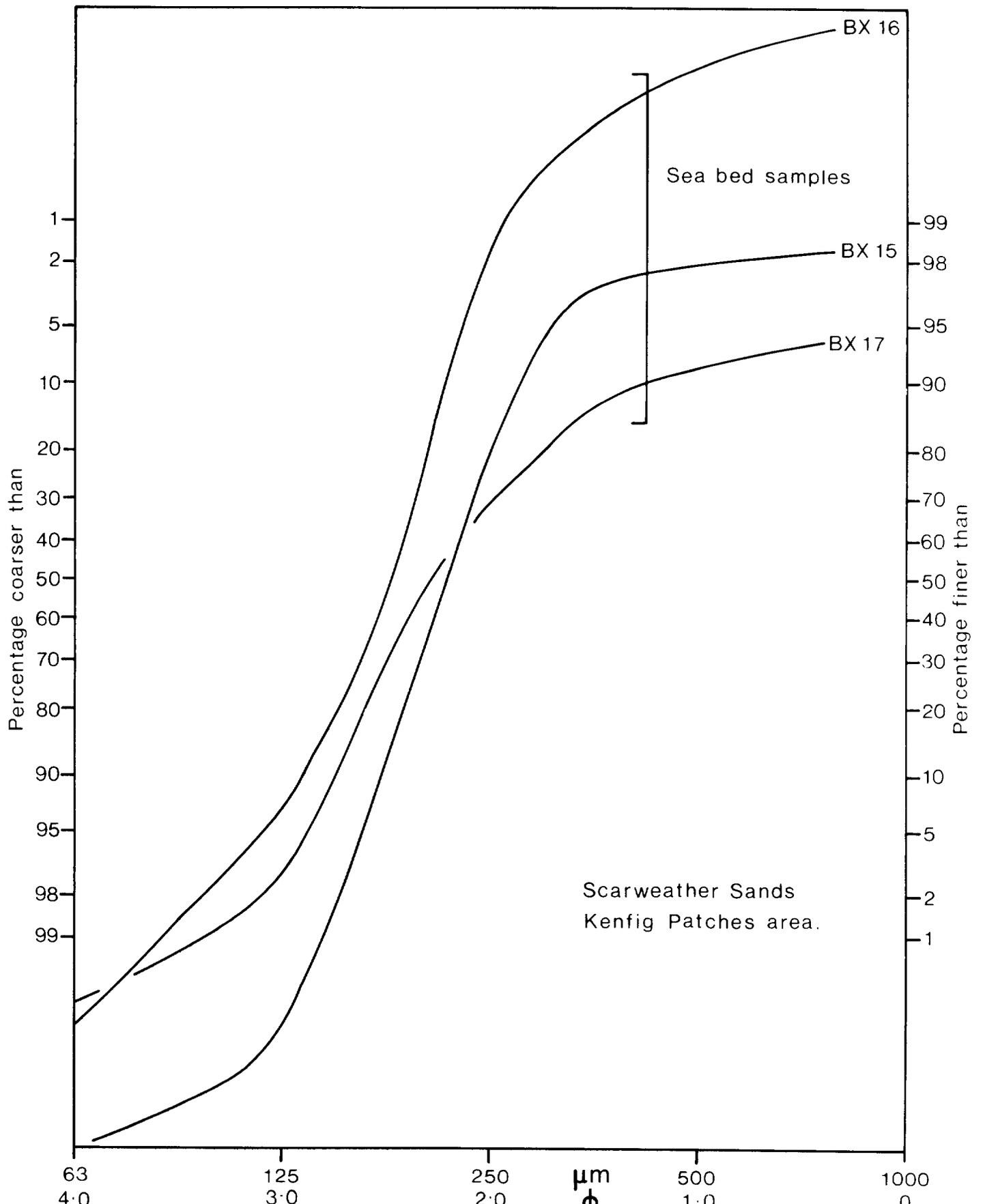
BX 16
Sea bed samples
BX 15
BX 17
Percentage coarser than
Percentage finer than
1
2
5
10
20
30
40
50
60
70
80
90
95
98
99
Scarweather Sands
Kenfig Patches area.
63
4·0
125
3·0
250
2·0
µm
ϕ
500
1·0
1000
0
Grain size

Fig.4

Figure 5 Tracer dispersion patterns at T1 and T2 approximately 2–3 days after injection. The initial dispersions reflect the phase of the tide following injection rather than the long term sediment drift which can only be established 10–20 days after the release of the tracer. Depths are in metres (m) and tracer activity in counts per second (cs $^{-1}$)

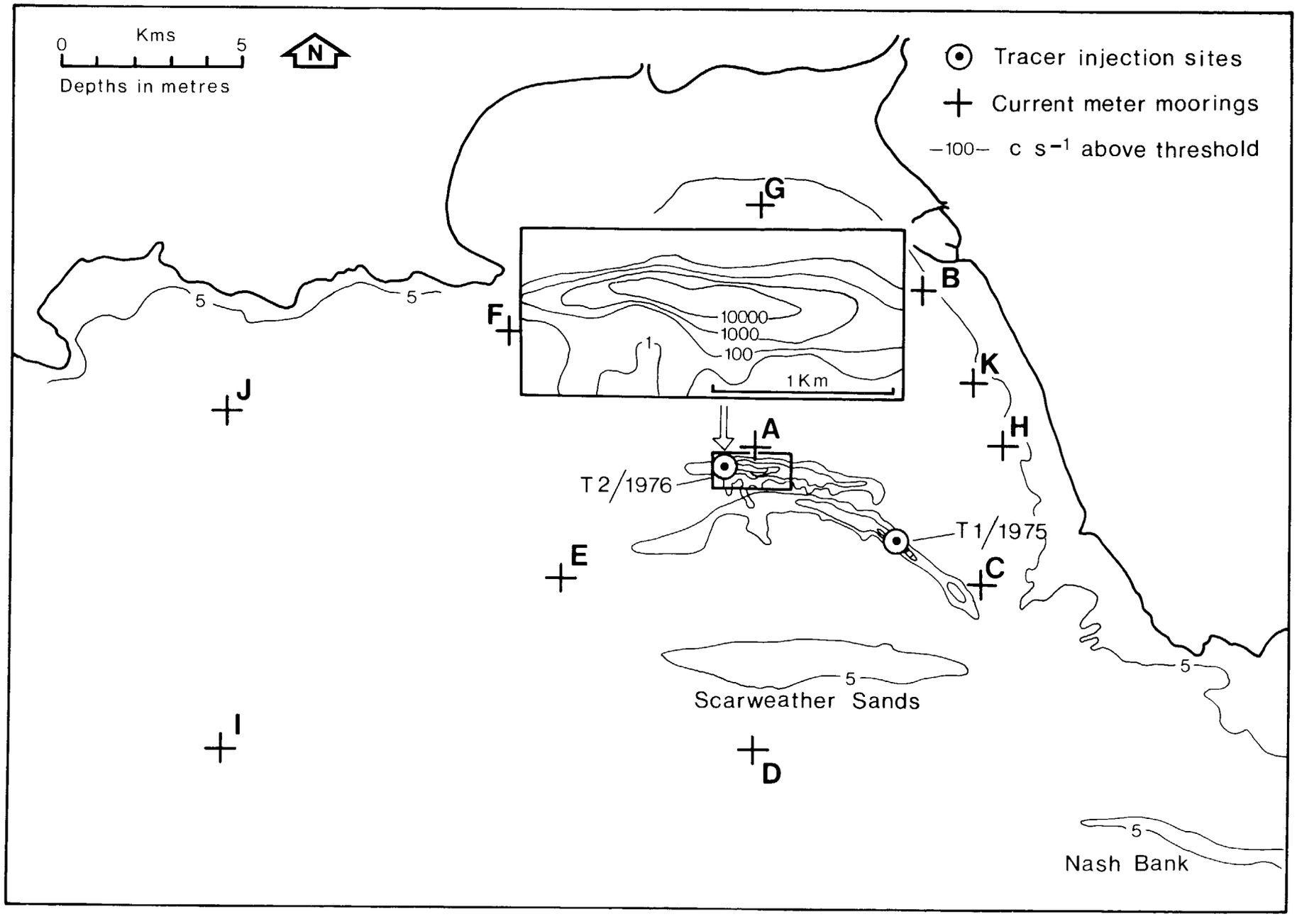
0 Kms 5
Depths in metres
N
Tracer injection sites
Current meter moorings
—100— c s⁻¹ above threshold
G
B
F
10000
1000
100
1
1 Km
5
5
J
K
A
H
T 2/1976
T 1/1975
E
C
5
Scarweather Sands
I
D
5
Nash Bank

Fig.5

Figure 6 Comparisons of observed and predicted net bed load transport rates ($\overline{q_{sb}}$). The maximum and minimum measured rates are derived from radioactive tracer experiments at T1 and T2. The overbar denotes averaging over a large number of tidal cycles.

Comparisons of measured and predicted net transport rates $(\overline{q_{sb}})$

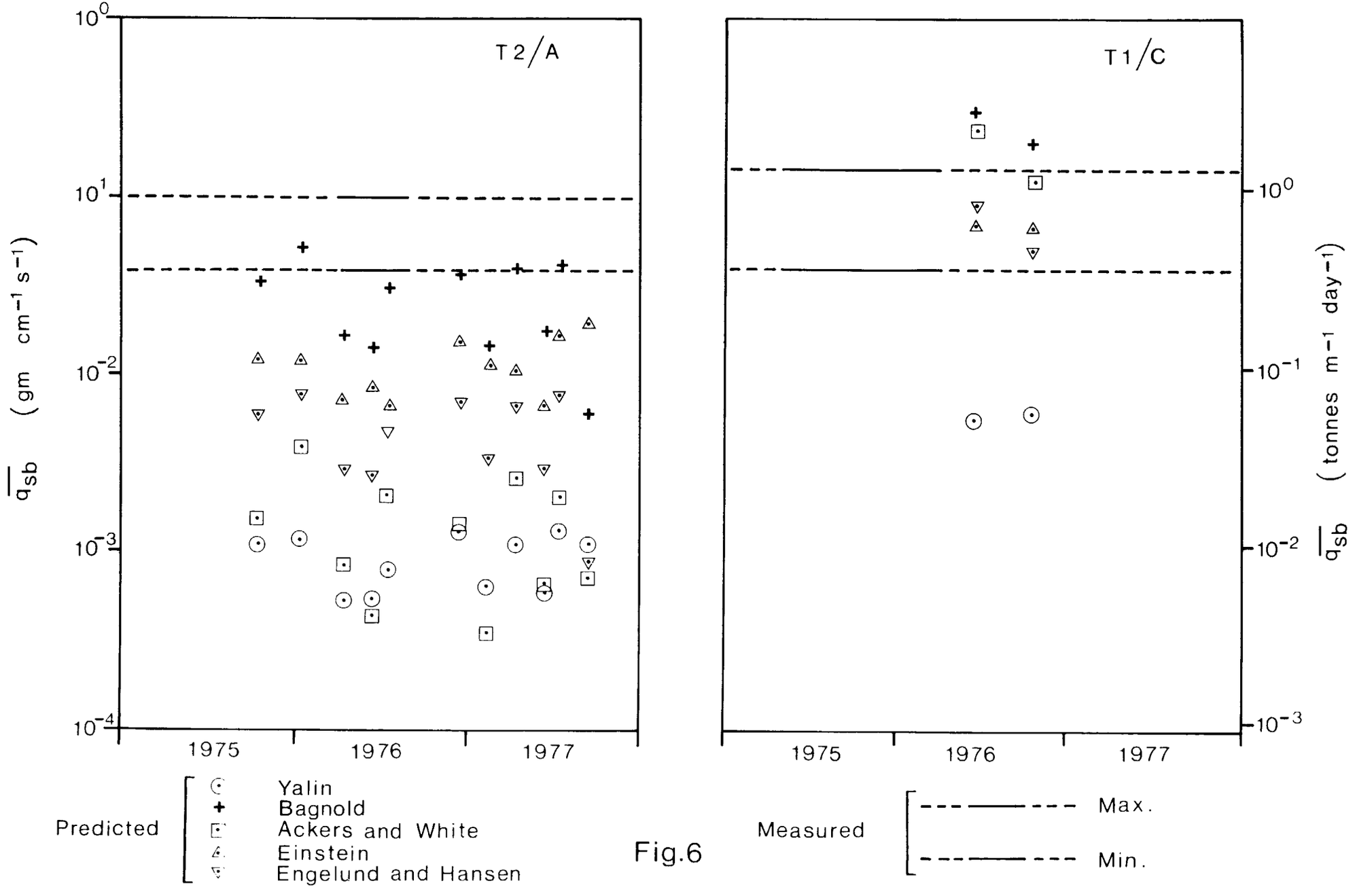

Fig.6

Figure 7 Equipment used to measure near-bottom velocity profiles and suspended sediment concentrations, showing the 4 Braystoke rotors and 6 pump sampling nozzles which are connected by electrically operated solenoid valves to a single hose. The probe is aligned with the mean flow by a large fin as it is lowered to the sea-bed.

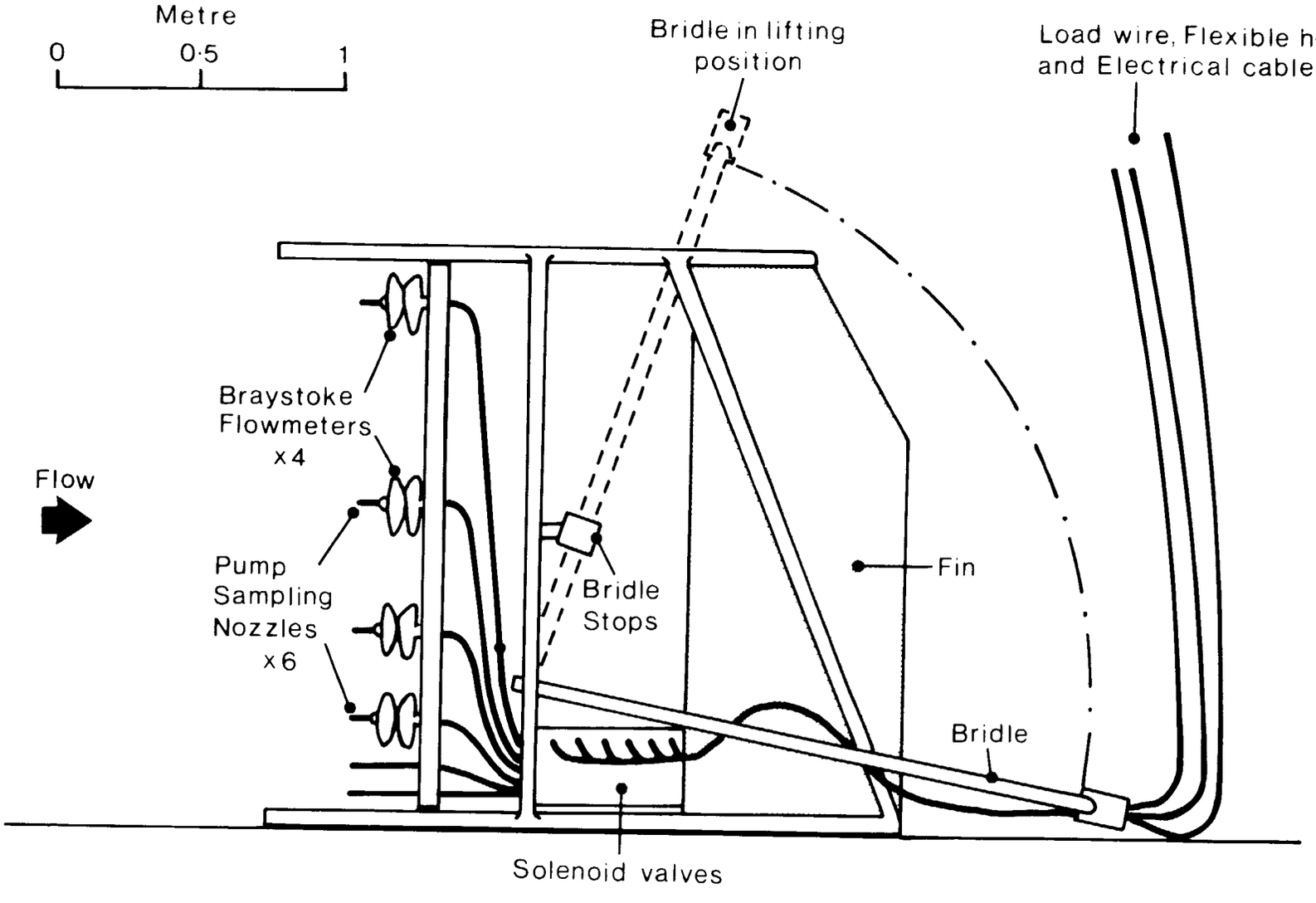
Metre
0
0·5
1
Bridle in lifting position
Load wire, Flexible hose and Electrical cables
Braystoke Flowmeters x4
Flow
Pump Sampling Nozzles x6
Bridle Stops
Fin
Bridle
Solenoid valves

Fig.7

Figure 8 Grain size analyses of sea-bed and suspended sediment samples in the vicinity of Station PS2 (see Figure 3) showing a median grain size for the suspensions and for the material on the seabed of about 70 μm .

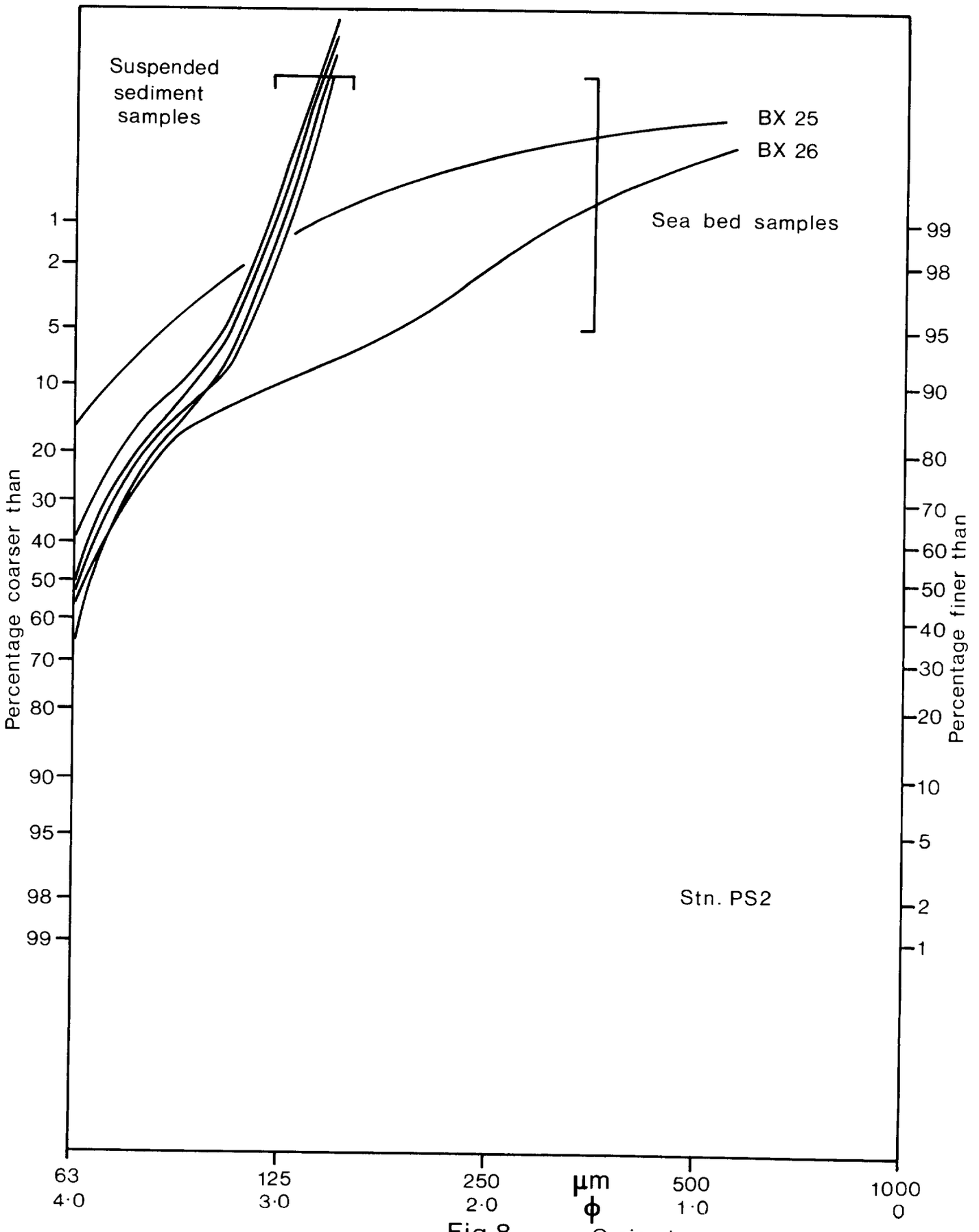
Suspended sediment samples
BX 25
BX 26
Sea bed samples
Stn. PS2
Percentage coarser than
Percentage finer than
1
2
5
10
20
30
40
50
60
70
80
90
95
98
99
63
4·0
125
3·0
250
2·0
µm
ϕ
500
1·0
1000
0
Grain size

Fig.8

Figure 9 Grain size analyses of sea bed and suspended sediment samples in the vicinity of Station PS5 (see Figure 3) showing a median grain size for the suspensions of 70 µm and a median grain size of sea bed samples of up to 150 µm .

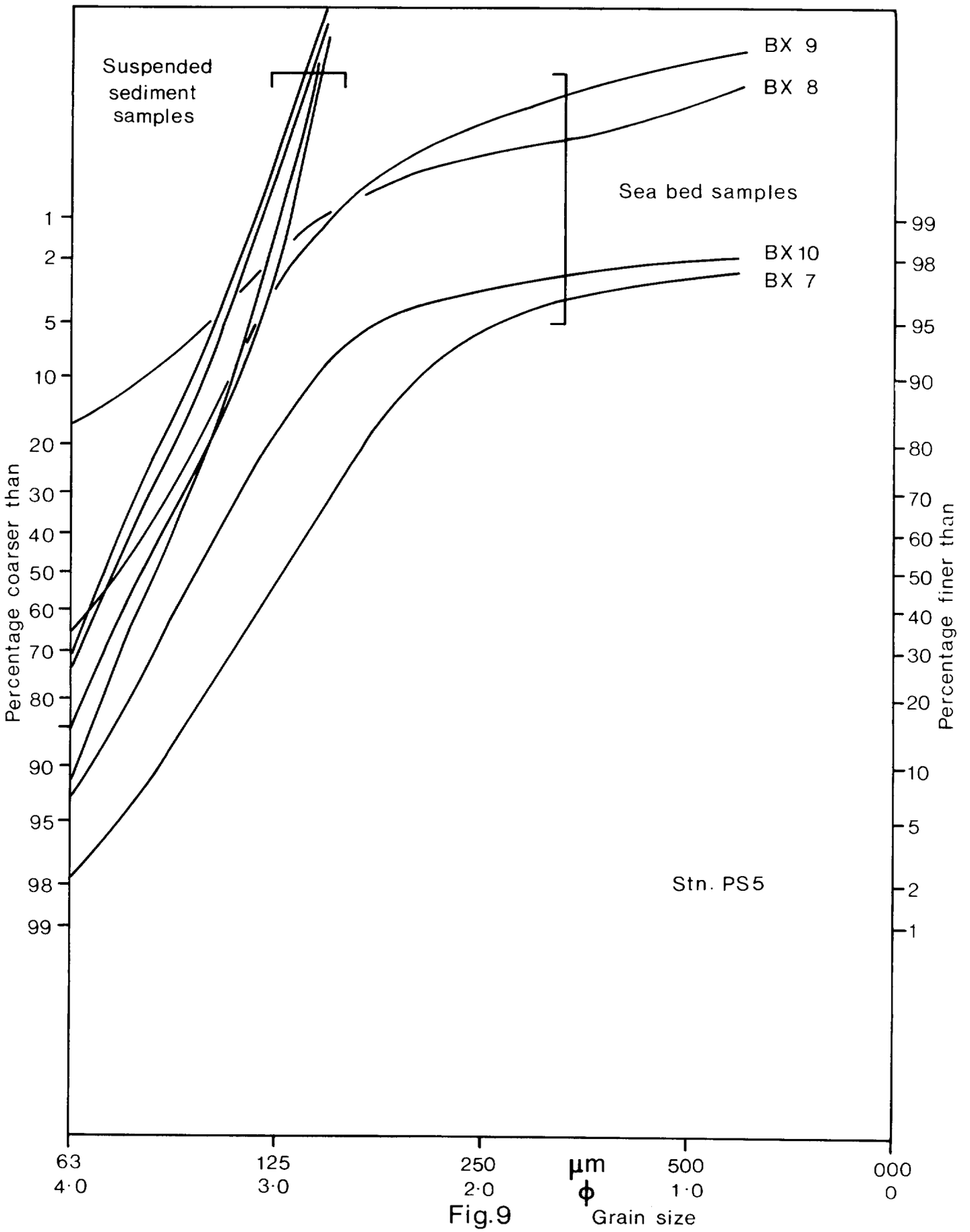
Suspended sediment samples
BX 9
BX 8
Sea bed samples
BX 10
BX 7
Stn. PS5
Percentage coarser than
Percentage finer than
1
2
5
10
20
30
40
50
60
70
80
90
95
98
99
63
4·0
125
3·0
250
2·0
µm
ϕ
500
1·0
000
0
Grain size

Fig.9

Figure 10 Suspended sediment concentration profiles from Stations PS4 and PS5 showing (a) up to two orders of magnitude difference between the total concentration ($d > 0$) and the concentration of the coarser fraction ($d > 40\mu m$): (b) almost uniform concentrations over the lower 2 m of the flow Spring tides.

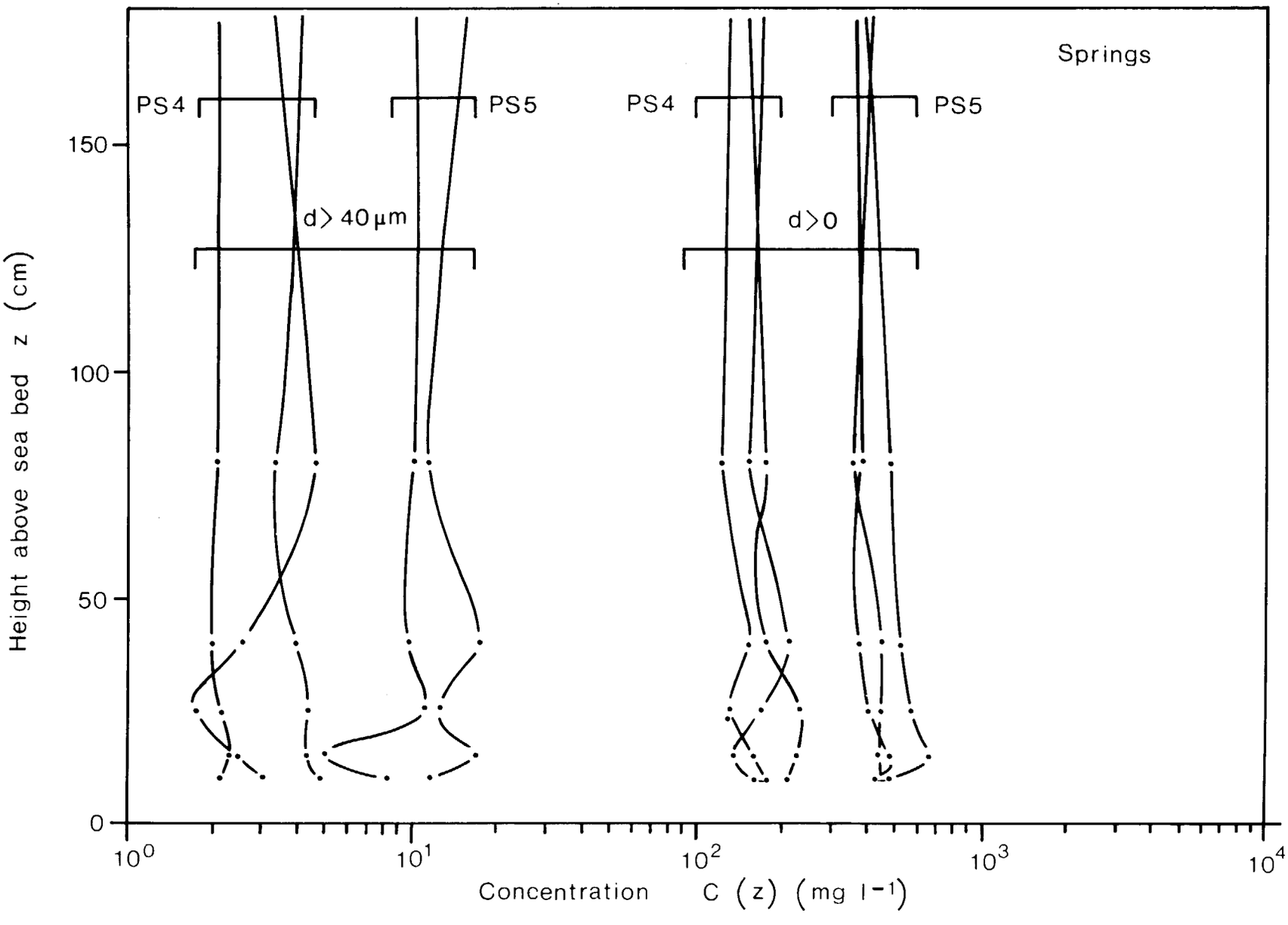
Springs
PS4
PS5
PS4
PS5
d> 40 µm
d>0
150
100
50
0
Height above sea bed z (cm)
10^0
10^1
10^2
10^3
10^4
Concentration C (z) (mg l^{-1})

Fig.10

Figure 11 Typical near bottom velocity profiles at Station PS2 measured over a period of about 1 hour at times of maximum tidal streaming on Spring tides. Values of the correlation coefficient (r) obtained by fitting logarithmic velocity profiles of the type given in equation (1) are indicated together with the values of r at the 5% and 1% significance levels. The solid curves indicate the observed trends.

PS2/ 4:4:77 Springs

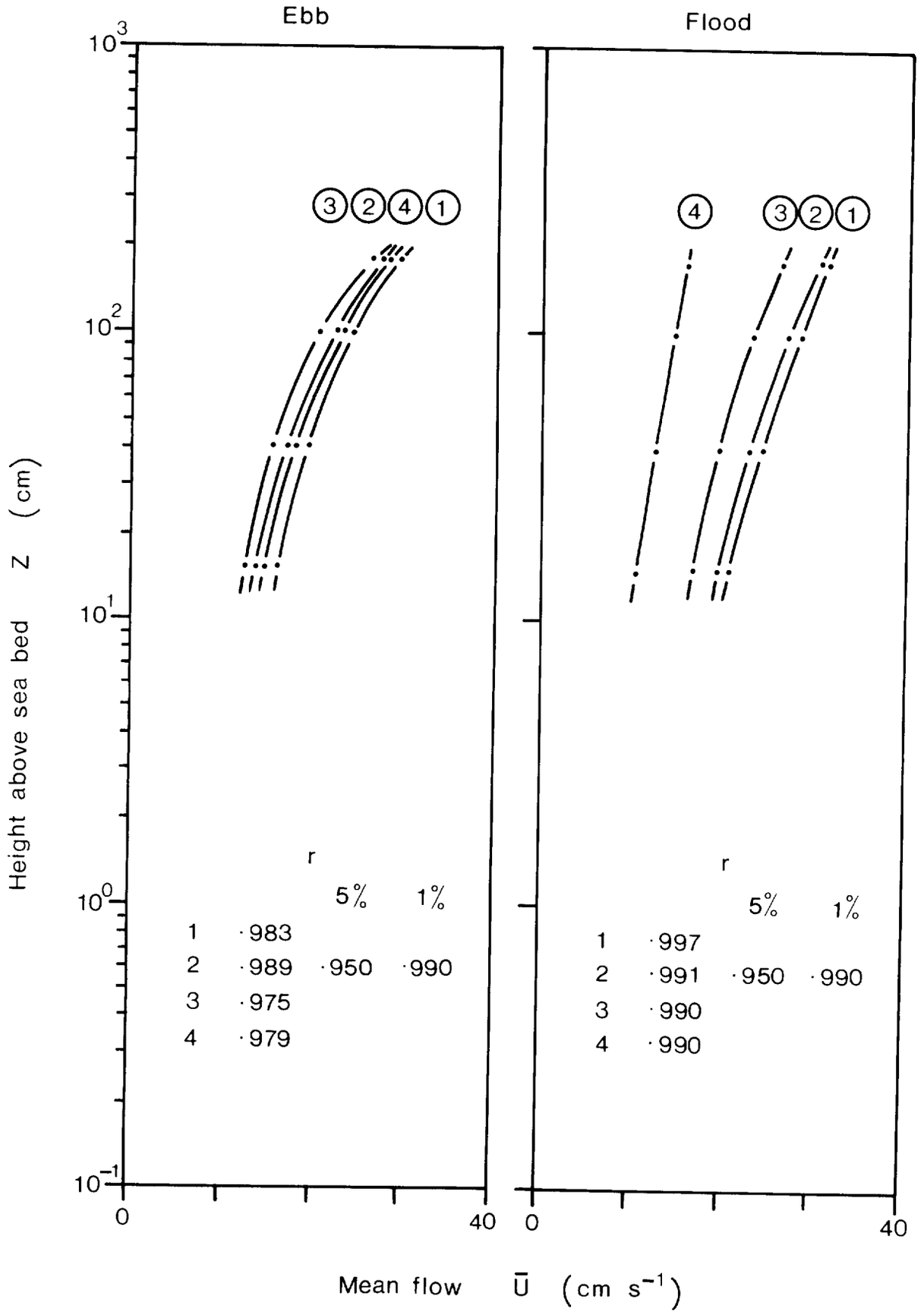

Fig.11

Figure 12 Typical near bottom velocity profiles at Station PS2 measured over a period of about 4 hours on the Ebb and Flood stages of a Neap tidal cycle. Values of the correlation coefficient (r) obtained by fitting a logarithmic velocity profile (equation 1) to these data are also shown. The solid curves indicate the observed trends.

PS2/29:3:77 Neaps

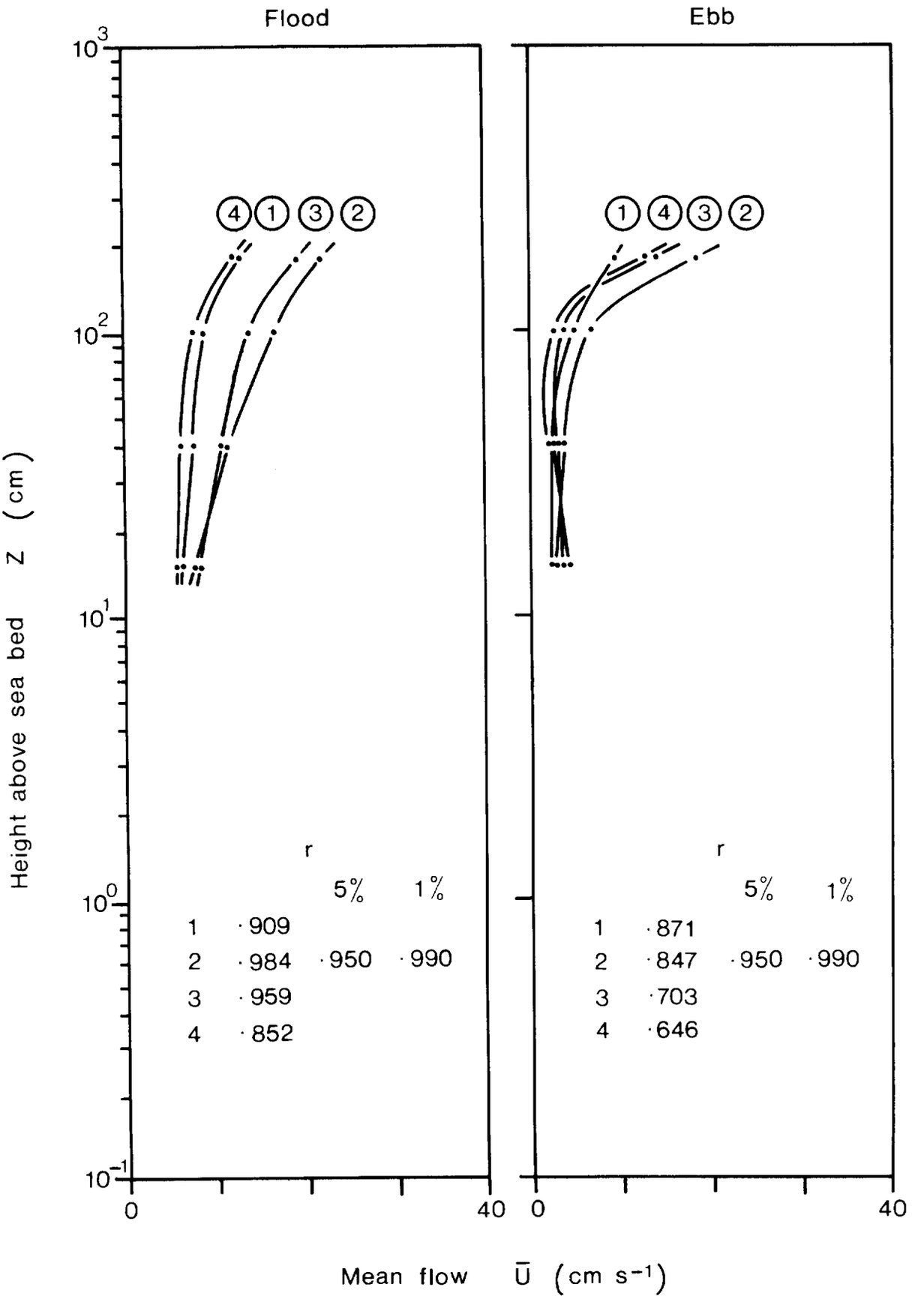

Fig.12

Figure 13 The variation of the suspended sediment concentration, $C(z)$, at heights of 10, 25, 80 and 180 cm above the seabed at Station PS2 (Neaps), with u_* and $\overline{u}_{100}$

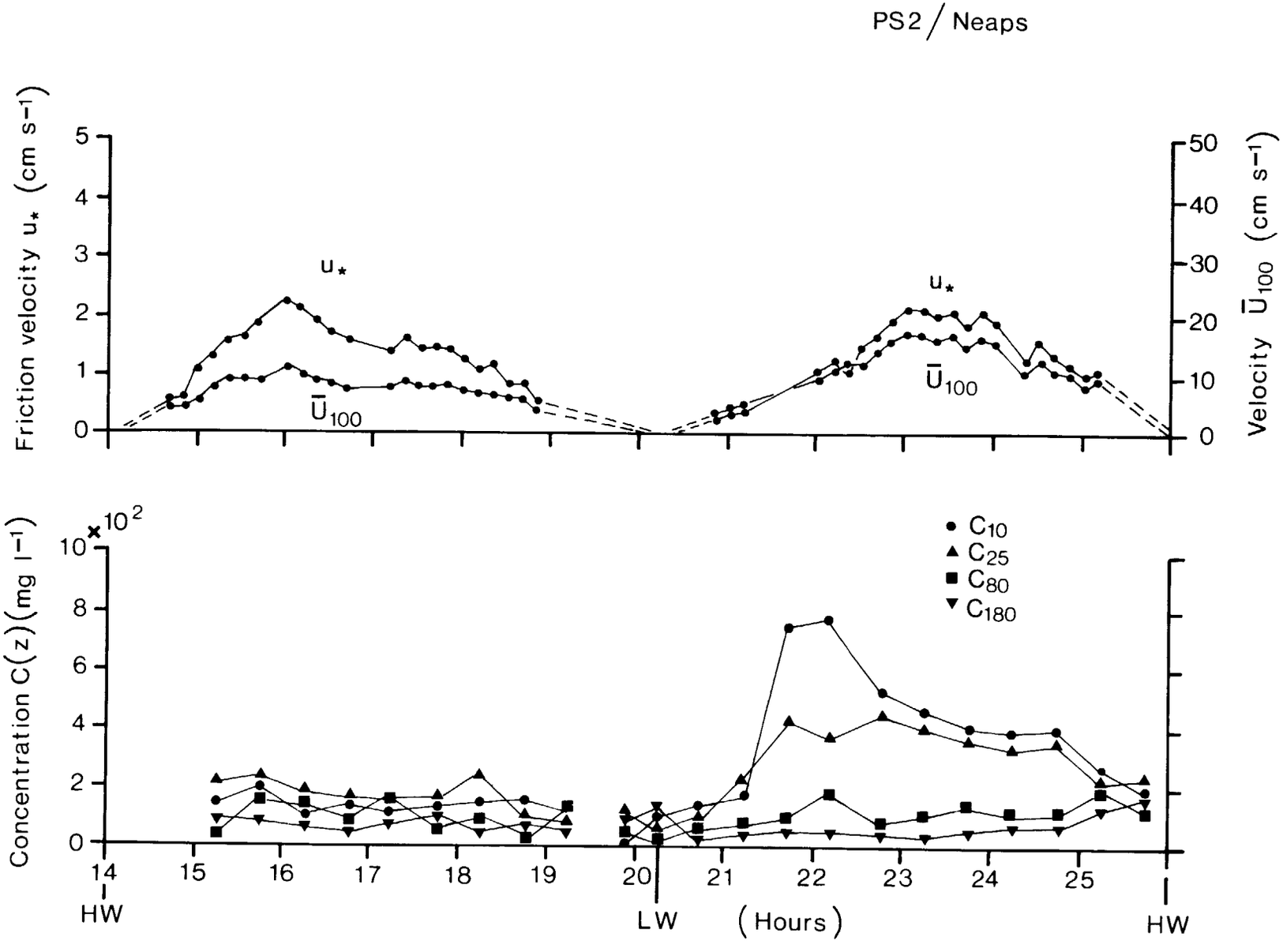
PS2 / Neaps
Friction velocity u_* (cm s^{-1})
Velocity $\bar{U}_{100}$ (cm s^{-1})
u_*
$\bar{U}_{100}$
u_*
$\bar{U}_{100}$
Concentration C(z) (mg l^{-1})
$\times 10^2$
C_{10}
C_{25}
C_{80}
C_{180}
HW
LW
(Hours)
HW

Fig.13

Figure 14 The variation of the suspended sediment concentration $C(z)$, at heights of 10 and 80 cm above the sea-bed at Station PS4 (Springs), with u_* and $\bar{u}_{100}$

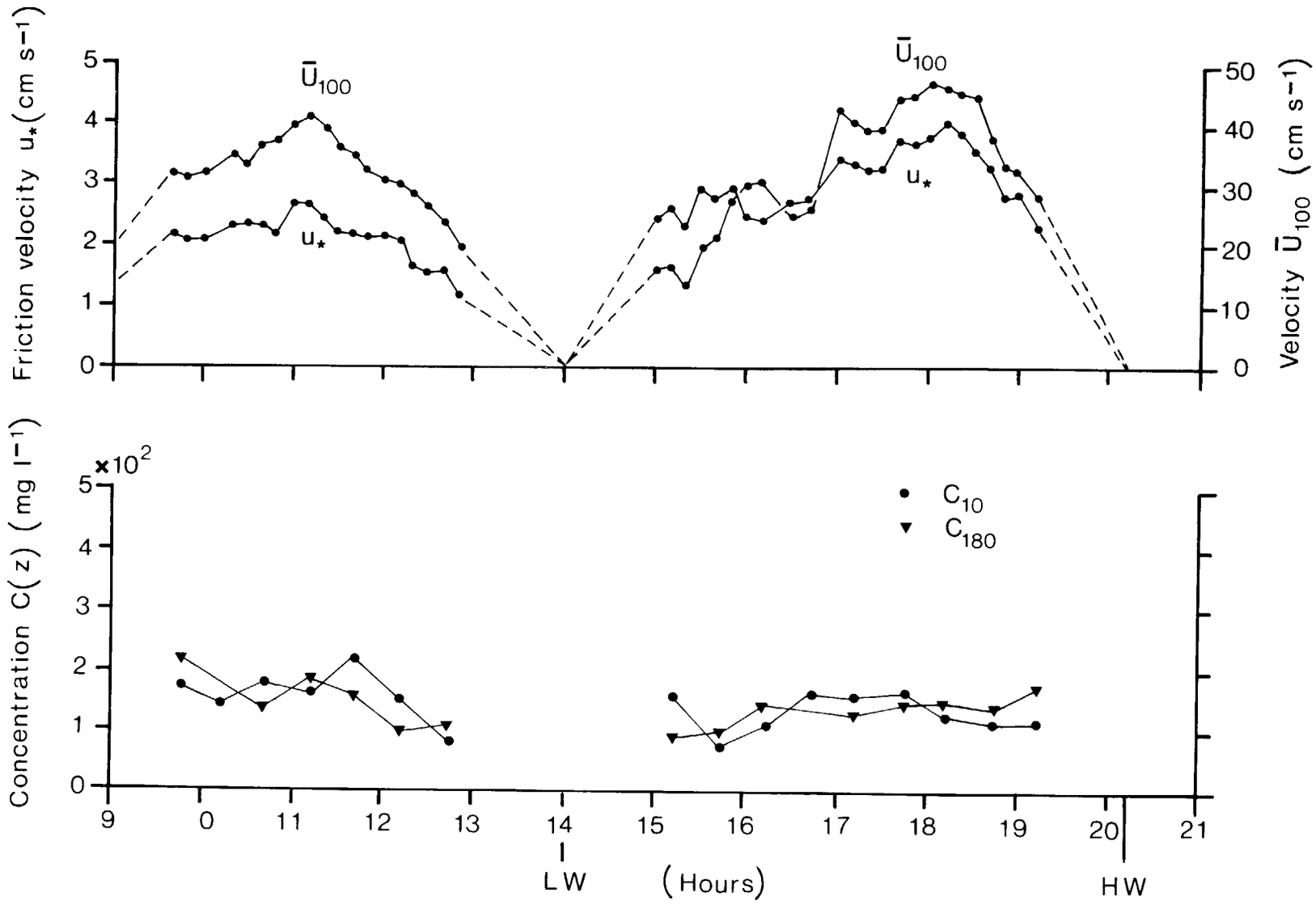
Friction velocity u_* (cm s^{-1})
$\bar{U}_{100}$
u_*
$\bar{U}_{100}$
u_*
Velocity $\bar{U}_{100}$ (cm s^{-1})
0
1
2
3
4
5
0
10
20
30
40
50
Concentration C(z) (mg l^{-1})
×10^2
C_{10}
C_{180}
0
1
2
3
4
5
9
0
11
12
13
14
15
16
17
18
19
20
21
LW
(Hours)
HW

Fig.14

Figure 15 The variation of roughness length (z_0) with friction velocity (u_*) at Station PS2 (Springs) showing an order of magnitude variation in z_0 . The broken line indicates a trend of $z_0 \propto u_*^4$ whereas the solid line indicates a significant correlation between z_0 and u_* of the form $z_0 = .10 u_*^{3.73}$

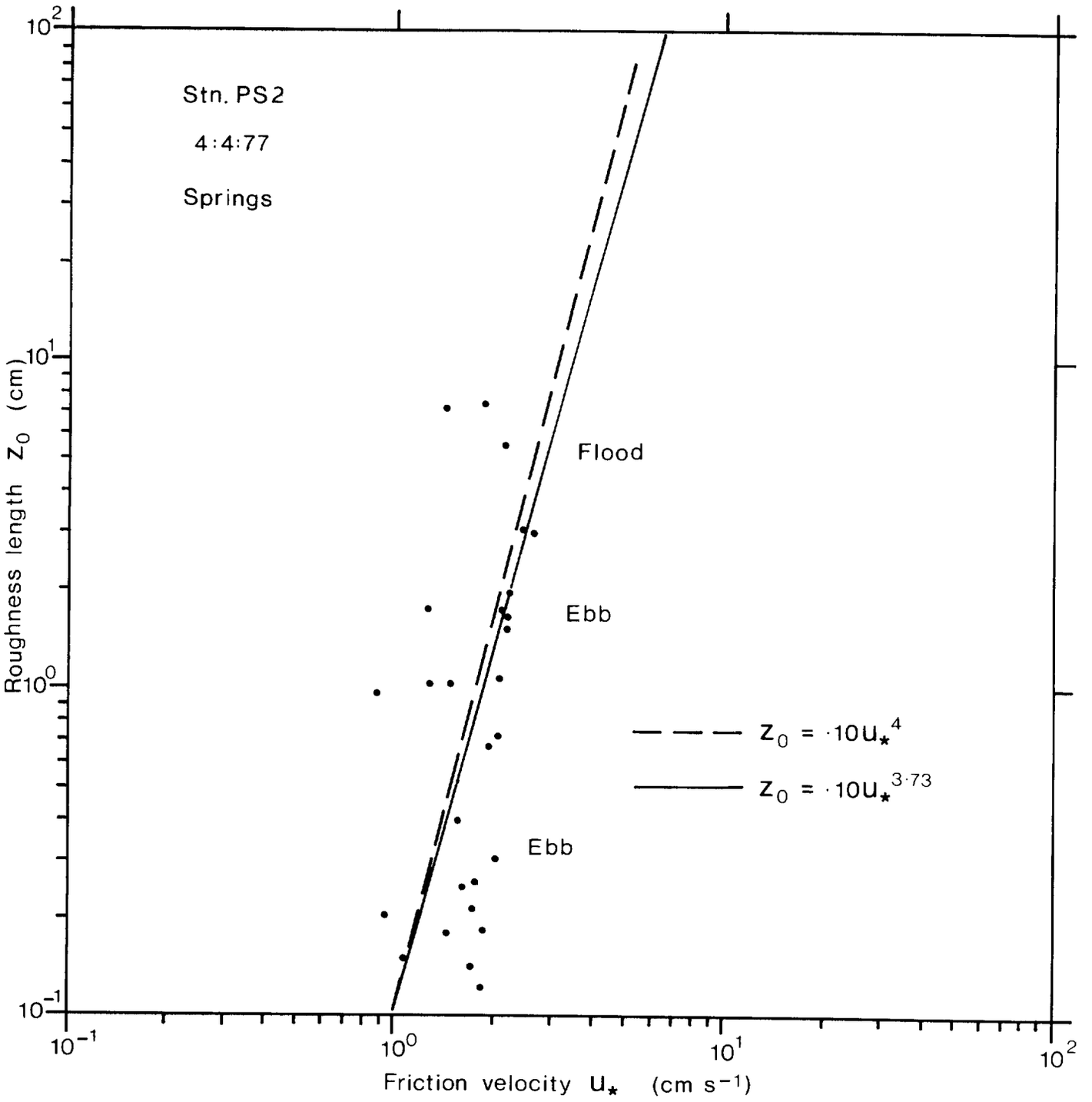
Stn. PS2
4:4:77
Springs
Flood
Ebb
Ebb
$Z_0 = \cdot 10 u_*^4$
$Z_0 = \cdot 10 u_*^{3.73}$
Roughness length Z_0 (cm)
Friction velocity u_* (cm s^{-1})
10^2
10^1
10^0
10^{-1}
10^{-1}
10^0
10^1
10^2

Fig.15

Figure 16 The variation of roughness length (z_o) with friction velocity (u_*) at Station PS4 (Springs) showing a similar variation to that in Figure 15 and illustrating flood z_o values higher than those observed during the ebb stage of the tidal cycle. The broken line indicates a trend of $z_o \propto u_*^4$ and the solid line a significant correlation of the form $z_o = .033\, u_*^{3.29}$

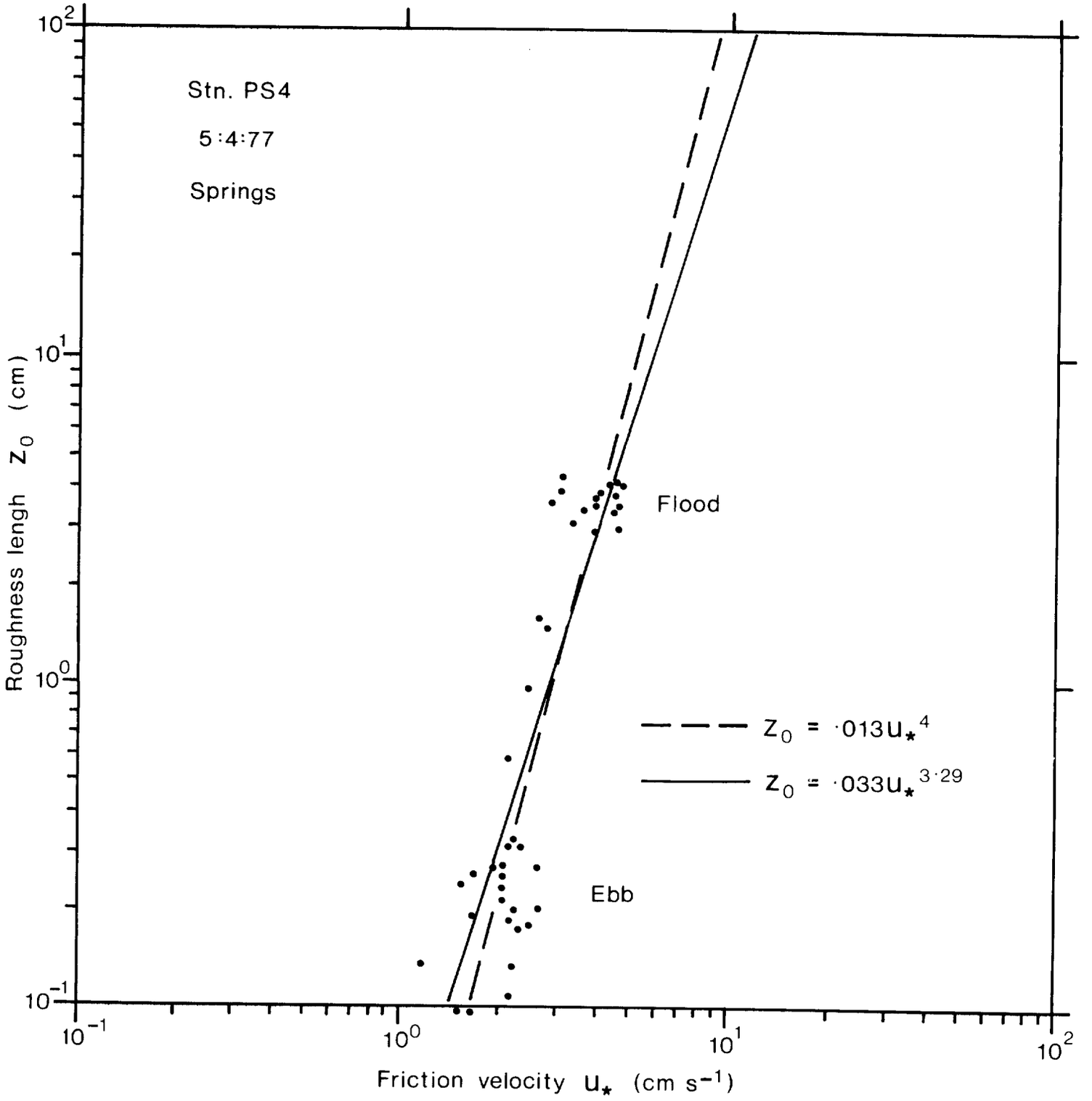
Stn. PS4
5:4:77
Springs
Flood
Ebb
$Z_0 = \cdot 013 u_*^4$
$Z_0 = \cdot 033 u_*^{3 \cdot 29}$
Roughness lengh Z_0 (cm)
Friction velocity u_* (cm s^{-1})
10^2
10^1
10^0
10^{-1}
10^{-1}
10^0
10^1
10^2

Fig.16

Figure 17 Velocity profile measurements (•) at Station PS5 (Springs). The broken lines show fitted logarithmic velocity profiles of the form given in equation (1). The solid curve represents a velocity profile modified by the effects of suspended sediment and of the form given in equation (10). Values of the correlation coefficient r obtained by fitting (1) to the measured currents are also indicated together with 5% and 1% significance levels.

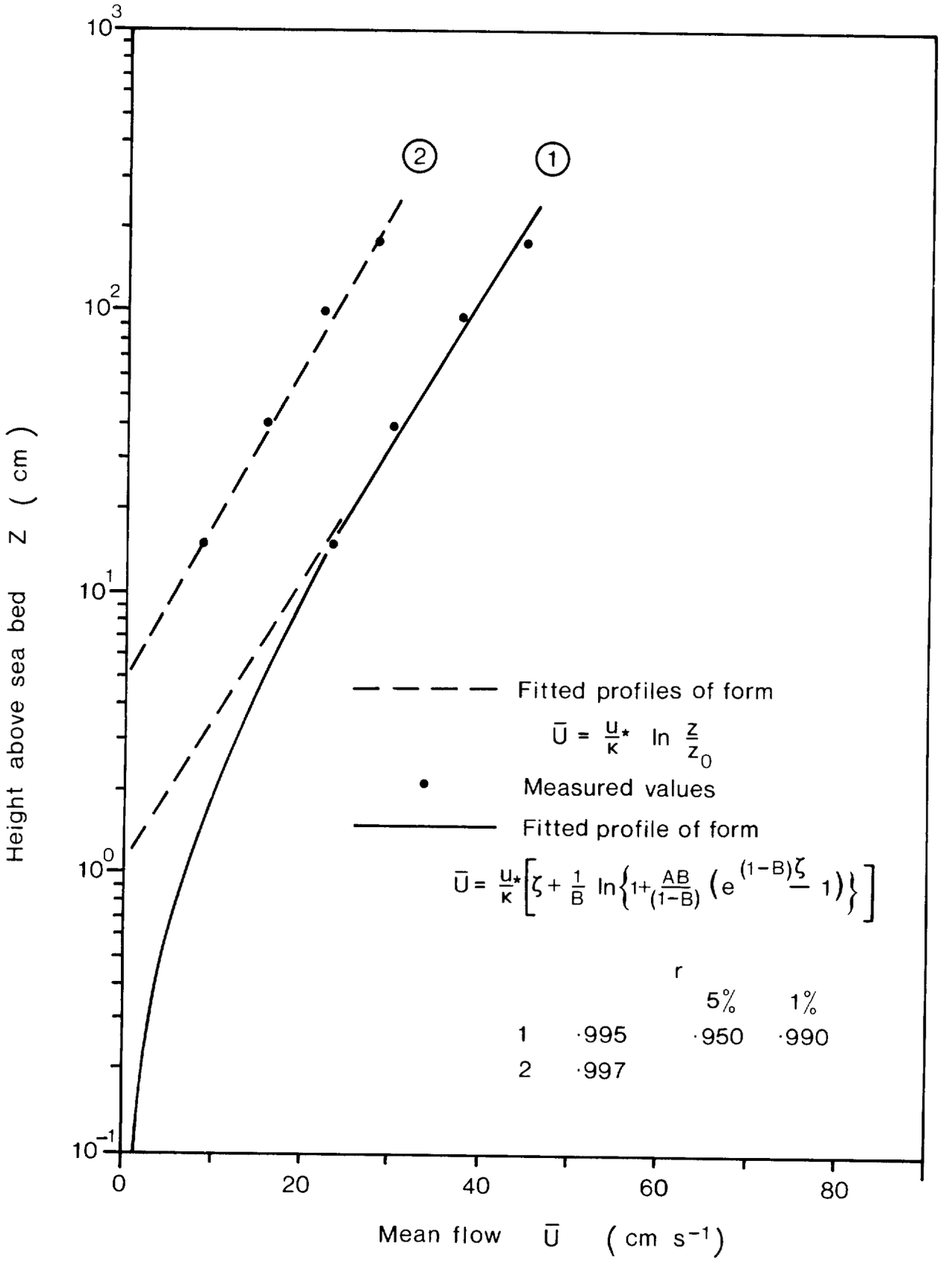
10^3
10^2
10^1
10^0
10^{-1}
0
20
40
60
80
Height above sea bed Z (cm)
Mean flow $\bar{U}$ (cm s^{-1})
②
①
Fitted profiles of form
$\bar{U} = \frac{u_*}{\kappa} \ln \frac{z}{z_0}$
Measured values
Fitted profile of form
$\bar{U} = \frac{u_*}{\kappa}\left[\zeta + \frac{1}{B} \ln\left\{1+\frac{AB}{(1-B)}\left(e^{(1-B)\zeta} - 1\right)\right\}\right]$
r
5%
1%
1 ·995 ·950 ·990
2 ·997

Fig.17

Figure 18 Suspended sediment concentration measurements (•), compared with profiles of the form given in equation (4) (broken line – large dashes) and equation (10) (solid line). The solid line is the modified concentration profile corresponding to velocity profile (1) in Figure 17, which has been fitted by iterating in u_* and z_o only. Thus the concentration profile will not necessarily pass through the measured values.

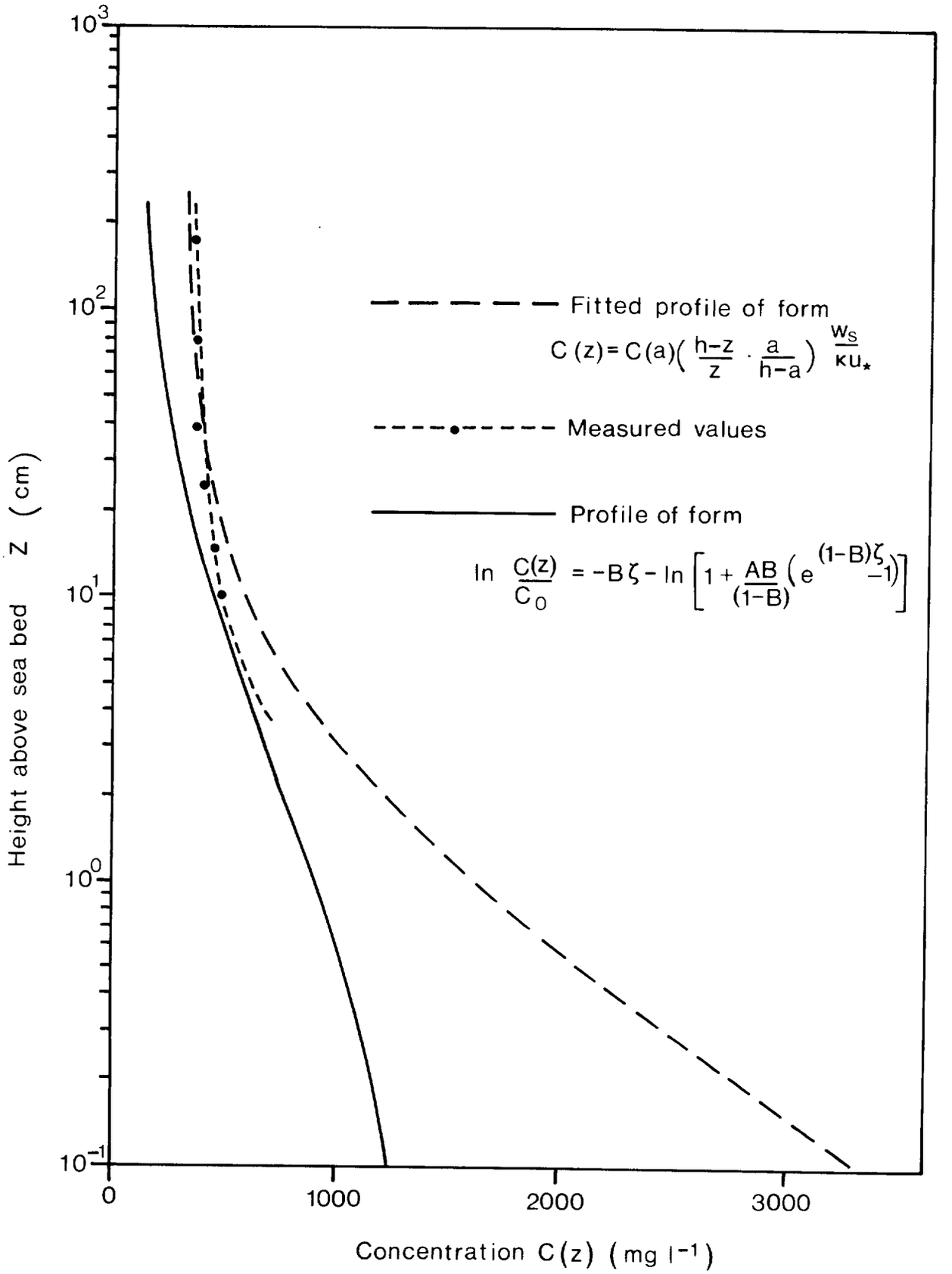
10^3
10^2
10^1
10^0
10^{-1}
Height above sea bed Z (cm)
0
1000
2000
3000
Concentration C(z) (mg l^{-1})
Fitted profile of form
$C(z) = C(a)\left(\frac{h-z}{z} \cdot \frac{a}{h-a}\right)^{\frac{w_s}{\kappa u_*}}$
Measured values
Profile of form
$\ln \frac{C(z)}{C_0} = -B\zeta - \ln\left[1 + \frac{AB}{(1-B)}\left(e^{(1-B)\zeta} - 1\right)\right]$

Fig.18

Figure 19 Predicted net bed load transport rates ($\overline{q_{sb}}$) and directions for the area, calculated using a modified form of Bagnold's (1963) sediment transport formulae. Transport rates are given in gm $cm^{-1}s^{-1}$. Two arrows are shown where it has been possible to indicate summer and winter variations.

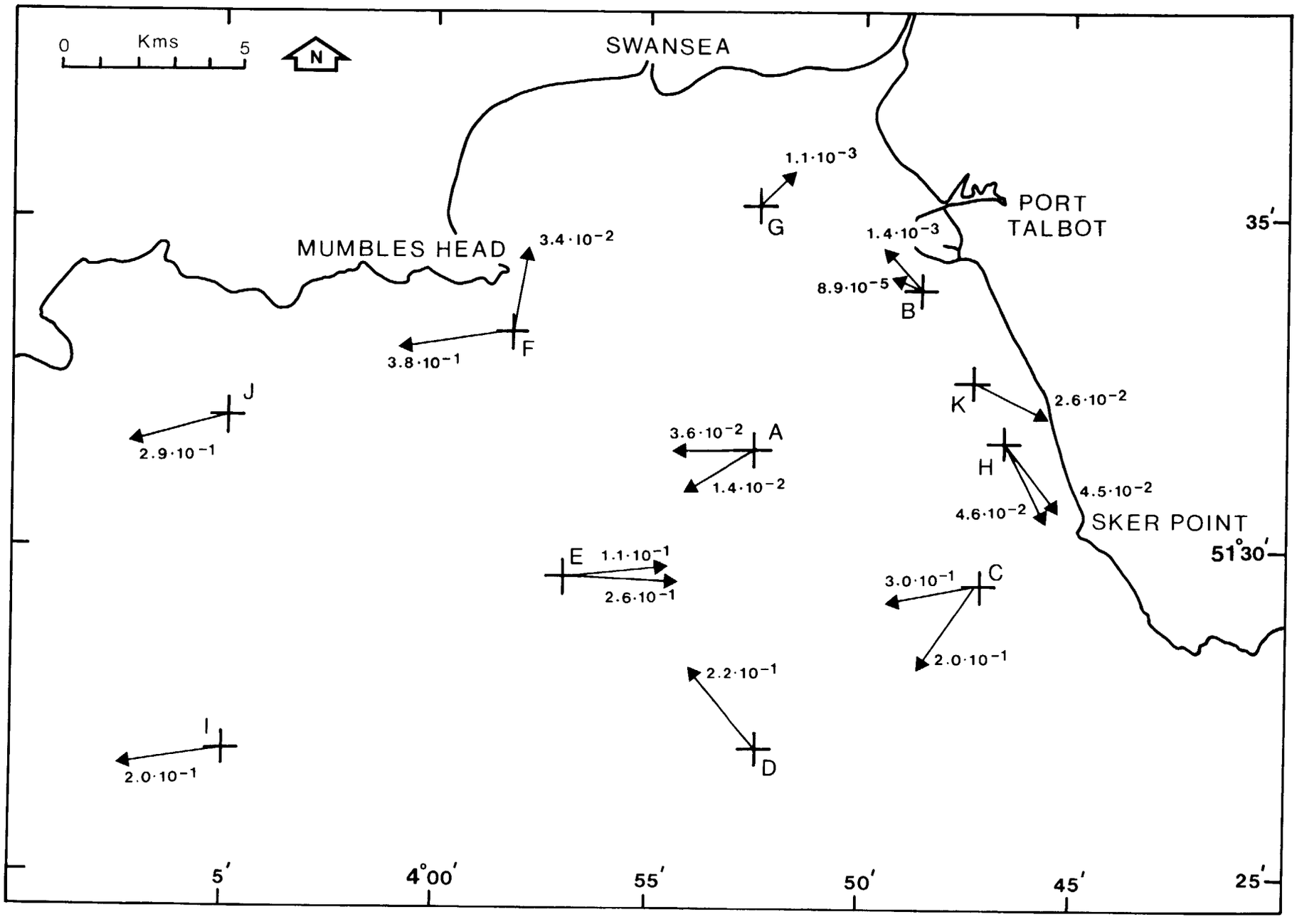
0 Kms 5
N
SWANSEA
MUMBLES HEAD
PORT TALBOT
SKER POINT
35′
51°30′
5′
4°00′
55′
50′
45′
25′
1.1·10⁻³
G
1.4·10⁻³
8.9·10⁻⁵
B
3.4·10⁻²
3.8·10⁻¹
F
J
2.9·10⁻¹
K
2.6·10⁻²
3.6·10⁻²
A
1.4·10⁻²
H
4.5·10⁻²
4.6·10⁻²
E
1.1·10⁻¹
2.6·10⁻¹
3.0·10⁻¹
C
2.0·10⁻¹
2.2·10⁻¹
D
I
2.0·10⁻¹

Fig.19

Figure 19a Summary of near-bottom (solid arrows) and mid-depth (open arrows) tidally induced residuals in Swansea Bay. Residual flow data have been presented in the manner suggested by Ramster et al (1978) and each measurement consists of a set of three figures indicating: the residual flow speed in cm s^{-1}, the steadiness factor $\mathcal{B}$, as a percentage, and the length of the record in days (in that order). (After Heathershaw and Hammond 1979.)

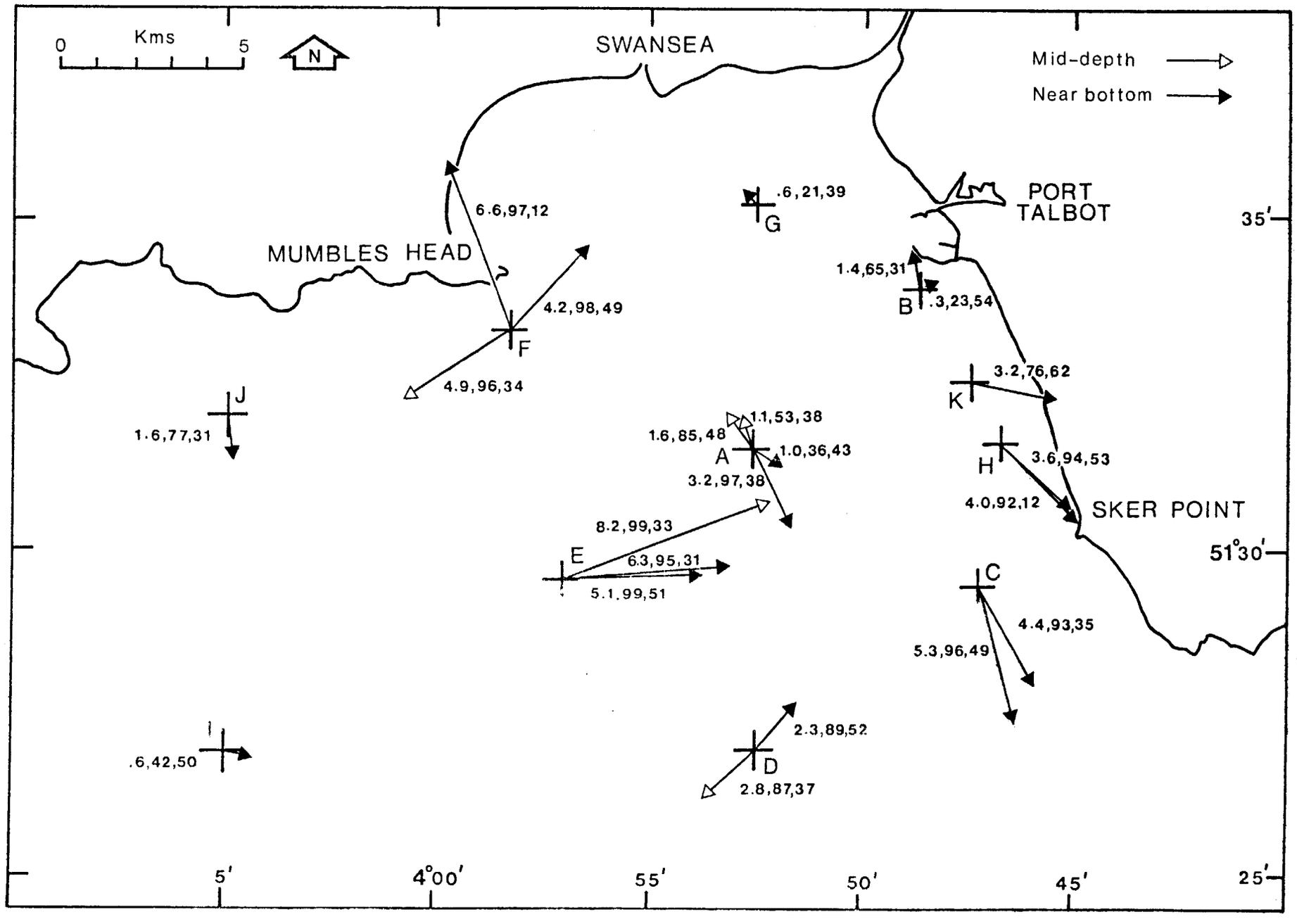
0 Kms 5
N
SWANSEA
Mid-depth
Near bottom
PORT TALBOT
MUMBLES HEAD
6.6,97,12
.6,21,39
G
1.4,65,31
B
.3,23,54
4.2,98,49
F
4.9,96,34
3.2,76,62
K
J
1.6,77,31
1.1,53,38
1.6,85,48
A
1.0,36,43
3.2,97,38
H
3.6,94,53
4.0,92,12
SKER POINT
8.2,99,33
E
6.3,95,31
5.1,99,51
C
4.4,93,35
5.3,96,49
I
.6,42,50
2.3,89,52
D
2.8,87,37
35′
51°30′
5′
4°00′
55′
50′
45′
25′

Fig.19a

Figure 20 The effect of waves on sediment transport. Bijker's (1967) magnification factor (γ) illustrating the effecting of increasing wave height (H) on bed load transport rates (q_{sb}) as a function of the current at a height of 100 cm above the bed ($\overline{u}_{100}$). These calculations have been carried out for a wave of 8 s period and a water depth of 20 m with a roughness length (z_o) of 0.25 cm (typical for the Swansea Bay area).

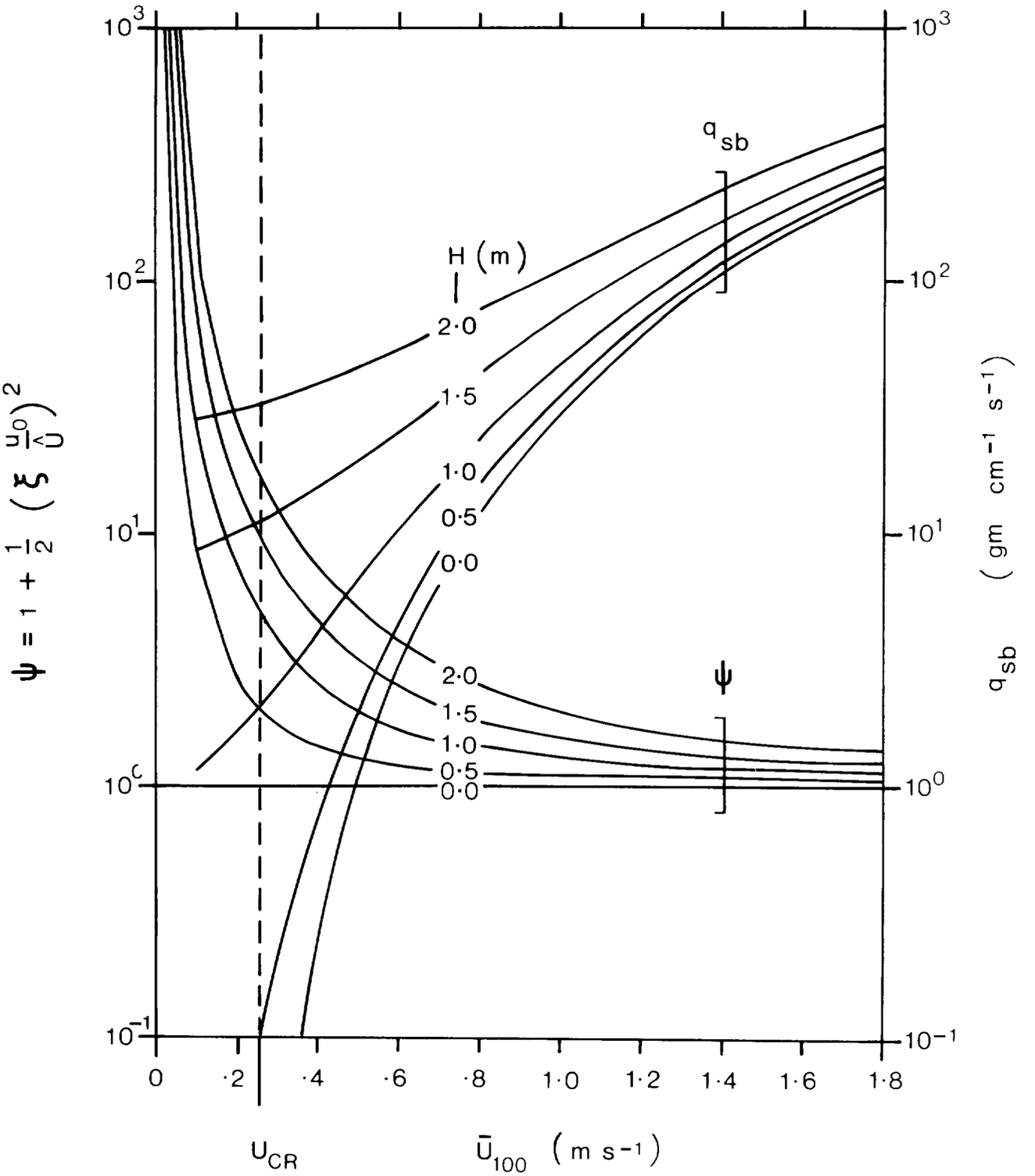
10^3
10^2
10^1
10^0
10^{-1}
q_{sb}
H (m)
2·0
1·5
1·0
0·5
0·0
ψ
$\psi = 1 + \frac{1}{2}\left(\xi \frac{u_0}{U}\right)^2$
q_{sb} (gm cm^{-1} s^{-1})
0
·2
·4
·6
·8
1·0
1·2
1·4
1·6
1·8
U_{CR}
$\bar{U}_{100}$ (m s^{-1})

Fig. 20

Figure 21 Wave induced and tidal current exceedance curves for Swansea Bay. These are based on near-bottom ($\overline{u}_{200}$) current measurements at Stations A and C and wave measurements near the Scarweather Light Vessel (see Figure 3). The threshold values of sand size sediment under waves and currents, u_{0cr} and u_{cr} are indicated. u_{0cr} has been calculated from equation (17).

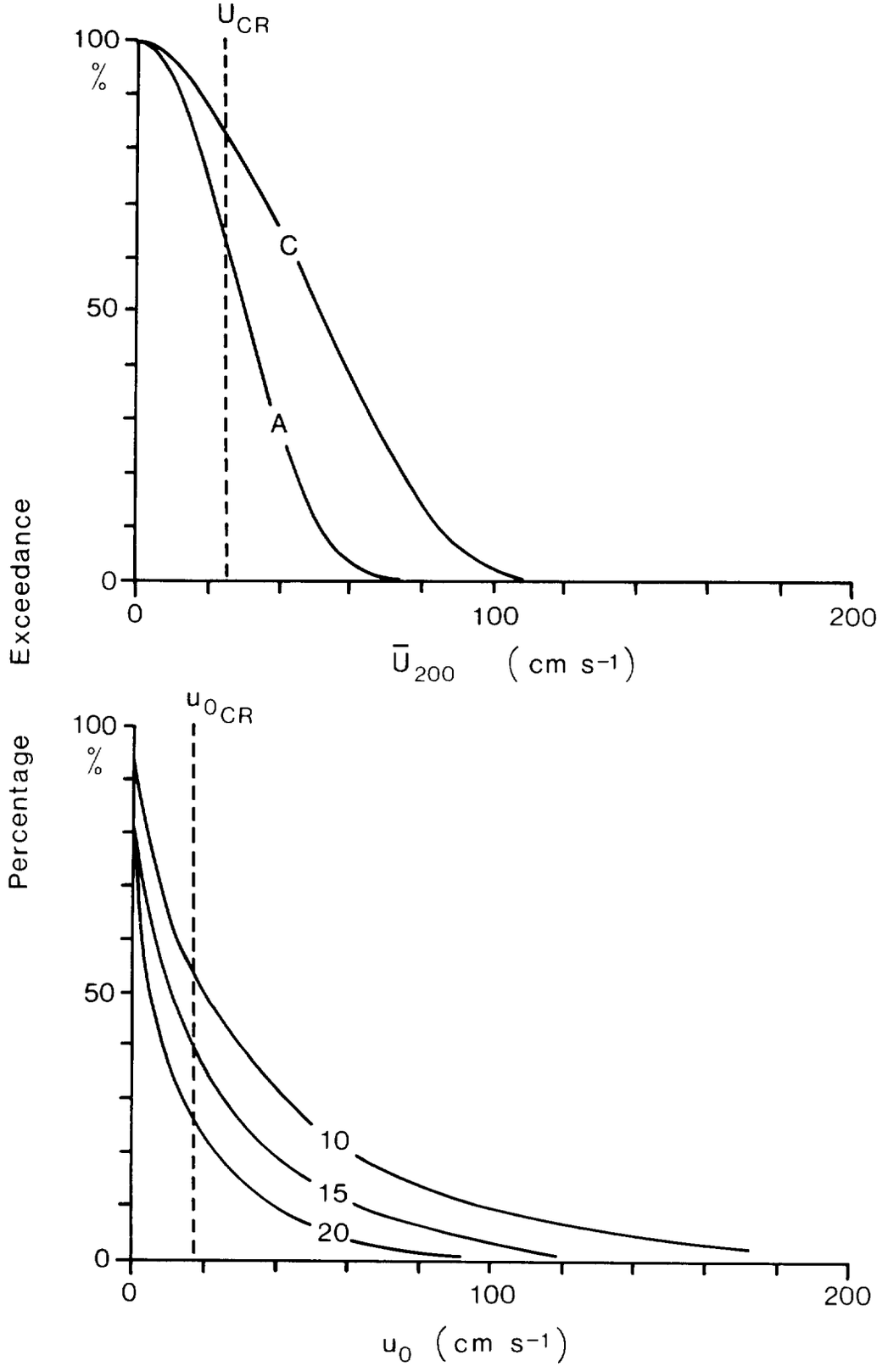
U_{CR}
100
%
50
0
C
A
Exceedance
0
100
200
$\bar{U}_{200}$ (cm s^{-1})
u_{0CR}
100
%
50
0
10
15
20
Percentage
0
100
200
u_0 (cm s^{-1})

Fig.21

Figure 22 Near-bottom tidal current exceedance curves, illustrating the variation in the proportion of time for which the threshold of sediment movement is exceeded, in moving offshore and alongshore from Port Talbot. The critical velocities (u_{cr}) have been calculated in the manner described in Appendix D. Figure 22 demonstrates the increased mobility of non-cohesive sediments in moving from the area of low tidal energy off Port Talbot, to the high tidal energy areas offshore (see Figure 23).

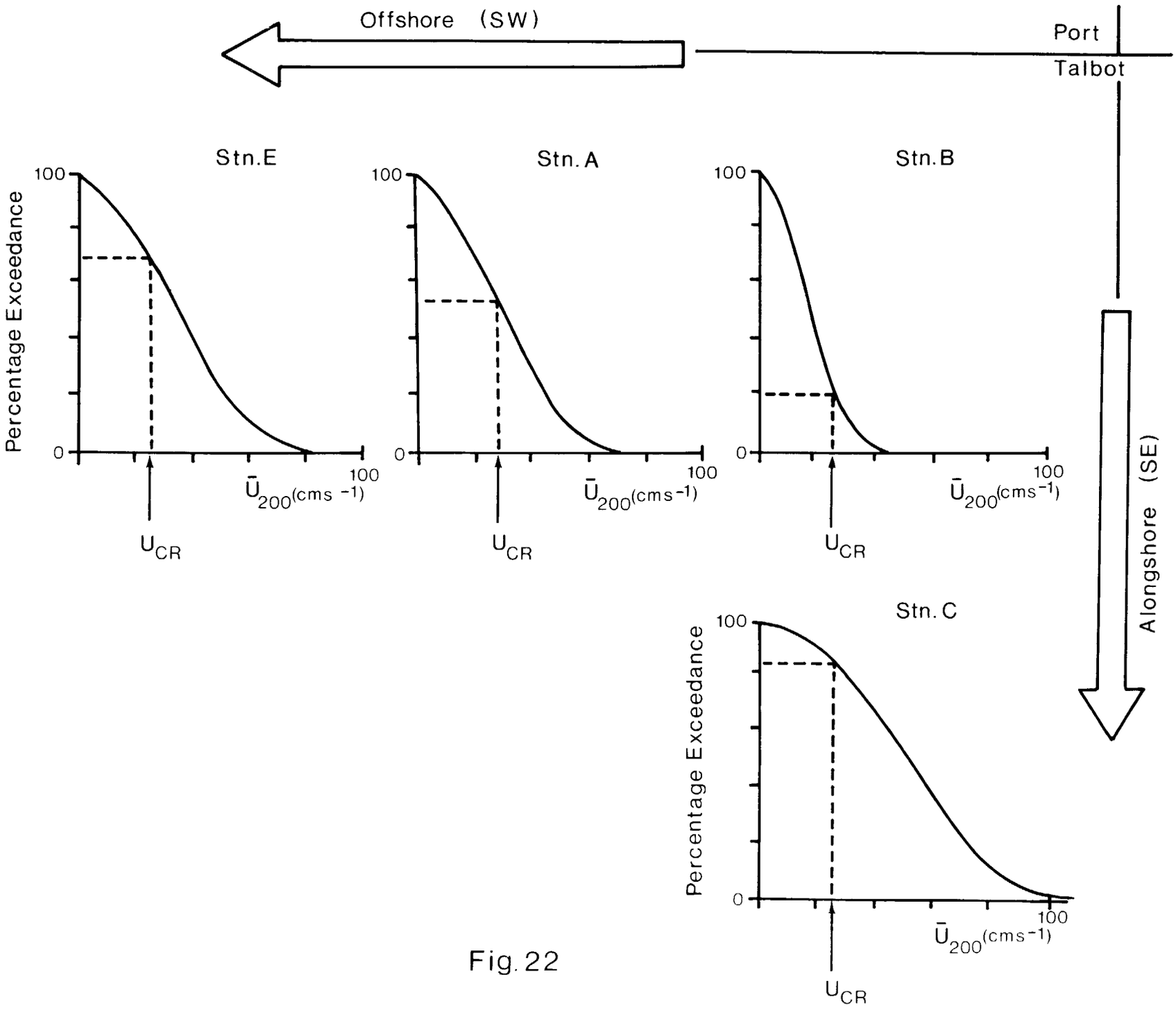
Offshore (SW)
Port
Talbot
Stn.E
Stn. A
Stn.B
Stn. C
Percentage Exceedance
100
0
100
$\bar{U}_{200(cms^{-1})}$
U_{CR}
Alongshore (SE)

Fig. 22

Figure 23 A schematic summary of sediment transport paths based upon the information presented in Figure 17, and the orientation of bedforms given by Collins et al (1979). The figure shows a two order of magnitude variation in bed load transport rates from about 2 tonnes m^{-1} day (figures in arrowheads) in the offshore areas to about .02 tonnes $m^{-1}day^{-1}$ in the vicinity of Port Talbot and Swansea. Important features are (a) the area of bed-load divergence to the S of Port Talbot and (b) the area of bed-load convergence in the vicinity of the Scarweather Sands. The broken arrows (c) indicate a possible wave induced transfer of material from the westward movement of sediment into the Bay.

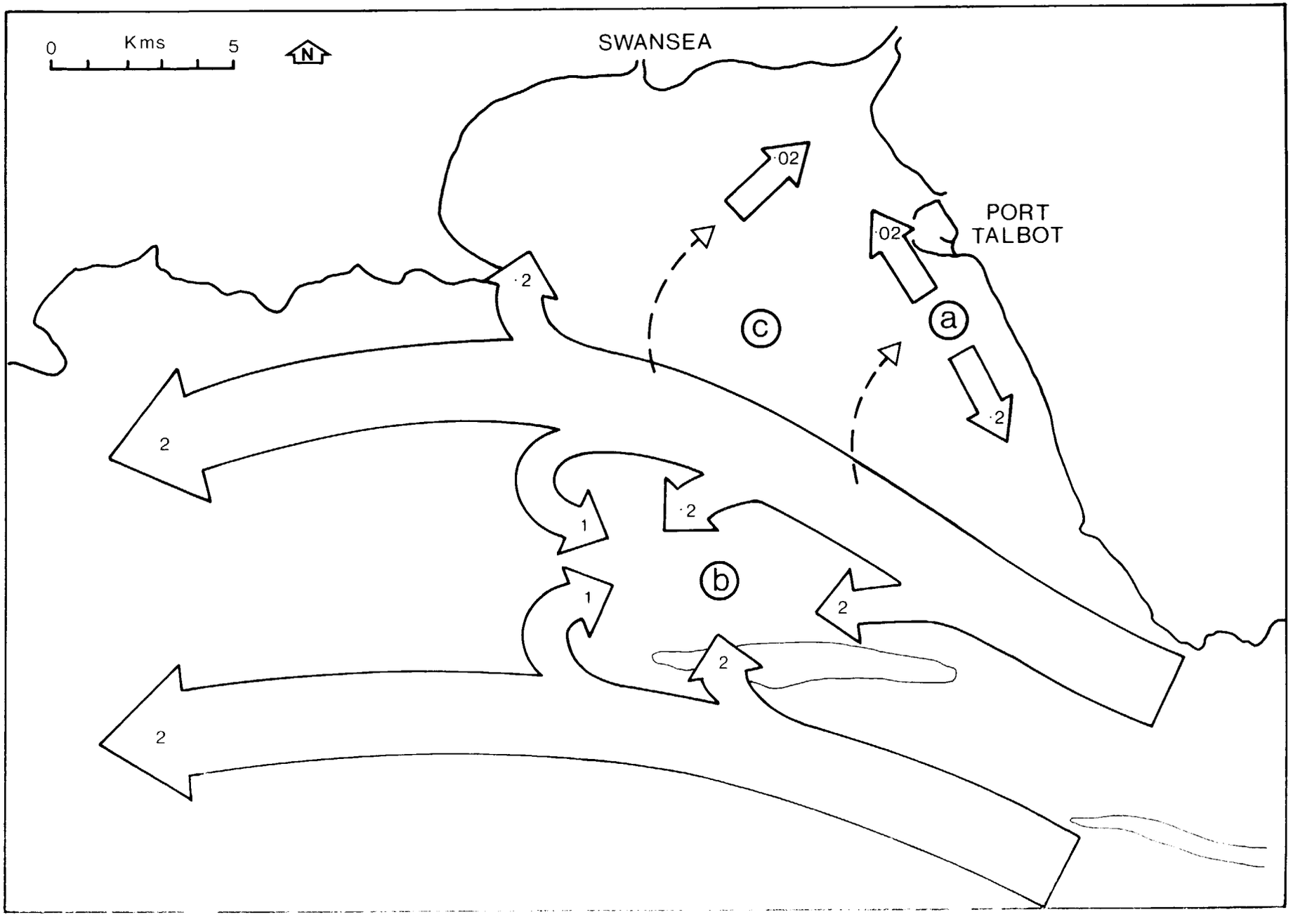

Fig.23

APPENDIX A

Grain size analyses.

The sediment transport formulae described in Appendix C of this report require either a d_{50} or d_{35} value to be specified. d_{50} is the median grain size while 35% of the sediment is finer than the d_{35} value.

Since this report is concerned with predicting the movement of sand size material of the type found on the foreshore on the E side of the Bay, it has been necessary to carry out grain size analyses of beach sediment samples to determine a typical d_{35} and d_{50} value. Similar analyses were carried out on a number of sediment samples from an area offshore and to the S of Port Talbot, to determine how similar these sediments were to those found on the foreshore.

The results of these grain size analyses are summarised in Tables A.1 and A.2.

In the calculation of sediment transport rates described in this report, d_{35} and d_{50} values of 150 and 170 μm respectively, have been used and assumed to be typical of the foreshore area and the offshore area in the vicinity of the Kenfig Patches, Hugo Bank and Scarweather Sands.

TABLE A.1

Grain size analyses

Mean d_{35} and d_{50} values for beach sediments.

Sample	Sorting	Grain sizes	
	S_o	$d_{35}(\mu m)$	$d_{50}(\mu m)$
RHW	1.30	172	185
RMW	1.35	155	175
RLW	1.49	123	141
PHW	1.22	165	180
PMW	1.30	168	185
PLW	1.34	161	185
NHW	1.25	176	192
NMW	1.29	163	182
NLW	1.43	143	165
LHW	1.21	183	195
LMW	1.48	172	198
LLW	1.29	97	108
ZHW	1.59	145	156
ZMW	1.36	125	135
ZLW	1.42	117	135
XHW	- a	- a	- a
XMW	1.29	165	182
XLW	1.26	135	144
VHW	1.44	210	233
VMW	1.41	162	180
VLW	1.51	120	137
THW	1.19	192	205
TMW	1.45	175	203
TLW	1.40	145	178
Mean values	$\overline{S_o}$ = 1.36	$\overline{d_{35}}$ = 155.17	$\overline{d_{50}}$ = 173.00

Notes: S_o calculated from $S_o = (d_{84}/d_{16})^{1/2}$

a: no analysis carried out

Prefix (eg R) denotes beach section (see Blackley, 1978, for details)

HW denotes High Water

MW denotes Mid Water

LW denotes Low Water

TABLE A.2

Grain size analyses

Mean d_{35} and d_{50} values for sediment in the vicinity of the Kenfig Patches and Scarweather Sands.

Sample	Sorting S_0		Grain sizes d_{35} (μm)		d_{50} (μm)	
GS6	2.01	a	260	a	332	a
GS11	1.12	b	142	b	147	b
BX6	1.54		122		140	
BX11	1.34		145		162	
BX12	1.22		157		168	
BX13	1.14		170		180	
BX14	1.14		155		158	
BX15	1.19		195		205	
BX16	1.16		170		182	
BX17	1.44		182		205	
BX19	1.16		142		152	
BX28	1.45		92		103	
BX29	1.33	b	145	b	158	b
BX33	1.44	b	105	b	120	b
BX35	1.55	a	145	a	166	a
BX36	11.29	a	4400	a	11800	a
BX38	2.25		11300		18800	
BX39	1.13		140		146	
BX40	1.11		133		137	
BX41	1.13		130		133	
BX42	1.66		145		180	
Mean values	$\bar{S}_0$ =1.25		$\bar{d}_{35}$ =149.53		$\bar{d}_{50}$ =161.07	

Notes: S_0 calculated from $S_0 = (d_{84}/d_{16})^{1/2}$

a: values omitted from mean calculations. Samples not well sorted.

b: values omitted from mean calculations. Samples outside area of interest.

GS denotes grab samples; BX denotes box-core samples.

Details of sample locations are given in Blackley (1978).

APPENDIX B

Calculation of measured sediment transport rates using the tracer balance method of Courtois and Sauzay (1966).

Tracer dispersion patterns (see Figure 5), corrected for the effects background and decay, were digitised (on a regular grid) and the centroids calculated from the expressions

$$\bar{x} = \frac{\sum_{i=1}^{M} x_i c_i}{\sum_{i=1}^{M} c_i} \quad \text{and} \quad \bar{y} = \frac{\sum_{i=1}^{M} y_i c_i}{\sum_{i=1}^{M} c_i}, \qquad \text{(B.1)}$$

where $\bar{x}$ and $\bar{y}$ are the position co-ordinates of the centroid and x_i and y_i are the position co-ordinates of the M concentration measurements c_i.

Sediment drift rates and directions were then calculated from the displacements of the centroids and the time elapsed between successive surveys. In order to obtain sediment transport rates from these data it is necessary to combine the measured sediment drift rates with an estimate of the depths to which tracer particles are incorporated in a notionally mobile sediment layer. This has been accomplished using the tracer balance method (Courtois and Sauzay, 1966; Courtois and Monaco, 1969).

The detector is assumed to have a reponse to tracer of unit activity per unit area buried in a thin layer at a depth z (taken as positive downwards) given by

$$f = f_0 e^{-\alpha z}, \qquad \text{(B.2)}$$

where f_0 is the response of the detector to unit activity per unit area at the surface (for the detector used in this study f_0 = 1.28 x 10^8 cps Ci^{-1} m^{-2}) and α is the adsorption coefficient. α depends on the density of the sediment and on the energy of the γ radiation. For Scandium-46 with the sediments in the area of this experiment, α has been taken as 17.5 m^{-1} (see later).

If the concentration of tracer as a function of depth in the sea-bed

is $C_T(z)$ then the output N of the detector is

$$N = \int_0^E C_T(z) f_0 e^{-\alpha z} dz , \qquad (B.3)$$

where E is the maximum depth of burial, referred to elsewhere in this report simply as the depth of burial.

To proceed it is necessary to assume a function for $C_T(z)$. Assuming first that the tracer is uniformly distributed down to a depth E, with none below, then $C_T(z)$ in (B.3) is a constant C_T giving

$$N = \frac{C_T f_0}{\alpha}(1 - e^{-\alpha E}) . \qquad (B.4)$$

The total activity per unit area is $C_T E$ which if it were all at the surface, would give a detector output N_0 of $f_0 C_T E$. Thus the effect of burial is to reduce the output of the detector by a factor

$$\frac{N}{N_0} = \frac{1 - e^{-\alpha E}}{\alpha E} . \qquad (B.5)$$

N is the actual measured output of the detector. By integrating it over the whole area and dividing it by f_0 we get an apparent total recovered activity of A. By assuming that the difference between this and the injected activity A_0 (with allowance being made for the decay of the radioactive element) is entirely due to burial, and that the depth of burial is constant (so that N/N_0 is constant), then

$$\frac{A}{A_0} = \frac{N}{N_0} \qquad (B.6)$$

and the depth of burial E can be calculated from (B.5).

If the concentration in the layer to E is not uniform but some other simple analytical function (eg linear or parabolic) then this can be inserted in (B.3) and integrated. Courtois and Sauzay introduced a factor Γ into the right hand side of (B.5) to account for these different profiles. For Iridium-192 they obtained an average value for Γ of 1.14, using $\alpha = 15.4 m^{-1}$ and burial depths of 0.05 to 0.10m. No figures for Scandium-46 are available, but since the values of α are comparable, so should be the values of Γ.

In this study due to the uncertainty in the form of the profile (see later discussion) Γ has been taken as unity. This is considered to be a reasonable assumption when considering the area as a whole and the diversity of sediment types and bedforms covered by the tracer. Thus E has been deduced graphically from (B.5) with $\Gamma = 1$, and the sediment transport rate $\bar{q}_{sb}$ per unit width calculated from,

$$\bar{q}_{sb} = \rho_B V E , \qquad (B.7)$$

where $\bar{q}_{sb}$ is the net or tidally averaged bed load transport, ρ_B is the bulk density of the sediment and V is the centroid velocity.

APPENDIX C

DETAILS OF SEDIMENT TRANSPORT FORMULAE AND COMPARISONS OF MEASURED AND PREDICTED TRANSPORT RATES.

C.1 Choice of sediment transport formulae

The choice of a suitable sediment transport formula for use in the marine environment is by no means clear for the following reasons:

(a) none have been developed specifically for use in the sea under oscillatory tidal currents,

(b) most are based on observations in unidirectional flows in rivers and flumes and finally

(c) none can intrinsically account for the effects of waves.

In standard texts on this subject Yalin (1972) lists 6 formulae, currently in use, Vanoni (1975) lists 13 and Graf (1971) describes 5. The most comprehensive comparisons of sediment transport formulae that we are aware of are those due to White (1972), Ackers and White (1973), White et al (1975, 1978), Flemming and Hunt (1976) and Swart (1976).

Ackers and White (1973) examined 15 sediment transport formulae and on the basis of comparisons with some 1000 observations developed a total load transport formula. This formula was examined independently by Swart (1976) and Flemming and Hunt (1976) who concluded that the Ackers and White formula gave the best agreement with observations.

However, Ackers and White's formula has not as far as we can determine been used previously for predicting transport rates under more or less open sea conditions and the only detailed comparisons of measured and predicted transport rates on the shelf, that we are aware of, are those due to Gadd et al (1978) who compared transport rates derived from radioactive tracer experiments with those predicted by Bagnold's (1963), Einstein's (1950) and Yalin's (1963) sediment transport formulae.

Our final choice of sediment transport formulae for comparisons of measured and predicted rates is summarised in Table 2 and included here for completeness:

TABLE C.1

Originator		Type	Load
Bagnold	1963	Deterministic	Bed
Yalin	1963	Deterministic	Bed
Einstein	1950	Stochastic	Bed
Ackers and White	1973	Deterministic	Total
Engelund and Hansen	1967	Deterministic	Total

These formulae were chosen on the basis of evidence presented by Swart (1976), Flemming and Hunt (1976) and Gadd et al (1978). Details of the formulae listed above are given in section C.2 of this report.

C.2 Details of sediment transport formulae

The following formulae (see Tables 2 and C.1) have been used to predict sediment transport rates from measurements of the mean flow at a height of 2m above the sea bed ($\bar{u}_{200}$). These formulae relate the transport rate to either the friction velocity u_*, the mean flow at a height of 1m above the sea bed, $\bar{u}_{100}$, the depth mean flow $\hat{u}$, or the critical shear stress τ_{cr}.

We have implicitly assumed the existence of a logarithmic velocity distribution, in the lower 2m of the flow, of the form

$$\bar{u}(z) = \frac{u_*}{\kappa} \ln \frac{z}{z_0} , \qquad (C.1)$$

to convert from $\bar{u}_{200}$ to the appropriate parameters (u_*, $\bar{u}_{100}$, $\hat{u}$, τ_{cr}). At each location z_0 has been prescribed using values given in Table 1 (see Section 4 of this report for discussion of the choice of z_0 values).

C.2.1 Einstein's (1950) bed load equation

Einstein's (1950) bed load equation differs in a number of ways from other formulae and in so doing achieves what is perhaps a more realistic representation of the physical processes of sediment transport. The important differences are:

(a) Einstein's equation is stochastic and relates sediment transport to random fluctuations in the velocity field rather than mean flow parameters.

(b) the difficulty of defining a threshold of sediment motion is avoided altogether in Einstein's equation.

According to Einstein (1950) the initiation of particle motion occurs when the instantaneous lift force is either greater than or less than the immersed weight of sediment. According to Einstein the probability (P) of this occurring is given by the normal error law

$$P = 1 - \frac{1}{\pi^{1/2}} \int_{-B_* \psi_* - 1/\eta_0}^{B_* \psi_* - 1/\eta_0} e^{-t^2} dt , \qquad \text{(C. 2)}$$

where η = .5 and B_* is a constant.

ψ_* is the 'flow intensity' given by

$$\psi_* = g\left(\frac{\rho_s - \rho}{\rho}\right) \frac{d}{u_*^2} . \qquad \text{(C.3)}$$

The bed load transport q_{sb} is then expressed in terms of a dimensionless bed load transport (ϕ) given by

$$\phi = \frac{q_{sb}}{\rho_s} \left(\frac{\rho}{(\rho_s - \rho) g d^3} \right)^{1/2} , \qquad \text{(C.4)}$$

which is related to the probability of particle motion occurring by

$$\frac{P}{1-P} = A_* \phi , \qquad \text{(C.5)}$$

where A_* is an empirically determined constant.

Thus the bed-load transport may be expressed in terms of P and A_* as

$$q_{sb} = \frac{P}{1-P} \cdot \frac{\rho_s}{A_*} \left(\frac{\rho_s - \rho}{\rho} \cdot g d^3 \right)^{1/2} . \qquad \text{(C.6)}$$

The coefficients A_* and B_* were originally obtained by Einstein using flume data and median particle sizes (d_{50}) of 0.785mm and 28.65mm (see Einstein, 1950, p37). This is considerably coarser than the sand size material found on the continental shelf and the size of material being examined in this study (d_{50} of order 150 - 200μm). Gadd et al (1978) found that the classically prescribed values of A_* and B_*

yielded predicted transport rates which differed from the extensive flume data compiled by Guy et al (1966). Gadd et al therefore recalibrated Eistein's equation against Guy et al's flume data to obtain values of A_* and B_* corresponding to the size of material which they were studying, which consisted of fine to medium sand in the range 110 - 560 μm. We have taken this particle size range to be sufficiently close to that being studied in this area, as to justify the use of Gadd et al's values of A_* and B_*. These are given in the table below together with Einstein's original values.

Gadd et al (1978)	Einstein (1950)
$A_* = 60.0$	$A_* = 43.5$
$B_* = 0.07$	$B_* = 0.143$
$d_{50} = 110 - 560 \mu m$	$d_{50} = 785 - 2865 \mu m$

To calculate q_{sb} using equation (C.6) it is necessary to evaluate the integral

$$\frac{1}{\pi^{1/2}} \int_{-B_* \psi_* - 1/\eta_0}^{B_* \psi_* - 1/\eta_0} e^{-t^2} dt .$$

Writing

$$\rho = -(B_* \psi_* + 1/\eta_0) \qquad (C.7)$$

and

$$q = (B_* \psi_* - 1/\eta_0) , \qquad (C.8)$$

we obtain

$$\frac{1}{\pi^{1/2}} \int_{\rho}^{q} e^{-t^2} dt = \frac{1}{\pi^{1/2}} \left(\int_0^q e^{-t^2} dt - \int_0^\rho e^{-t^2} dt \right),$$

$$= \frac{1}{2} (\operatorname{erf} q - \operatorname{erf} \rho) .$$

The error functions $\operatorname{erf} q$ and $\operatorname{erf} \rho$ were evaluated using a rational approximation (see Abramowitz and Stegun, 1965) as follows:

$$\operatorname{erf} x = \frac{2}{\pi^{1/2}} \int_0^x e^{-t^2} dt = 1 - (a_1 t + a_2 t^2 + a_3 t^3) e^{-x^2} + \epsilon(x)$$

where $t = 1/(1 + rx)$, $r = .47047$, $a_1 = .3480242$,

$a_2 = 0.0958798$ and $a_3 = 0.7478556$.

This expression gives an error in $erf\ x$ of the order $|\epsilon(x)| \leq 2.5 \times 10^{-5}$.

C.2.2 Bagnold's(1963) bed load equation

Bagnold's (1963) original formula expresses the bed load transport rate q_{sb} in terms of the stream power, ω, and an efficiency factor K. That is

$$q_{sb} = \frac{\rho_s}{(\rho_s - \rho)g} \cdot K\omega . \tag{C.9}$$

The power per unit area expended on the sea bed by the fluid, ω, can be expressed as

$$\omega = \tau u_* , \tag{C.10}$$

which since $\tau = \rho u_*^2$ may also be written as,

$$\omega = \rho u_*^3 . \tag{C.11}$$

This expression forms the basis of the dynamical arguments outlined in section 2 of this report. The efficiency factor K was originally thought to depend only on sediment characteristics (see Bagnold, 1963). However, it has recently been shown by Kachel and Sternberg (1971) that K depends not only on the grain size but also on the excess shear stress $(\tau - \tau_{cr})/\tau_{cr}$, where τ_{cr} is the threshold shear stress, ie that stress at which initial motion occurs. This dependence has been removed by Gadd et al (1978), who, using the flume data of Guy et al (1966) expressed (C.9) in terms of the mean flow at a height of 1m above the sea bed ($\bar{u}_{100}$) and a threshold velocity (u_{cr}) so obtaining

$$q_{sb} = \beta(\bar{u}_{100} - u_{cr})^3 , \tag{C.12}$$

where β is a constant obtained from flume data.

Bagnold's original expression (equation C.9) contains no threshold condition and predicts sediment motion at all flow speeds. From a physical point of view this must be regarded as something of a shortcoming and the

formulation proposed by Gadd et al (1978) goes some way towards overcoming this difficulty.

Gadd et al obtained two values of β from Guy et al's (1966) flume data, for different grain sizes. These are as follows:

d_{50} = 180 μm	d_{50} = 450 μm
β = 7.22 x 10^{-5}	β = 1.73 x 10^{-5}
u_{cr} = .16m s^{-1}	u_{cr} = .19m s^{-1}

In this study we have taken a value of β = 7.22 x 10^{-5} corresponding to d_{50} = 180 μm, as being most representative for the Swansea Bay area, (note : β has dimensions gm cm^{-4} s^{-2}).

C.2.3 Yalin's (1963) bed load equation

Yalin's (1963) formula is one of the simplest to apply and considers the average lift forces exerted on a sediment particle. In Yalin's theory particles are assumed to move over the bed by saltation and any increase in transport is brought about by an increase in the particle path length and not necessarily an increase in the number of particles. The existence of a critical shear stress is assumed. Yalin thus obtained a bed load transport rate q_{sb} given by

$$q_{sb} = .635\, g(\rho_s - \rho)\, d\, u_* \, s\left[1 - \frac{1}{as}\ln(1+as)\right], \qquad (C.13)$$

where

$$a = 2.45\left(\frac{\rho}{\rho_s}\right)^{.4}\left(\frac{\tau_{cr}}{[\rho_s - \rho]\, g\, d}\right)^{1/2} \qquad (C.14)$$

is a constant for given values of d and τ_{cr}.

s is the non-dimensional excess shear stress given by

$$s = (\tau - \tau_{cr})/\tau_{cr} . \qquad (C.15)$$

Gadd et al (1978) found that Yalin's formula (equation C.13) calibrated for a grain size of 450 μm, gave good agreement with Guy et al's (1966) flume data for grain sizes of 190 and 450 μm at velocities near threshold. For higher velocities the predicted values are less than those obtained in the flume experiments. However, despite this difficulty we have used the empirically determined constants as they appear in equations (C.13) and (C.14).

Strictly speaking Yalin's formula (equation C.13) is restricted to plane beds, to fully developed turbulent flows and to large depth/diameter (h/d) ratios.

It is particularly instructive to examine the limiting values of equation (C.13) since these illustrate the range of power law dependencies referred to in section 2 of this report.

Case 1. Low transport rates, ie $as \to 0$

By expanding the term $\ln(1+as)$ in equation (C.13) as a series we obtain

$$\frac{1}{as}\ln(1+as) = \frac{1}{as}\left[as - \frac{(as)^2}{2} + \frac{(as)^3}{3} - \frac{(as)^4}{4} \cdots\right] \qquad (C.16)$$

$$= 1 - \frac{as}{2} + \quad \text{..... smaller terms.} \qquad (C.17)$$

$$\therefore \lim_{as\to 0}\left[\frac{1}{as}\ln(1+as)\right] \simeq 1 - \frac{as}{2} . \qquad (C.18)$$

Thus equation (C.13) becomes

$$q_{sb} \simeq .635\, g d (\rho_s - \rho)\left(\frac{\tau}{\rho}\right)^{1/2}\frac{as^2}{2}, \qquad (C.19)$$

which, since $\tau \propto u_*^2$ and $s \propto u_*^2$, gives

$$q_{sb} \propto u_*^5 . \qquad (C.20)$$

Case 2. High transport rates, ie $as \to \infty$

Consider the term $\frac{1}{as}\ln(1+as)$. Applying L'Hospital's rule (see Yalin, 1972) to the limit gives

$$\lim_{as\to\infty}\left[\frac{1}{as}\ln(1+as)\right] \simeq 0 . \qquad (C.21)$$

Thus

$$q_{sb} \simeq .635\, g d (\rho_s - \rho)\left(\frac{\tau}{\rho}\right)^{1/2} s, \qquad (C.22)$$

which since $\tau \propto u_*^2$ and $s \propto u_*^2$ gives

$$q_{sb} \propto u_*^3. \qquad (C.23)$$

C.2.4 Ackers and White's (1973) total load formula

It is beyond the scope of this report to review in full the derivation of Ackers and White's formula. Full details of the theory and calibration techniques can be found elsewhere, eg Ackers, (1972), White, (1972), Ackers and White, (1973), White et al,(1975), White et al, (1978).

The general function of Ackers and White is one of the most recent and comprehensive transport formulae to be developed. It is based on physical and dimensional considerations and expressed in terms of three dimensionless groups as follows:

$$G_{gr} = C\left\{\frac{F_{gr}}{A} - 1\right\}^m, \qquad (C.24)$$

where G_{gr} is the dimensionless sediment transport given by

$$G_{gr} = \frac{c}{\varrho_s}\frac{d}{a}\left(\frac{u_*}{v}\right)^n. \qquad (C.25)$$

Here c is the concentration by weight of sediment which is related to the total load transport rate q_{st} by $q_{st} = cq$.

F_{gr} is a dimensionless mobility given by

$$F_{gr} = \frac{u_*^n}{(gd[\frac{\varrho_s}{\varrho} - 1])^{1/2}}\left(\frac{v}{2.46\, d \ln(10h/d)}\right)^{1-n}. \qquad (C.26)$$

The coefficients A, C, m and n are given in terms of a dimensionless grain size

$$D_{gr} = d\left\{\frac{g(\varrho_s/\varrho - 1)}{\nu^2}\right\}^{1/3}. \qquad (C.27)$$

For coarse sediments ($D_{gr} > 60$) these four coefficients take the following values:

$A = 0.170$

$C = 0.025$

$m = 1.50$

$n = 0.0$

For the transitional sizes ($1 \leq D_{gr} \leq 60$)

$$A = \frac{0.23}{D_{gr}} + 0.14 , \tag{C.28}$$

$$\log C = 2.86 \log D_{gr} - (\log D_{gr})^{1/2} - 3.53 . \tag{C.29}$$

The dimensionless parameters F_{gr} , D_{gr} and G_{gr} may be expressed as follows:

$$F_{gr} = \left(\frac{\text{shear forces}}{\text{immersed weight}}\right)^{\frac{1}{2}} ,$$

$$D_{gr} = \left(\frac{\text{immersed weight}}{\text{viscous forces}}\right)^{\frac{1}{3}} ,$$

$$G_{gr} = \left(\frac{\text{shear forces}}{\text{immersed weight}}\right) . E , \tag{C.30}$$

where E is an efficiency of transport based upon the work done in moving the material per unit time and the total stream power.

The coefficients n and A have physical meaning. The coefficient n relates to the transition zone of particle size; For fine sediment $n = 1$ ($D_{gr} = 1$) and correlation of F_{gr} and G_{gr} (ie of the sediment transport) is with the total shear measured in terms of the friction velocity u_* ; For coarse sediments $n = 0$ ($D_{gr} \geq 60$) and correlation of F_{gr} and G_{gr} is with grain shear, measured in terms of skin fricition velocity, $\hat{u}$ and λ/a being the representative variables.

The important points which emerge from Ackers and White's formula may be summarised as follows:

(1) A general sediment transport function has been developed in terms of three dimensionless groups:

(a) the dimensionless grain size D_{gr}

(b) the dimensionless grain mobility F_{gr}

(c) the dimensionless sediment transport G_{gr}

The function is based upon almost 1000 flume experiments in flow depths up

to .4m.

(2) The function may be applied in the range $1 < D_{gr} < 60$ that is for particle sizes d in the range $40 < d < 4000 \mu m$.

(3) On the basis of correlations with observed transport rates it has been found that the transport of fine materials is best related to the gross shear, friction velocity (u_*) being the representative variable, and that the transport of coarse material is best related to the net grain shear, depth mean velocity ($\hat{u}$) being the representative variable.

(4) The new function is based upon experiments in which there was established sediment motion and the equations forecast initial movement conditions which give reasonable agreement with previous investigations of incipient motion.

(5) The relationships are <u>not</u> sensitive to bed form and may be applied to plain, rippled and duned configurations up to an upper phase transport limit given by Froude numbers $F_r > 0.8$.

(6) The new function incorporates a transition exponent, n , which effects the change from friction velocity u_* to the depth mean velocity $\hat{u}$ through an intermediate range of particle sizes.

C.2.5 Engelund and Hansen's (1967) total-load formula

Engelund and Hansen's (1967) formula expresses the total load transport q_{st} in terms of a friction factor C_f , a dimensionless sediment discharge ϕ and a dimensionless bed shear stress τ . Thus

$$C_f \phi = 0.1 \theta^{5/2}, \tag{C.31}$$

where

$$C_f = 2 u_*^2 / \hat{u}^2, \tag{C.32}$$

$$\phi = \frac{q_{st}}{\rho_s \left(g \left(\frac{\rho_s}{\rho} - 1 \right) d_{50}^3 \right)^{1/2}} \tag{C.33}$$

and

$$\theta = \frac{\tau}{(\rho_s - \rho) g d} . \tag{C.34}$$

To apply this formula it is necessary to specify the friction velocity u_* and the depth mean flow $\hat{u}$. These quantities have been calculated from an assumed logarithmic velocity profile (see equation 11) and assumed roughness length z_o as described in section 4.1 of this report.

C.3 Comparisons of measured and predicted transport rates

Near bottom current measurements from Station A in Swansea Bay (the long-term mooring, see Figure 3) have been used to predict sediment transport rates for comparison with those measured with radioactive tracers at position T2, approximately 1km to the E where it has been assumed that the hydraulic regime is similar to that at Station A (tracer measurements could not of course be made at Station A due to the risk of radioactive contamination of the current meter mooring). A similar comparison has been carried out between the tracer measurements at position T1 and the current measurements at Station C. This latter comparison is considered to be less reliable due to the distance between the current meter mooring and the tracer injection site (approximately 3kms). It should be noted that comparisons of the various sediment transport formulae has been made in terms of net or tidally averaged quantities, since the radioactive tracer experiments can only provide information of this type. The net sediment transport rates are thus the resultants obtained by vector averaging each current meter record, converted to sediment transport rates and direction, over many tidal cycles.

In this study we have been concerned principally with predicting the movement of material of the type found on the foreshore in the sedimentary system as a whole. Sediment distribution maps (see Figure 2) show that material of this size is also found offshore in an area to the south of the beach and the results of some grain size analyses (see Appendix A) from these two areas show that the mean grain sizes of the surficial deposits are broadly similar (see Table A1 and A2).

Bagnold's, Yalin's, Einstein's and Engelund and Hansen's formula require the specification of a median grain size (d_{50}) whereas Ackers and White's formula requires the specification of a d_{35} grain size, that is that size for which 35% of the material is finer.

Comparisons of predicted and observed sediment transport rates are shown in Figure 6. This shows the vector mean rates predicted from near bottom current measurements ($\overline{u_{200}}$) at Stations A and C over a period of approximately 2 years, and the measured transport rates from tracer

observations at T2 and T1.

It is apparent from these observations (see Figure 6) that there is very nearly a two order of magnitude spread in the transport rates predicted by the five formulae listed in Table 2. Figure 6 shows that in the deeper parts of the Bay as typified by tracer injection site T2, Ackers and White's (1973) total load formula consistently underestimates the measured rates whereas Bagnold's (1963) bed load formula yields the highest estimates. At tracer injection site T1, typical of the shallower environments of the Bay it is apparent that Ackers and White's (1973) formula gives considerably higher estimates which are in closer agreement with Bagnold's formula and with the measured transport rates from radioactive tracer experiments.

Of these predictions Bagnold's (1963) fall consistently within limits which are (approximately) a factor of 2 higher or lower than the observed transport rates (see Table 3). In fact, bearing in mind that the comparisons are between tidally averaged or net transport rates, this agreement is remarkably good. However, as remarked previously, in the absence of tracer estimates and in terms of median performance Engelund and Hansen's (1967) or Einstein's (1950) formula might well have been chosen. Indeed the higher measured rates may simply be a reflection of the effects of wave activity which cannot be accounted for in any of the formulae used here.

It is interesting to note that Ackers and White's (1973) formula, widely considered to be the most successful formula produced to date, gives the poorest comparisons with the observed transport rates.

APPENDIX D

Calculation of critical friction velocities for use in sediment transport formulae

Yalin (1972, p82) gives the critical friction velocity u_{*cr} in terms of a modified Shields' (1936) function

$$Y_{cr} = \Phi(X_{cr}), \qquad (D.1)$$

where Y_{cr} is determined graphically from values of X_{cr} calculated from the expression

$$X_{cr} = \left(\frac{g(e_s - e)\alpha^3}{e\nu^3}\right)^{1/2}. \qquad (D.2)$$

Thus u_{*cr} is given by

$$u_{*cr} = \left(Y_{cr} \cdot \frac{g(e_s - e)\alpha}{e}\right)^{1/2}. \qquad (D.3)$$

Here ν is the kinematic viscosity of the fluid and the remaining terms have their usual meanings. ν will depend on temperature of the sea and taking a mean value for the area of 10°C (which is lower than the annual mean figure of 11.5°C given by Bowden (1955) for the outer Bristol Channel) gives a value of $\nu = .01278 cm^2 s^{-2}$.

The computer calculation of sediment transport rates requires the specification of a critical velocity u_{cr}. This has been calculated from the critical friction velocity (u_{*cr}) obtained from Yalin's (1972) modified Shields' curve and equations (D.1) to (D.3). These give a value of u_{*cr}, for grain sizes in the range 100 - 200 μm, of $1.31 cm\ s^{-1}$. This value has been used to calculate u_{cr} at heights corresponding to those at which the current measurements were made and either converted to the critical velocity at a height of 100cm above the sea bed (ie Bagnold's (1963) formula) or converted to a critical bed shear stress τ_{cr} (ie Yalin's (1963) formula) as appropriate. This conversion was carried out using an assumed logarithmic velocity profile and appropriate roughness length. The range of u_{cr} and z_0 values used in this study is summarised in Table D1. It should be noted that the u_{cr} figures have

been rounded up or down to the nearest whole figure, the recording current meters only giving flow speeds to the nearest whole figure (see Table 1).

TABLE D.1

Values of the critical velocity (u_{cr}) and roughness length (z_o) used in this study for grain sizes in the range 100 - 200 μm

	z_o (cm)	u_{cr} (cm s^{-1}) .05cm	.1cm	.5cm
z (cm)				
100		24.89	22.62	17.35
200		27.16	24.89	19.62
300		28.49	26.22	20.95

Notes: z corresponds to the height of the flow measurement.

See Table 1 for summary of z_o and u_{cr} values in relation to sediment types and the positions of current meter moorings.

APPENDIX E

Smoothed progressive vector diagrams for residual sediment movements in Swansea Bay. Sediment transport rates have been calculated using Bagnold's (1963) formula (see Appendix C)

Figure	Station
E1.1 - E1.2	A
E2.1 - E2.2	B
E3.1 - E3.2	C
E4.1	D
E5.1 - E5.2	E
E6.1 - E6.2	F
E7.1	G
E8.1 - E8.2	H
E9.1	I
E10.1	J
E11.1	K

Notes: (1) the header code on each progressive vector diagram indicates the following;

eg 629F6	:	File name
6:6:76	:	Date record starts
SWB	:	Area (eg Swansea Bay)
A	:	Station
2M	:	Height above sea bed in metres
B SED	:	Sediment transport formula used in calculations.

(2) the scales of the progressive vector diagrams are not the same.

629F6 6:6:76 SWB : A : 2M : B SED

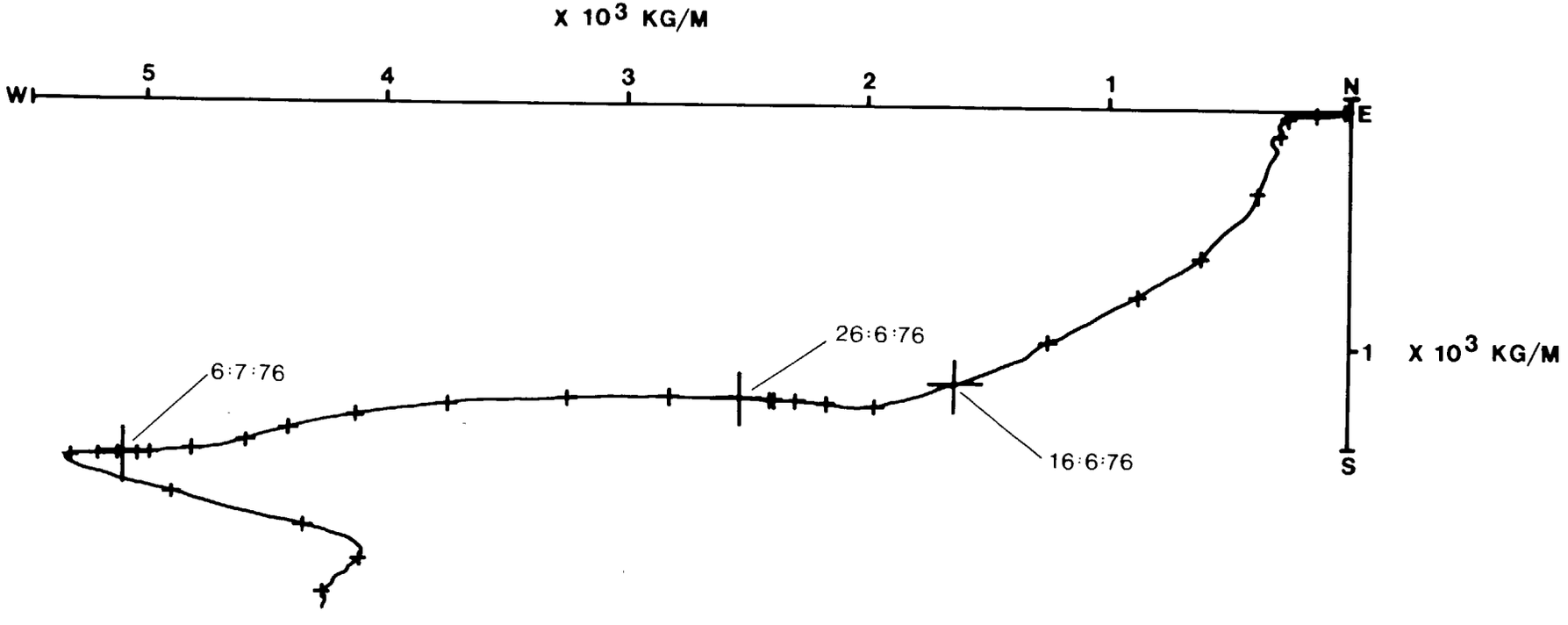

100

Fig. E1.1

680M6 4:12:76 SWB : A : 2M : B SED

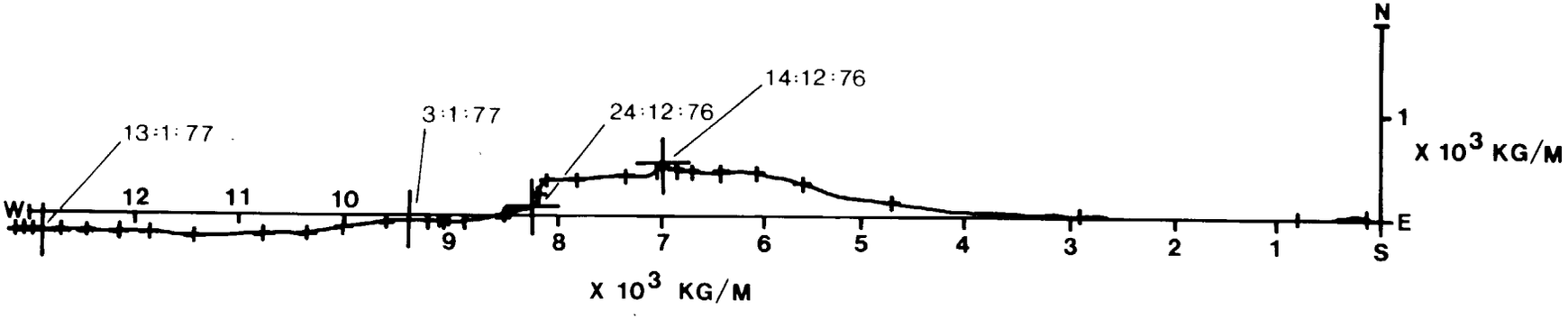

Fig. E1.2

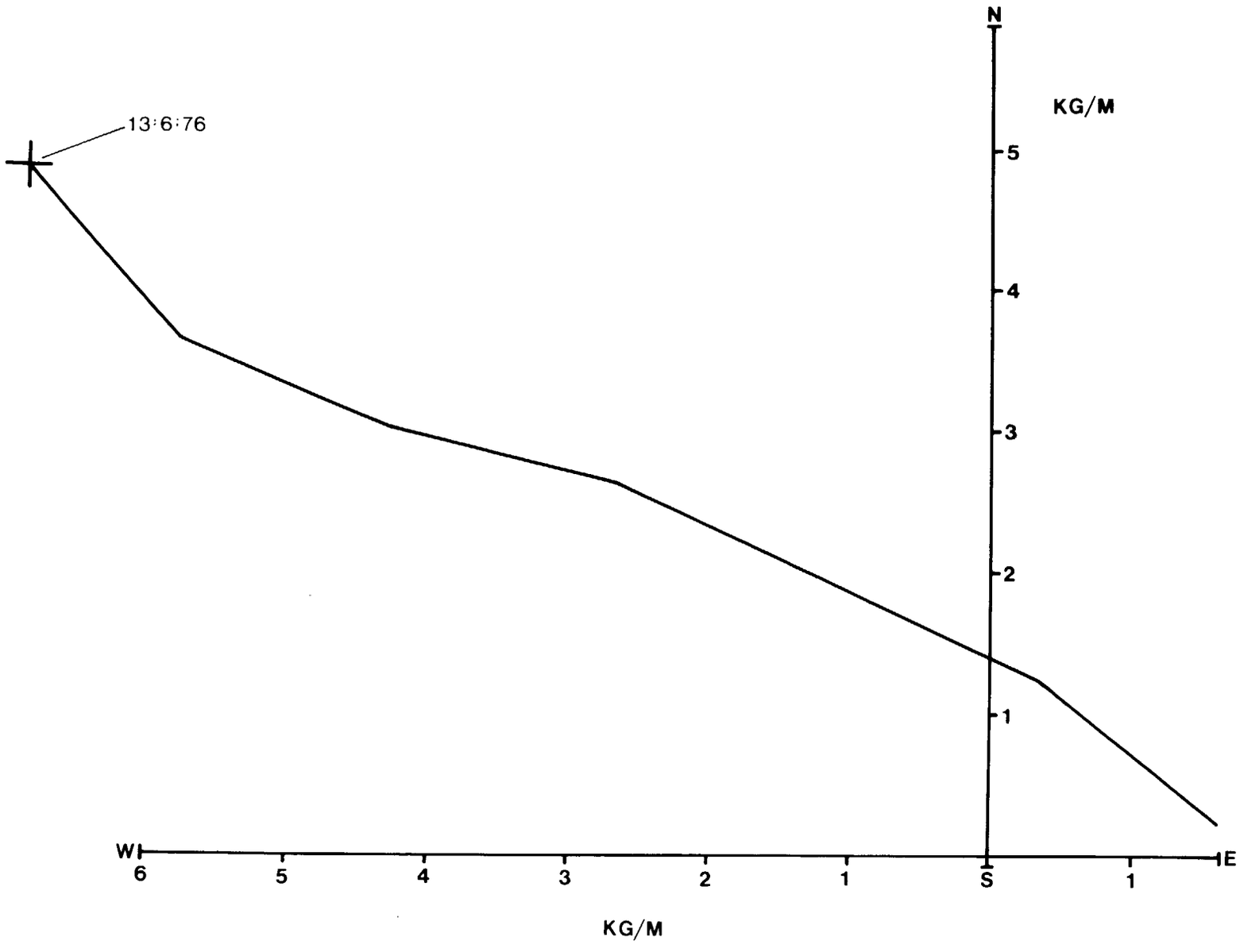

Fig. E 2.1

680K6 29:10:76 SWB:B:2M:B SED

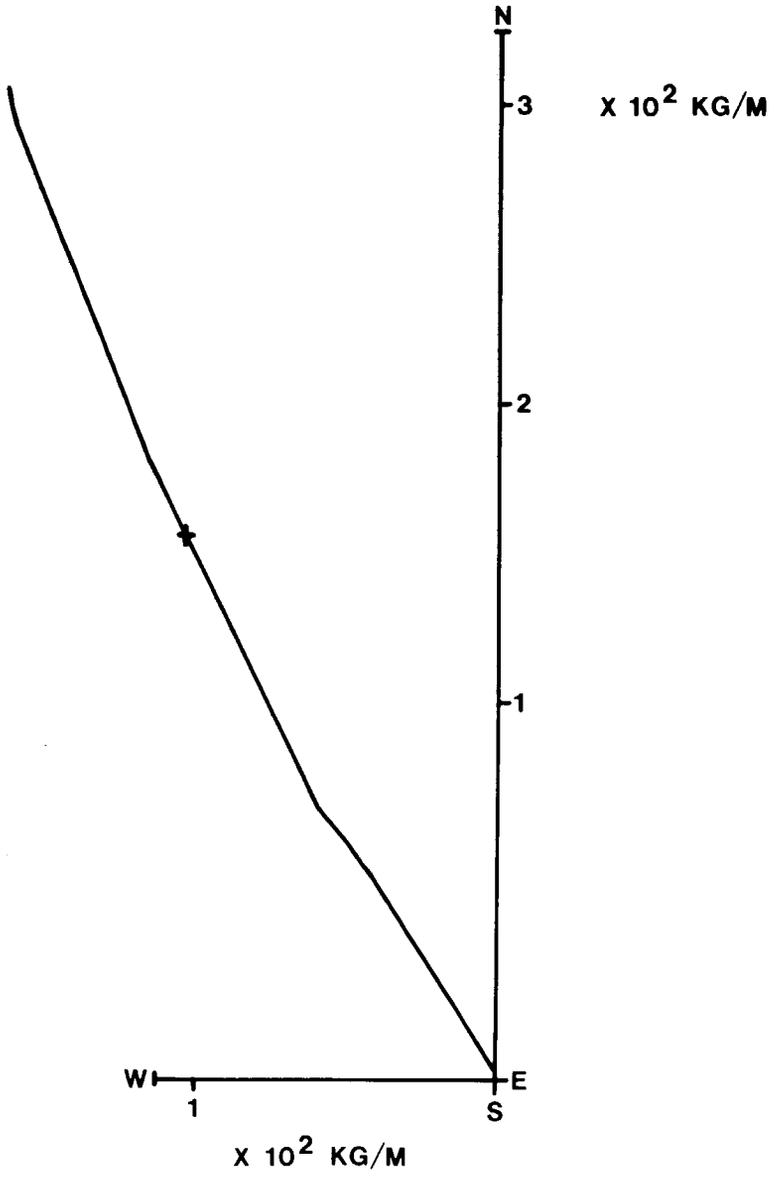

Fig. E 2.2

667 F6 6:6:76 SWB : C : 2M : B SED

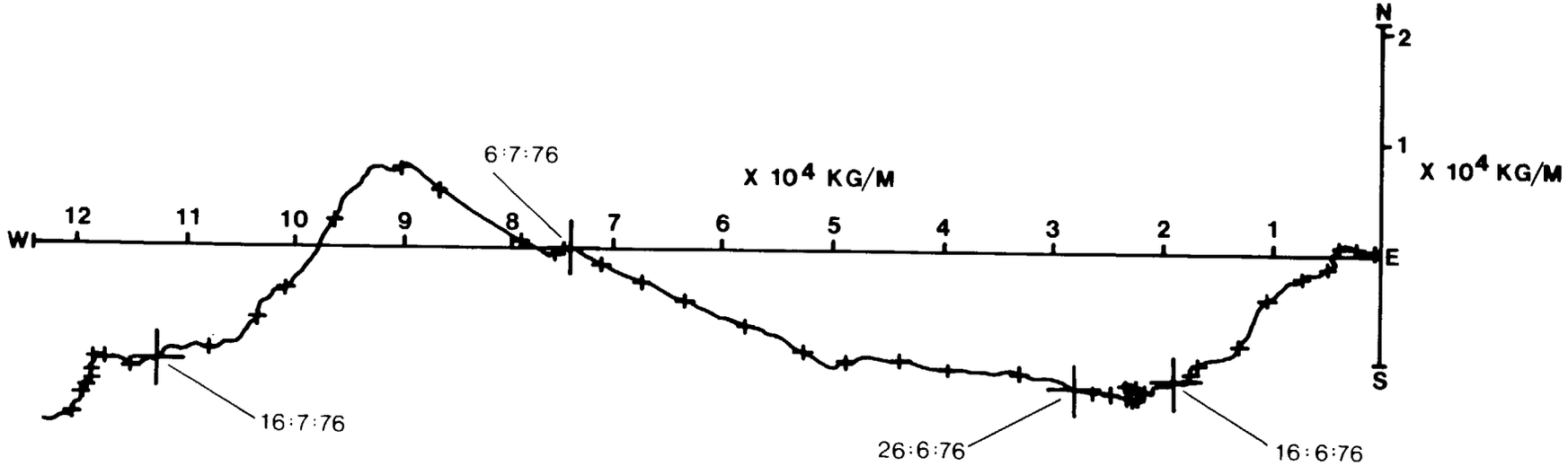

Fig. E 3.1

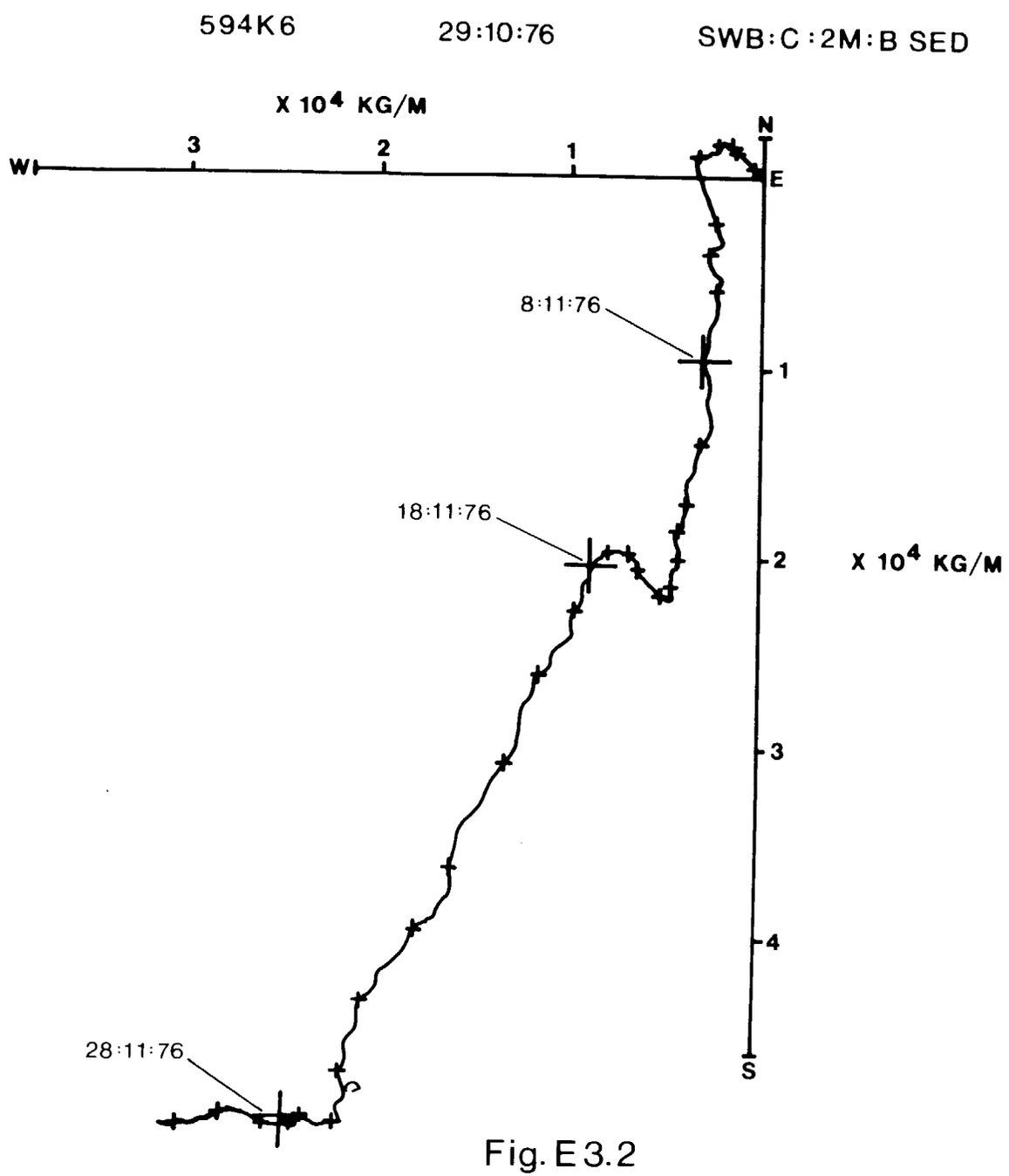
594K6
29:10:76
SWB:C:2M:B SED
X 10⁴ KG/M
3
2
1
W
N
E
8:11:76
18:11:76
28:11:76
1
2
3
4
S
X 10⁴ KG/M

Fig. E3.2

877F6 4:6:76 SWB : D:2M : B SED

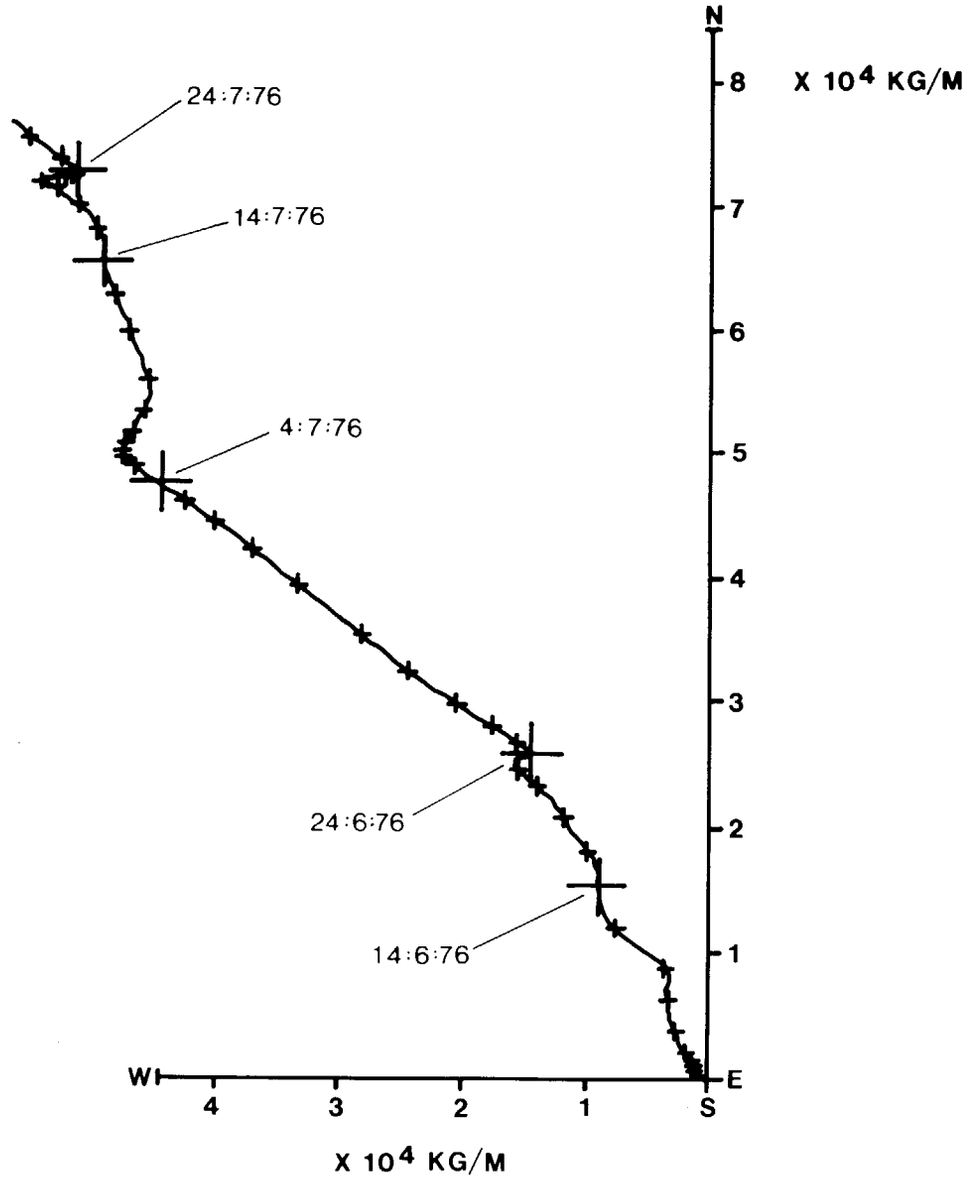

Fig. E 4.1

878 F 6 4:6:76 SWB : E : 2M : B SED

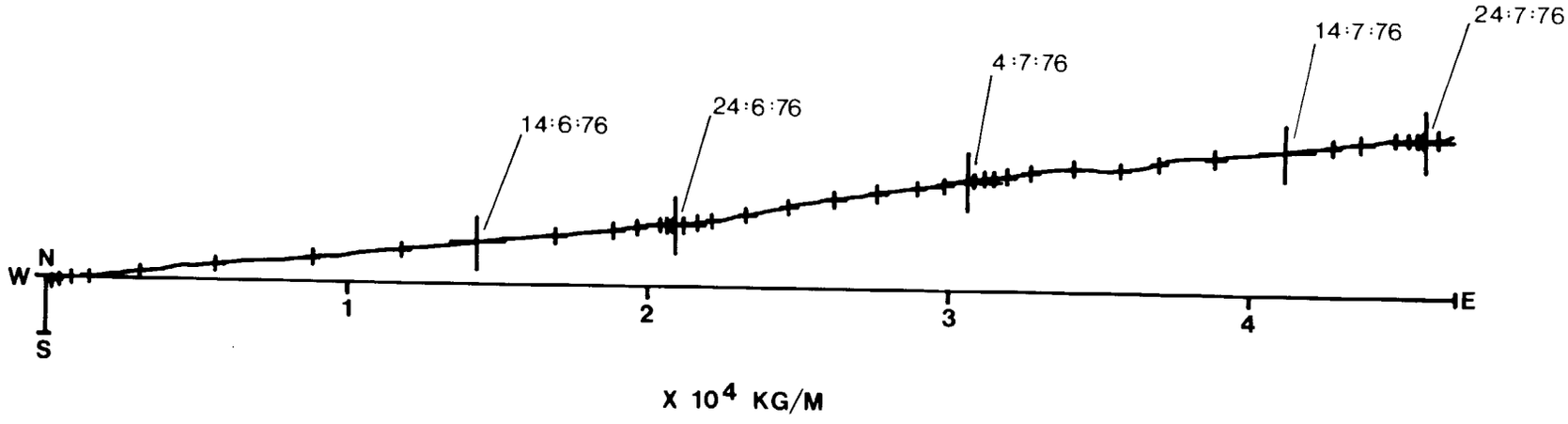

Fig. E 5.1

667K6 26:10:76 SWB : E : 2M : B SED

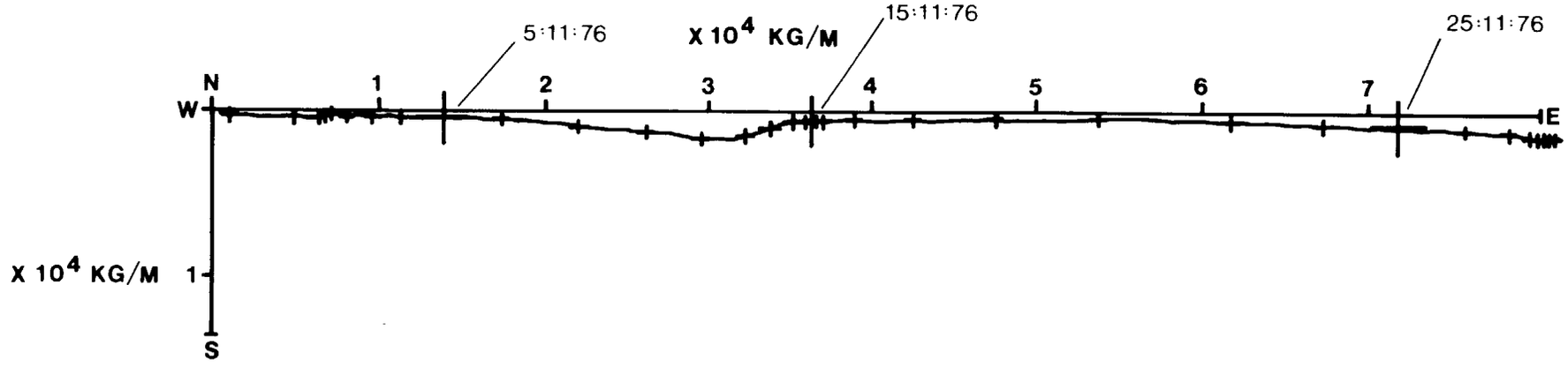

Fig. E5.2

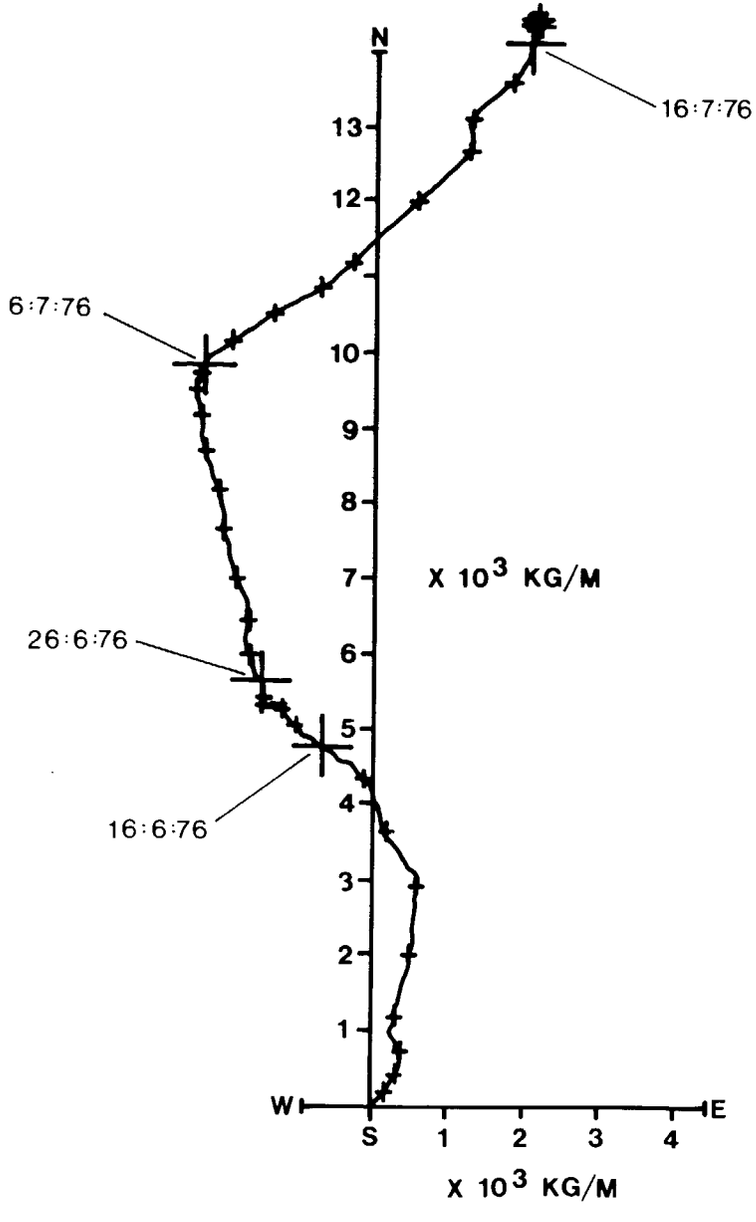
N
13
12
10
9
8
7
6
5
4
3
2
1
W
S
1
2
3
4
E
X 10³ KG/M
X 10³ KG/M
16:7:76
6:7:76
26:6:76
16:6:76

Fig. E 6.1

560L6 8:11:76 SWB : F : 2M : B SED

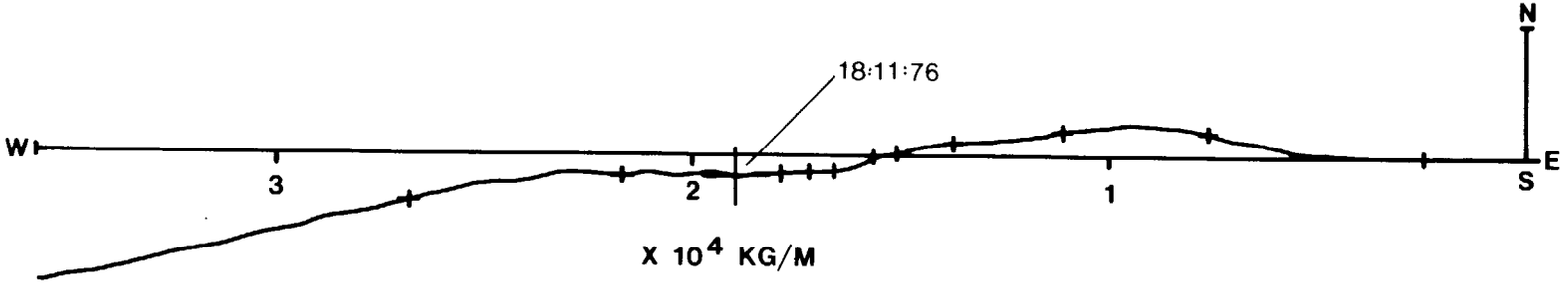

Fig. E6.2

573K5 16:10:75 SWB:G:1M:B SED

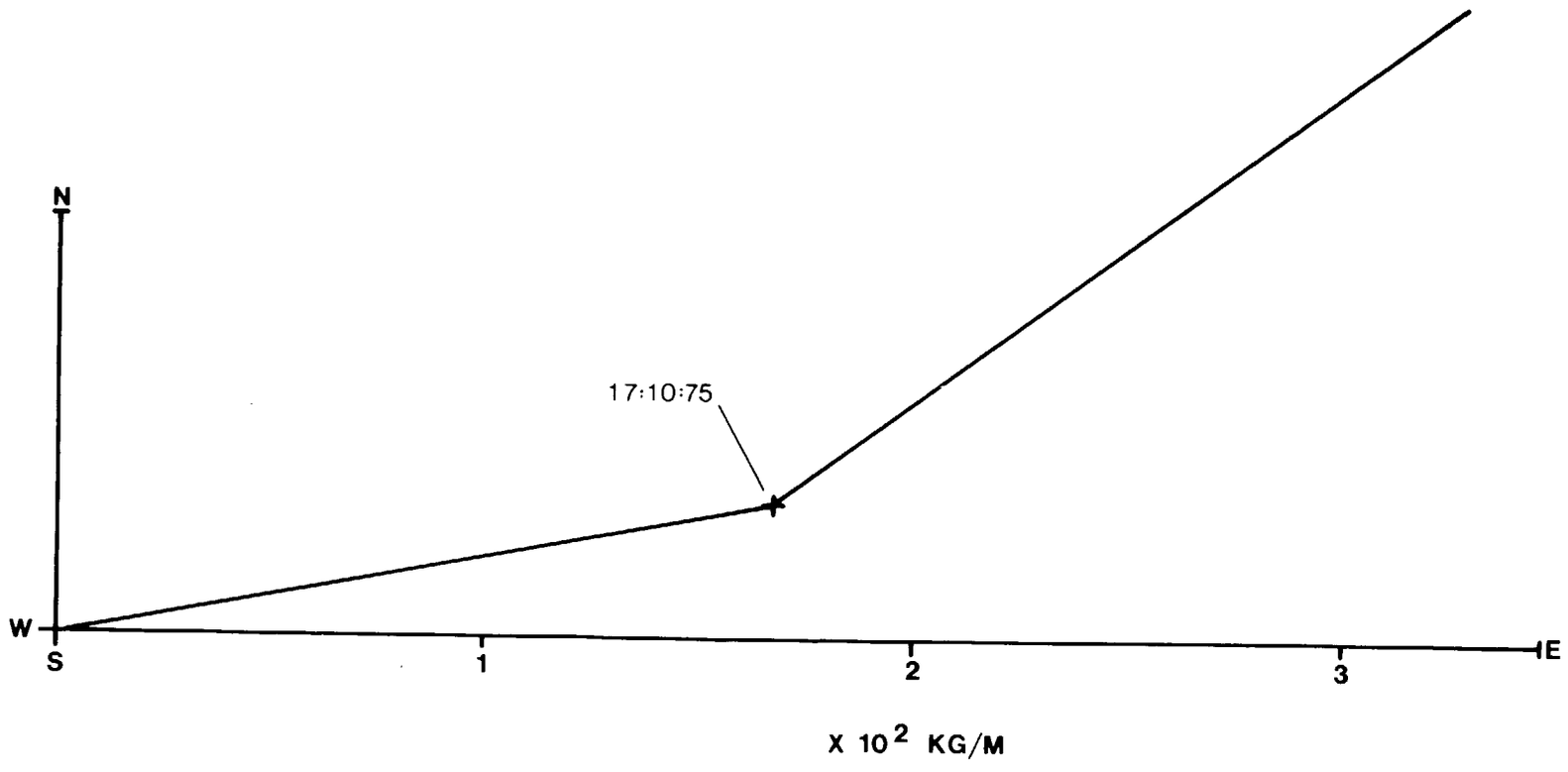

Fig. E7.1

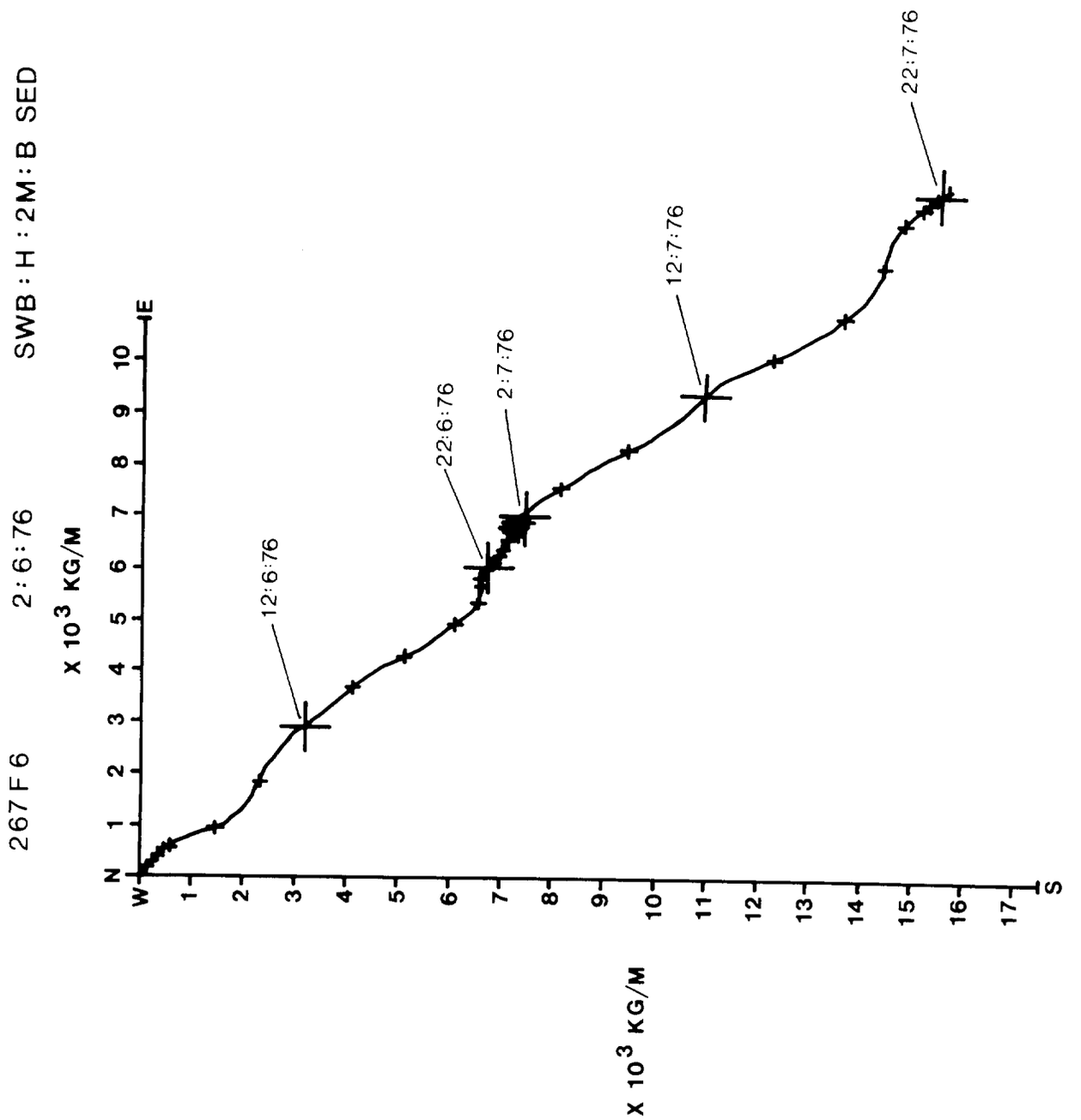
267 F 6
2:6:76
SWB : H : 2M : B SED
X 10³ KG/M
N
W
E
S
1
2
3
4
5
6
7
8
9
10
11
12
13
14
15
16
17
12:6:76
22:6:76
2:7:76
12:7:76
22:7:76
X 10³ KG/M

Fig.E8.1

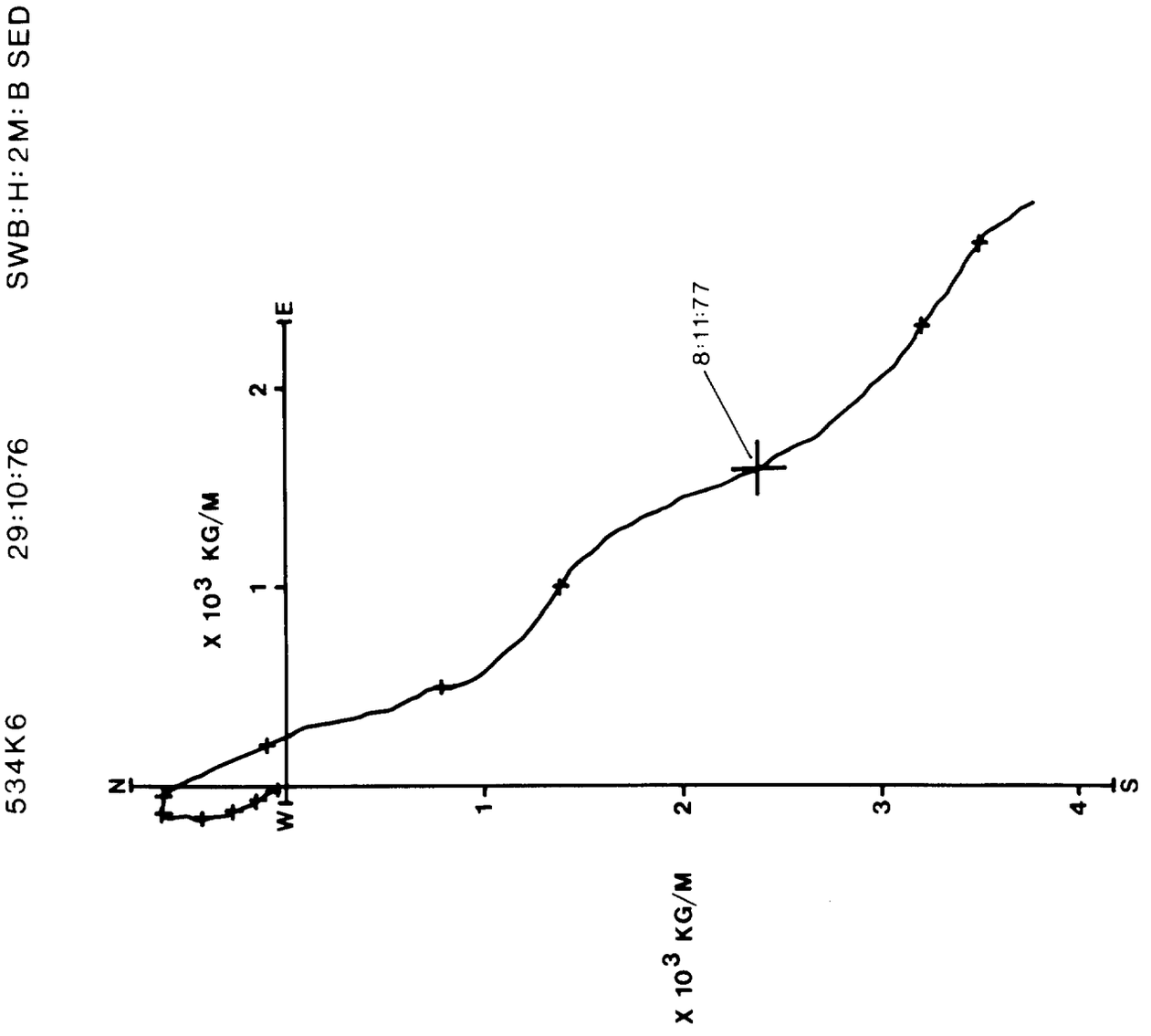

Fig.E8.2

534 F6 7:6:76 SWB : I : 2M : B SED

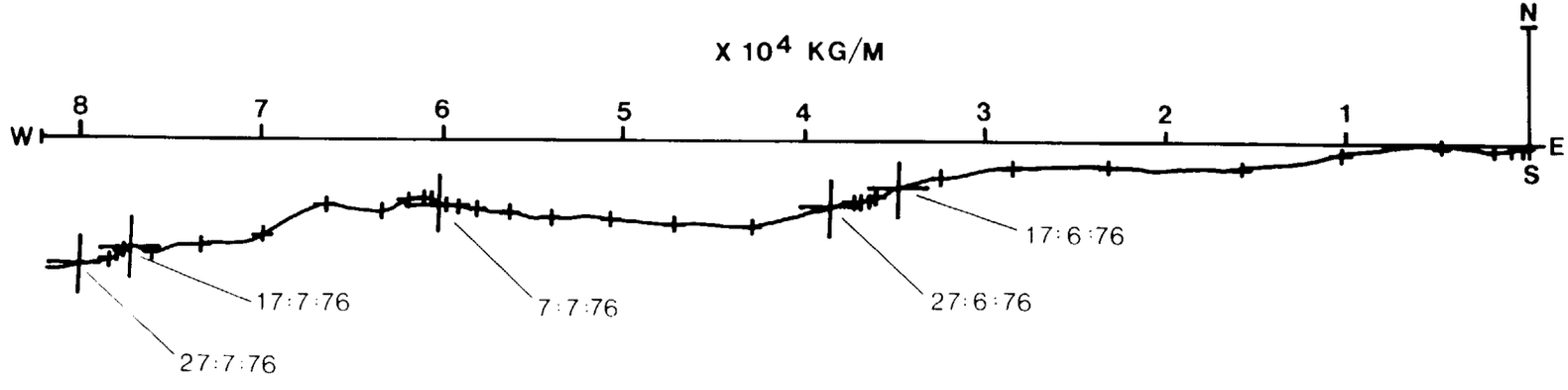

Fig. E 9 1

532 F6 11:6:76 SWB : J : 2M : B SED

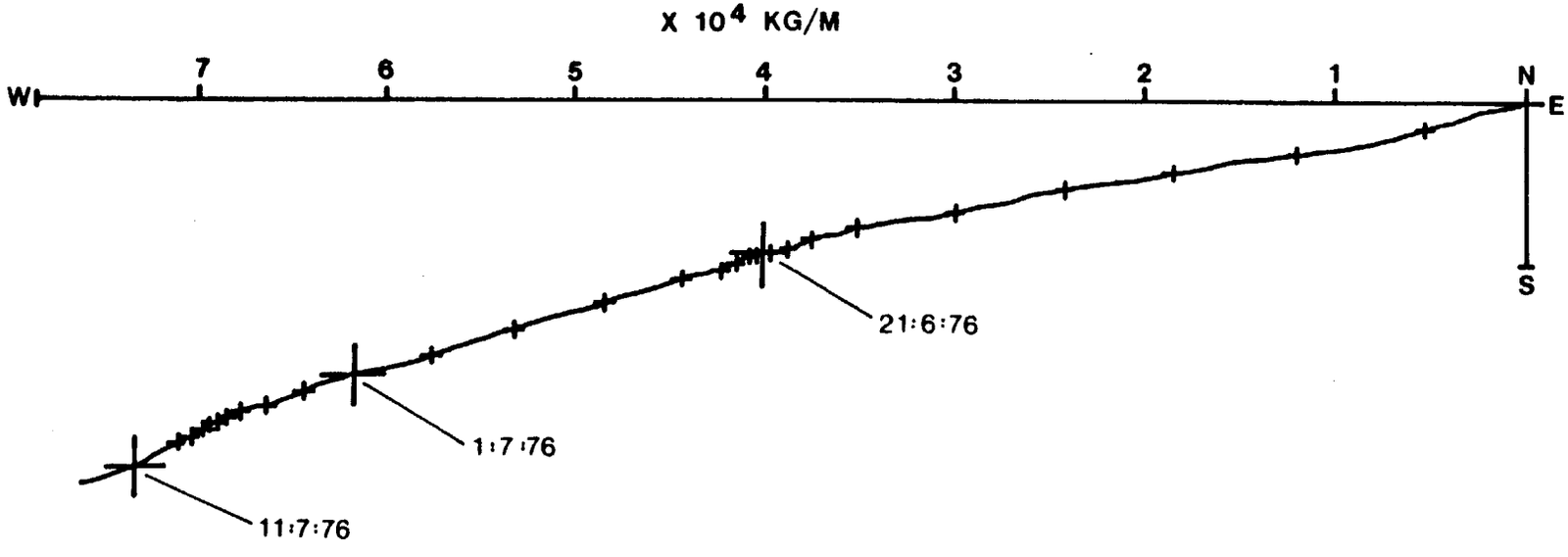

Fig. E 10.1

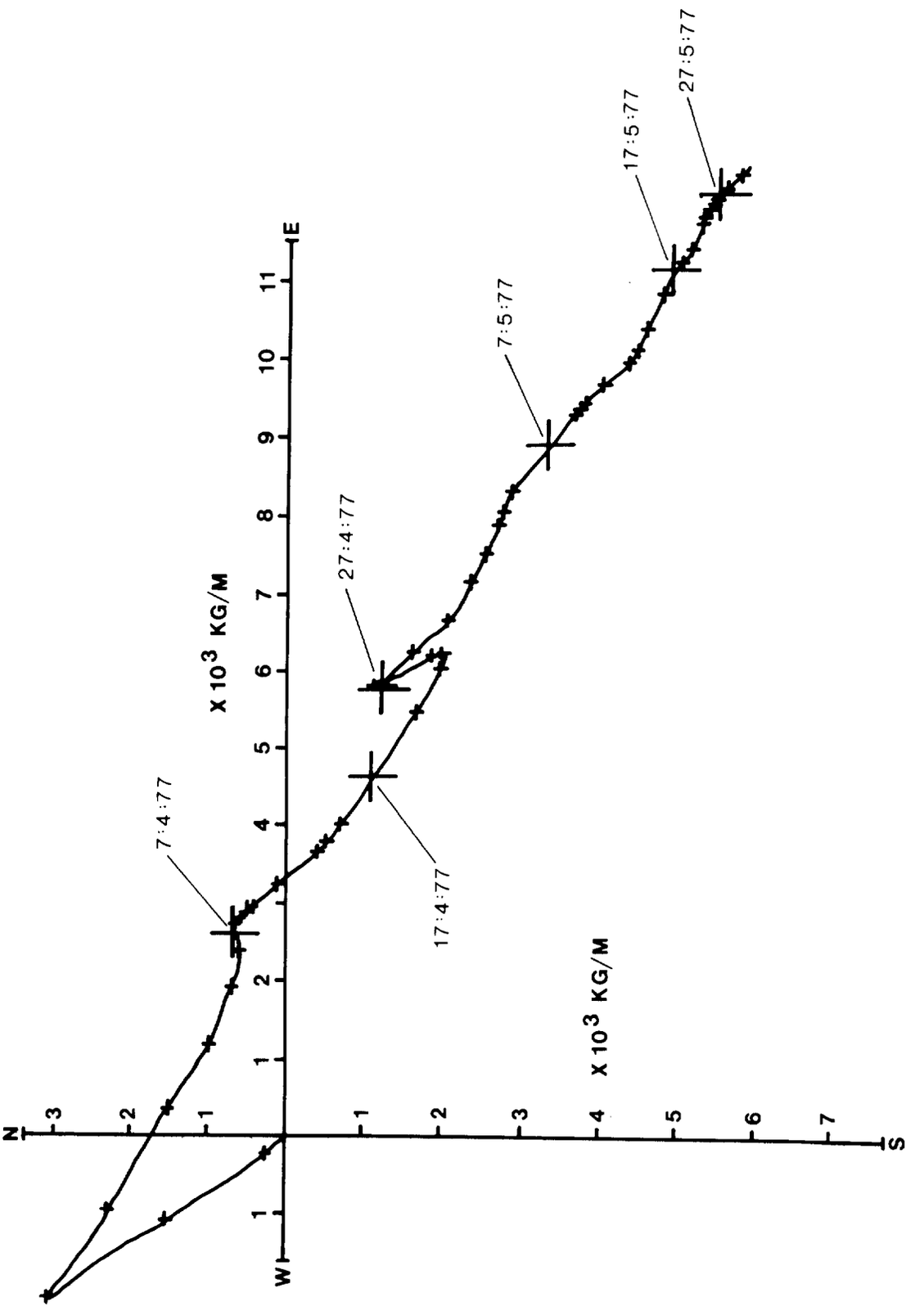
669C7
29:3:77
SWB:K:2M:B SED
N
S
E
W
X 10³ KG/M
X 10³ KG/M
7:4:77
17:4:77
27:4:77
7:5:77
17:5:77
27:5:77

Fig.E11.1

APPENDIX F

Suspended sediment and near-bottom velocity profile measurements

Measurements of near-bed suspended sediment concentrations and velocity profiles were made in Swansea Bay at the locations shown in Figure 3.

The objective of these measurements was:

(a) to examine the alongshore variations in suspended sediment concentrations immediately offshore of the area being studied on the foreshore (insufficient time prevented this aspect from being studied in full);

(b) to examine the onshore-offshore variations in suspended sediment concentrations moving from the low tidal energy area near the coast to the high energy area offshore.

In both cases it was intended to examine these variations over the Neap-Spring cycle.

Pumped sampling (PS) techniques were introduced to determine the quantities and particle size distributions of the material in suspension. This equipment also enables simultaneous measurement of the near-bottom velocity profiles to be made.

The PS equipment was designed and built at IOS Taunton and is shown schematically in Figure 7. The sea-bed unit consists of a tubular steel frame having a triangular base. The frame also supports an instrument post on which may be mounted up to six 9.5mm bore stainless steel nozzles for suspended sediment sampling. Also supported on the post were 4 Braystoke flowmeters for current speed measurements. Further provisions were made for the mounting of 2 electromagnetic flowmeters (not used in this study), the mounting of various electronic units, an underwater television system, and an inclinometer. Also mounted on the frame was a solenoid valve unit which enabled water samples to be taken from any one of the six nozzles and pumped to the surface via a single hose; this was accomplished by energizing the appropriate solenoid from the surface.

The underwater unit was lowered onto the sea-bed on a single load-wire with separate electrical cables to carry electrical power and signals between the solenoids, Braystoke flowmeters and inclinometer, and the surface. A single 50m 12.5 mm bore PVC hose carried sea-water to the

surface and the shipboard pump and filtration units.

Alignment of the probe with the mean flow was achieved by a large PVC fin on the rear of the frame, while the latter was being lowered to the sea-bed.

Provision was also made on the shipboard pump and filtration units for the simultaneous measurement of suspended sediment fluxes at an intermediate depth with a roving unit. The latter consisted of a nozzle attached to a Braystoke direct reading current meter with a separate 50m PVC hose (the roving unit was not used in this study).

Water samples were pumped to the surface with JABSCO 0.25 HP electrical pumps (one for the sea-bed unit and one for the roving unit) through 40μm polyester gauze filters clamped in Sartorius 142mm PVC pressure filter holders. Total flows and flow rates were monitored with Neptune rotary piston flow meters. Sediments finer than 40μm were collected in 250 ml water samples for subsequent concentration measurements by drying and weighing and by optical techniques using an EEL long cell absorptiometer. Typically 10% of a batch of samples would be dried and weighed to provide a calibration curve for the absorptiometer.

The measurements described in this report were made at the following heights above the sea-bed.

Height of concentration measurement (cm)	Height of speed measurement (cm)
180	180
–	100
80	–
40	40
25	15
15	
10	

Information on near-bed flow rates provided by the Braystoke flowmeters was monitored continuously by a PDP8 computer on board the surface vessel. Thus the number of rotor revolutions at all four elevations was listed routinely every 60s and punched on paper tape which was returned to the Laboratory for subsequent analysis.

Calibrations of the PS equipment showed that pump-line velocities of the order .7 – .8 ms^{-1} could be obtained. These figures are lower than

the required minimum of 1.0 m s^{-1} obtained by the Hydraulics Research Station (see Crickmore and Aked, 1975) with similar equipment, but should still be great enough to prevent settling of particulate matter in the pump line. The flushing time for the 50 m hose was found to be of the order of 60–90 s.